NASA CONTRACTOR REPORT

NASA CR-966

NASA CR-966

DISTRIBUTION STATEMENT A
Approved for public release;
Distribution Unlimited

19960628 091

AN INVESTIGATION OF THE MECHANISMS OF HEAT TRANSFER IN LOW-DENSITY PHENOLIC-NYLON CHARS

by E. D. Smyly, C. M. Pyron, Jr., and C. D. Pears

Prepared by
SOUTHERN RESEARCH INSTITUTE
Birmingham, Ala.
for Langley Research Center

NATIONAL AERONAUTICS AND SPACE ADMINISTRATION • WASHINGTON, D. C. • DECEMBER 1967

DEPARTMENT OF DEFENSE
PLASTICS TECHNICAL EVALUATION CENTER
PICATINNY ARSENAL, DOVER, N. J.

DTIC AD 10832

DISCLAIMER NOTICE

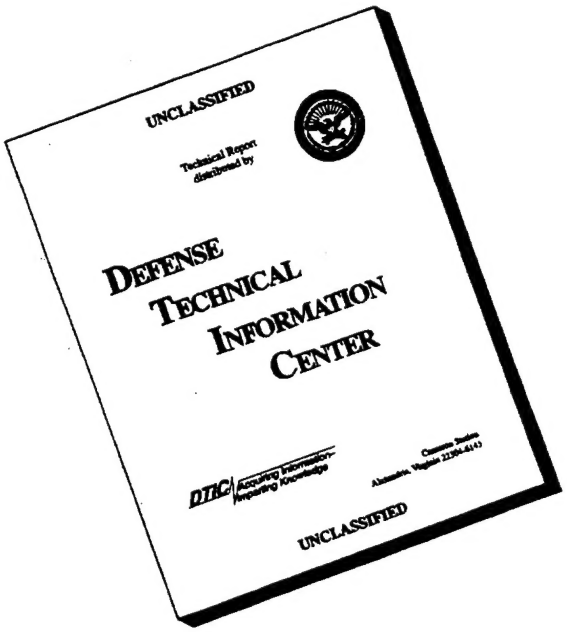

THIS DOCUMENT IS BEST QUALITY AVAILABLE. THE COPY FURNISHED TO DTIC CONTAINED A SIGNIFICANT NUMBER OF PAGES WHICH DO NOT REPRODUCE LEGIBLY.

NASA CR-966

AN INVESTIGATION OF THE MECHANISMS OF HEAT TRANSFER IN LOW-DENSITY PHENOLIC-NYLON CHARS

By E. D. Smyly, C. M. Pyron, Jr., and C. D. Pears

Distribution of this report is provided in the interest of information exchange. Responsibility for the contents resides in the author or organization that prepared it.

Prepared under Contract No. NAS 1-5448 by
SOUTHERN RESEARCH INSTITUTE
Birmingham, Ala.

for Langley Research Center

NATIONAL AERONAUTICS AND SPACE ADMINISTRATION

For sale by the Clearinghouse for Federal Scientific and Technical Information
Springfield, Virginia 22151 – CFSTI price $3.00

CONTENTS

	Page
SUMMARY	1
INTRODUCTION	2
SYMBOLS	4
SPECIMEN MATERIAL	7
Composition	7
Charring Procedure	7
True and Bulk Density and Porosity	9
Micrographic Evaluations	10
THERMAL CONDUCTIVITY DETERMINATIONS	11
Apparatus	12
Specimens	12
Specimen Buildup	13
Uncertainty in Measurements	13
Data and Results	16
Summary of Data	19
THERMAL ANALYSIS	21
Analyses of Porous Materials	21
Development of the Thermal Model	22
Physical and Thermal Model	22
Radiation	23
Solid Conduction	26
Gas Conduction	27
Convection	28
Equation for Apparent Thermal Conductivity of Char	29
Thermal Conductivity of Gases	31
Correlation of Thermal Model with Measurements	32
Correlation of Thermal Model with Prior High Temperature Data	34
CONCLUSIONS	37
APPENDIX A	39
APPENDIX B	49
REFERENCES	96

AN INVESTIGATION OF THE MECHANISMS OF HEAT TRANSFER IN LOW-DENSITY PHENOLIC-NYLON CHARS

By E. D. Smyly,
C. M. Pyron, Jr., and C. D. Pears
Southern Research Institute

SUMMARY

The heat transfer mechanisms in phenolic-nylon chars were investigated. In order to separate the effects of solid and gas conduction and radiation, the thermal conductivities of three phenolic-nylon chars having porosities of 0.79, 0.82, and 0.88 were measured in vacuum, nitrogen, and helium environments. The temperature range covered was from 400°F (477°K) to 1000°F (811°K). The pressure range was from 0.002 to 760 torr.

The specimens were obtained from virgin materials with densities of 19 lb/ft^3 (304 kg/m^3), 30 lb/ft^3 (409 kg/m^3), and 42 lb/ft^3 (673 kg/m^3) by charring in a 30 percent nitrogen-70 percent argon plasma for 125 to 180 seconds. The input cold-wall heat flux density was 170 Btu/sec-ft^2 (193 x 10^4 W/m^2).

The thermal conductivity increased on changing the environment from vacuum to either nitrogen or helium. The increase noted was in each instance greater than could be accounted for by the simple addition of the thermal conductance of the environmental gas to the thermal conductivity measured in vacuum. This discrepancy was explained as an effect due to the "thermal shorting" of internal delaminations within the char. From 30 to 50 percent of the flow paths through the char contain delaminations. The heat flow is essentially blocked by these delaminations at vacuum. When a gas is introduced it serves to "short" the delaminations and effectively increase the conduction area. The higher the thermal conductivity of the gas the more effective is the thermal shorting. A thermal model which takes the delaminations into account was developed and correlated with the data. The correlation of this model with the measured data allowed the isolation of one important intrinsic property of the char, the thermal conductivity of the matrix, assuming that the model describes the physical situation. Data at other conditions will be required to properly confirm the model.

The matrix thermal conductivity, reduced from the data, ranged from 155×10^{-5} Btu/sec-ft-°F (10.3 W/m-°K) to 250×10^{-5} Btu/sec-ft-°F (16.7 W/m-°K). It is believed that the variation represents differences in the charring histories of the specimens.

It was found that the heat transfer by radiation and gas convection was negligible below 1000°F (811°K). Gas convection was negligible because of geometric considerations plus the experimental arrangement. A study of the radiation parameters in the thermal model led to the conclusion that radiation was negligible.

The thermal analysis was extended to include some prior high temperature thermal conductivity data obtained in a steady-state apparatus to see if the analysis satisfies observed high temperature measurements. This analysis pointed out that further knowledge about certain parameters is required for an understanding of the "in-flight" behavior of the char. Some possible means of resolving these uncertainties are recommended.

INTRODUCTION

This program complements the studies performed under Contract No. NAS 1-2978, Task Orders 1, 2, 3 (reported in Reference 1) and 4 (see Reference 2) and represents a continuation of the efforts to provide a definition of the characteristics and intrinsic properties of low-density phenolic-nylon in both the virgin and charred states. Specifically, the work performed under this task order involved measurements of the thermal conductivity of chars produced from three different virgin densities of phenolic-nylon and the development of a thermal model for the porous structure. The measurements were made in vacuum, nitrogen, and helium and covered the temperature range from 400°F to 1000°F and a range of pressures from approximately 0.002 torr to 760 torr.

The virgin material was supplied by the NASA Langley Research Center in densities of 19, 30 and 42 lb/ft^3. The chars were prepared in Southern Research Institute's plasma torch from samples of the material provided.

Measurements were made of the bulk density, true density, and pore size distribution of the char produced from each of the virgin materials.

An effort was made to separate the effects of solid conduction, gas conduction, gas convection, and radiation on the apparent thermal conductivity of the char. A thermal model was developed in order to explain these effects.

SYMBOLS

Letter Symbols

$a = \dfrac{2\rho + \epsilon}{4\sigma\epsilon T_m^3}$

a_1, a_2 = accommodation coefficients for surfaces 1 and 2, respectively

A = total area normal to heat flow

A_1 = area of lower reference normal to heat flow

A_2 = area of upper reference normal to heat flow

A_d = $(1-f)(1-F)A$ = radiation and gas conduction area normal to heat flow across delaminations

A_g = $(1-f)(1-F)\,P^{2/3}A$ = gas conduction area of delaminated heat flow channels normal to heat flow

A_g' = $(1-f)FP^{2/3}A$ = gas conduction area of undelaminated heat flow channels normal to heat flow

A_G = $(1-f)\,FP^{2/3}A$ = gas conduction and radiation area of undelaminated heat flow channels normal to heat flow

A_m = $(1-f)(1-F)(1-P^{2/3})A$ = solid conduction area of delaminated heat flow channels normal to heat flow

A_m' = $(1-f)\,F\,(1-P^{2/3})A$ = solid conduction area of undelaminated heat flow channels normal to heat flow

A_r = $(1-f)(1-F)\,P^{2/3}A$ = radiation area of delaminated heat flow channels normal to heat flow

A_r' = $(1-f)\,FP^{2/3}A$ = radiation area of undelaminated heat flow channels normal to heat flow

A_R = fA = radiation and gas conduction area normal to heat flow through cracks

A_s = area of specimen normal to heat flow

$c = \dfrac{nt}{L}$ = ratio of total crack length in a flow channel to the overall thickness

c_v = specific heat at constant volume

f = fraction of total cross-sectional area normal to the heat flow occupied by the cracks which are parallel to the heat flow

F = fraction of the heat flow paths which are undelaminated

F_g = a factor which depends on the type of thermal guarding (matched or unmatched in some manner) and the geometry of the apparatus

F_{ir_2} = reradiation shape factor for heat flow through cracks parallel to heat flow

SYMBOLS - Continued

$F_K = k_i \left(\frac{1}{k_r} - \frac{1}{k_s}\right)$

H = heat transferred per unit area per unit time
k_1 = thermal conductivity of lower reference
k_2 = thermal conductivity of upper reference
k_a = apparent thermal conductivity
k_g = thermal conductivity of gas
k_i = thermal conductivity of insulating powder
k_m = thermal conductivity of matrix
k_r = thermal conductivity of references
k_s = thermal conductivity of specimen
K = overall thermal conductance
K_{dg} = thermal conductance of gas across delaminations
K_{dr} = radiant thermal conductance across delaminations
K_g = thermal conductance of gas in pores
K_g' = gas thermal conductance through undelaminated heat flow channels
K_G = thermal conductance of gas in cracks
K_m = solid thermal conductance in delaminated heat flow channels
K_m' = solid thermal conductance in undelaminated heat flow channels
K_r = radiant thermal conductance in delaminated flow channels
K_r' = radiant thermal conductance through undelaminated heat flow channels
K_R = radiant thermal conductance through cracks
L = thickness across which heat is being transferred
n = number of delaminations
p = pressure
P = porosity
Q = heat flow per unit time
r = ratio of specific heat at constant pressures to the specific heat at constant volume
R = gas constant
t = average delamination thickness
T_m = absolute temperature
x = characteristic radiant length

SYMBOLS - Concluded

Greek Symbols

α	=	correction term for heat bypass error in thermal conductivity measurements
ΔT	=	temperature difference
Δx	=	gage length
ϵ	=	emittance
ρ	=	reflectance
ρ_b	=	bulk density
ρ_t	=	true density
σ	=	Stefan-Boltzmann constant

Subscripts

1	=	lower reference
2	=	upper reference
s	=	specimen

SPECIMEN MATERIAL

Composition

This low-density phenolic-nylon composite was molded and consisted of the following materials: (1) 40% (weight) powdered 66 nylon, Dupont's Zytel 103; (2) 25% (weight) phenolic resin, Union Carbide Corporation's BRP-5549; (3) 35% (weight) phenolic Microballoons, Union Carbide Corporation's BJO-0930.

The virgin materials of all three densities had the same composition. The three densities were obtained by variation of molding pressure. The composition of this material was identical with that of the material used for the measurements reported in Reference 2.

A more thorough description of the individual constituents is included in Reference 2. The only difference in composition noted between this material and the low-density phenolic-nylon used for the measurements reported in Reference 1 was the difference in percentages of the phenolic Microballoons and nylon powder within the composite.

Charring Procedure

The char samples were produced at Southern Research Institute in an induction plasma torch. The chars evaluated under the previous task orders were prepared in the arc tunnel at the NASA Langley Research Center. A schematic diagram of the plasma torch is shown in Figure 1. As can be seen from the figure, the torch consisted of a quartz tube which was surrounded at one end with a five turn rf coil. Argon or mixtures of argon and nitrogen were introduced in a tangential flow pattern through a brass housing at the opposite end of the quartz tube. The rf coil was energized by a Lepel 25 kW power supply at a frequency of 2.5 to 5 Mc. The plasma was generated by inserting a graphite rod in the field of the coil while maintaining an argon flow rate of 25 to 30 scfh. The graphite rod heated and caused ionization of the argon, which initiated the plasma. The argon flow and the power level were increased to provide the desired flame properties. In order to provide a nitrogen plasma, the nitrogen was slowly introduced as the argon flow was decreased. It was found that the torch could be operated at stable conditions with 30 percent nitrogen and 70 percent argon. Higher nitrogen flow rates caused the flame to be unstable.

Heat flux density was measured on a 23 percent nitrogen flame at maximum power, and the values obtained averaged about 170 Btu/sec-ft^2 at a distance of 1 inch from the end of the quartz tube. This heat flux density was sufficient to produce chars of proper quality and is slightly higher than the heat flux density used at the NASA Langley Research Center to produce the chars evaluated and reported in References 1 and 2 (140 Btu/sec-ft^2). Heat flux densities were measured with a copper slug calorimeter. This calorimeter was basically a copper disc of known weight and size instrumented with a thermocouple and mounted in a refractory brick. Heat flux densities were calculated from measurements of temperature rise of the copper disc versus time (monitored by an X-Y recorder). It was found during the initial runs that the induced voltage caused sufficient current flow through the calorimeter thermocouple circuit to burn out the wire. This current drain also extinguished the flame. Several filter circuits were tried without success. Therefore, the rate of temperature rise was monitored by obtaining the slug temperature immediately before and after exposure to the flame and measuring length of time during exposure. The thermocouple circuit was switched open during flame exposure. This method, although more approximate, did confirm the general level of the heat flux density.

The specimens from which the chars were made were $1\frac{1}{4}$ inch diameter discs mounted in a refractory brick holder, which was inserted in the flame 1 inch away from the end of the quartz tube. At this location, with the power settings used, the "cold-wall" heat flux density, as mentioned previously, was approximately 170 Btu/sec-ft^2. To reduce oxidation of the char, the specimens were placed in a chamber immediately after the charring was completed. The chamber was purged with nitrogen.

During the runs, surface temperatures of the specimens were monitored with an optical pyrometer to determine the consistency of the charring conditions for each run. The pyrometer data obtained were not corrected for the effects of surface emittance and plasma characteristics; however, these data ascertained the consistency of all the runs. The pyrometer readings also provided an approximate temperature distribution over the front surface of the specimen. A typical temperature distribution is shown in Figure 2.

During the runs, the temperature rise rate of the specimens varied with the density of the material, the temperature rise rate of the lowest density material being more rapid. For example, the observed temperature of the phenolic-nylon of 19 lb/ft^3 virgin density increased to 4000°F in approximately 4 seconds, whereas 10 seconds were required to achieve the same surface temperature with the 42 lb/ft^3 material. The steady-state temperatures toward the ends of the runs were the same for all of the materials. It was also noted that the charring rate was higher for the lower density materials. Therefore, the total times of exposure were varied for the different densities to obtain chars of $\frac{1}{2}$ inch thickness which were required for the thermal conductivity specimens.

The chars prepared for this program were exposed for a longer period of time than the prior chars prepared in the arc tunnel at the NASA Langley Research Center in order to obtain chars of sufficient thickness from which to prepare thermal conductivity specimens. The exposure times for producing the chars were 125 seconds, 165 seconds, and 180 seconds for the 19 lb/ft^3, 30 lb/ft^3, and 42 lb/ft^3 virgin density materials, respectively. The chars used for the measurements reported in Reference 2, which were produced by the NASA Langley Research Center, were exposed for 90 seconds.

True and Bulk Density and Porosity

The bulk densities of the chars were determined by weighing the specimens on an analytical balance and dividing weight by the calculated volume (the specimens had a cylindrical geometry). The specimens had been impregnated with polyalphamethylstyrene (for machinability) and then baked out before the thermal conductivity runs. Some attempts were made to determine the bulk density by using a water displacement method, after paraffin coating, in accordance with ASTM C311-58. However, the results obtained by this method were not satisfactory.

True density measurements were made on pulverized samples by employing a pycnometer. The particle size distribution in the pulverized powder was as follows:

2 microns or less	-	75 percent
3 - 5 microns	-	20 percent
6 - 12 microns	-	5 percent

The results of the true and bulk density measurements are given in Table 1 for each sample evaluated. Note for Specimen 19-4 that there was only a 4 percent change in bulk density as measured before and after the thermal conductivity evaluation.

Porosity was calculated from the relation

$$P = 1 - \frac{\rho_b}{\rho_t} \tag{1}$$

where

P - porosity
ρ_b - bulk density
ρ_t - true density

The results of the porosity calculations are given in Table 1. Note that while the bulk densities of the three materials varied by more than a factor of 2, the porosity variation was only from 0.79 to 0.88. This results from the fact that the importance of the bulk density is reduced by about $\frac{1}{5}$ in the porosity calculation since the true density is about 5 times as large as the bulk density.

Micrographic Evaluations

A micrographic evaluation was also performed on the char to determine the average pore size and relative frequency distribution. One char sample of each virgin density was mounted and polished using standard techniques. The specimens used for the photomicrographic evaluations were not impregnated. The specimens were viewed at 100X magnification in a plane parallel to the charring direction. The measurements were made in a central zone midway between the front and back surfaces of the sample. Two traverses a few mils apart were made across the char at this location. The pores were counted and their diameters measured with a calibrated eye-piece which read in filar units. When grossly irregular pores were encountered, the diameter was approximated. Cracks which ran parallel to the charring direction were not included in the measurements. Only openings which were nearly enclosed were counted as pores. Some areas appeared to represent locations where several pores had been blown out.

Since these areas were enclosed by pores on all sides, they were counted as large pores since they probably were created during the charring process. Shown in Figure 3 are photomicrographs of the char produced from the three materials of different virgin densities. Photomicrographs 3(a) and 3(c) are typical, whereas pictures 3(b) and 3(d) are not typical (as many large openings as are shown do not appear in the typical photomicrograph). The porous areas shown in Figure 3(b) (away from the large openings) are typical. The samples shown in Figures 3(a), 3(b), and 3(c) were used for the pore size measurements.

Histograms of the distribution of pore diameters are shown in Figures 4, 5, and 6 for the chars of 0.88, 0.82, and 0.79 porosities, respectively. The average pore diameters of the materials with porosities of 0.88, 0.82, and 0.79 were 69, 18, and 35 microns, respectively. For comparison the histogram obtained for a material with a porosity of 0.86 (36 lb/ft^3 virgin density)(reference 2) is shown in Figure 7. Note that the mean pore diameter for this material was 29 microns. This mean pore diameter is greater than that for the material of 0.82 porosity and less than that for the material of 0.79 porosity. There was no apparent correlation between the pore diameter distribution and the bulk density of either the virgin material or the char. However, the histograms give reasonable agreement and indicate the approximate range of pore diameters. Apparently, the average pore diameter decreases with increasing bulk density up to a point and then increases. Perhaps the porosity of the virgin structure permits outgassing through paths following the existing voids up to a point where the existing voids cannot handle the gas evolution and then larger paths (and pores) are formed to provide gas release.

THERMAL CONDUCTIVITY DETERMINATIONS

The thermal conductivity was determined in one direction (in the charring direction) using the comparative rod apparatus. The apparatus was placed inside a vacuum chamber which was connected to a 15 cfm mechanical pump and a 4 inch diffusion pump. With this system, it was possible to achieve a vacuum level of 0.002 torr. Pressures were measured with a thermocouple vacuum gage below 0.1 torr, a McLeod vacuum gage between 0.1 torr and 5 torr, a Dubrovin vacuum gage between 1 torr and 20 torr, and a bourdon tube gage above 20 torr.

Apparatus

The comparative rod apparatus is described in detail in Appendix A. Basically, this apparatus consists of a stacked column with the specimen sandwiched between two references of known thermal conductivity. Heat is made to flow through the column, and the thermal conductivity is measured by referencing the temperature drop across the specimen material to the temperature drop through the references.

Guard heaters are employed to minimize radial heat losses and axial bypasses. The guard section is concentric with the specimen column, and the annulus between the column and the guard is filled with diatomaceous earth as an insulation. The thermal conductivity is calculated from the measurements by using the relation

$$k_s = \left(\frac{k_1 \Delta T_1}{\Delta x_1} + \frac{k_2 \Delta T_2}{\Delta x_2} \right) \frac{\Delta x_s}{2 \Delta T_s} \qquad (2)$$

where k is the thermal conductivity, ΔT is the temperature difference over the gage length, Δx, and the subscripts s, 1 and 2, refer to the specimen, lower reference and upper reference, respectively.

Specimens. - The machining of the specimens was performed after impregnating the char with polyalphamethylstyrene to provide sufficient mechanical strength. Machining was performed by first cleaning up the front (plasma-heated) surface until it was flat (this usually required the removal of only a small amount of material since this was the smoothest surface), then reducing the thickness a minimum amount until the back surface was flat and parallel with the front surface. The specimen was then turned to 1 inch outside diameter, and 0.040 inch thermocouple holes were drilled 0.093 inch from either surface. Table 2 gives the gage length (between thermocouple holes) and overall thickness of each specimen.

The specimens were baked at 700 °F under a nitrogen purge to remove the impregnant. Specimen 42-3 was baked in a helium purge. All of the specimens baked out well except those from the highest density material. The back surface of two of these specimens after bake out consisted of a grayish white residue about 0.1 inch thick, which indicated that these specimens had not charred to the same depth as the lower density specimens or had a different composition in the char products near the rear face. This

residue was not noticeable before impregnating. Of course, those specimens which baked out poorly were not evaluated. Pictures of Specimen 30-6 before and after exposure are shown in Figure 8.

Specimen Buildup. - The specimens were built up for the runs as shown in Figure 9. For all of the runs except the second run on Specimen 42-3 (when an attempt was made to measure the thermal conductivity variation across the specimen) the buildup was as shown in Figure 9(a). Note that the guard thermocouples were located opposite the thermocouples in the references. The surface of the specimen which had been heated during the charring process always was situated so that the heat flow was from the front to the back surface.

Uncertainty in Measurements. - The basic uncertainty in the thermal conductivity measurements made with this apparatus is 5 percent. This uncertainty applies to measurements on materials with a thermal conductivity above about 230×10^{-5} Btu/sec-ft-°F. The uncertainty was increased for these measurements because the thermal conductivity of the chars was lower than the thermal conductivity of the reference materials. The uncertainty is increased because of the difference between the temperature profiles in the references and the specimens due to the higher conductivity of the references. This makes it difficult to match the guard profile with the column profile. For the range of values expected for the char specimens, there was a choice of two reference materials, Code 9606 Pyroceram or Pyrex. Pyroceram is suitable as a reference up to 1500°F, and Pyrex is suitable to 577°F. Above 577°F, the radiation component through the Pyrex introduces an increased uncertainty in its thermal conductivity. Over the temperature range of the measurements on the char, the reference materials had the following range of thermal conductivities:

Pyroceram: 57.6×10^{-5} to 49.3×10^{-5} Btu/sec-ft-°F (300°F to 1100°F)
Pyrex: 19.9×10^{-5} to 22.6×10^{-5} Btu/sec-ft-°F (300°F to 577°F)

The values for the Pyrex match the measured values better than the values for the Pyroceram. However, as mentioned, the temperature range is limited using Pyrex.

Analyses have been made of the errors which are introduced in comparative rod measurements when there is a mismatch between the thermal conductivity of the references and the specimen. The analyses undertook to account for the heat flow through the references which bypassed the specimens. Physically, this can be explained as follows: some of the heat flow through the upper reference will bypass the specimen and flow to the lower reference

through the insulation surrounding the specimen. This results in less heat flow through the specimen than indicated by the references. Consequently, the temperature difference across the specimen will be reduced, resulting in an apparently higher thermal conductivity than would be measured if there were no heat losses.

The equation for the conductivity containing the correction for the heat bypass may be written

$$k_s = (1 + \alpha)\left(\frac{\frac{k_1 \Delta T_1}{\Delta x_1} + \frac{k_2 \Delta T_2}{\Delta x_2}}{\frac{2 \Delta T_s}{\Delta x_s}} \right) \tag{3}$$

Note that equation (3) is identical with equation (2) except for the term α which represents the error term for the mismatch. The error may be written

$$\alpha = F_k F_g \tag{4}$$

where

$$F_k = k_i \left(\frac{1}{k_r} - \frac{1}{k_s} \right) \tag{5}$$

F_g = a factor which depends on the type of thermal guarding (matched or unmatched in some manner) and the geometry of the apparatus

In equation (5), k is used for the thermal conductivity, and the subscripts i, r, and s refer to the insulation, reference, and specimen, respectively. Observe that in equation (5), the term F_k will be negative if k_s is less than k_r.

The factor, F_g, can be maintained at less than 2 if the guard temperatures are matched with the column temperatures. During the runs it was not possible to maintain matched guarding and still maintain the heat flows through the upper and lower references equivalent within 10 percent. This was due in large part to a severely nonlinear temperature gradient through the specimen which probably resulted from a conductivity gradient through the

specimen. Almost invariably a good match of the column and guard temperatures could be achieved for the upper reference and the central portion of the specimen. However, the temperature of the lower guard usually was about 50°F to 100°F higher than the temperature of the lower reference because of the severe temperature drop between the lower specimen thermocouple and the lower face of the specimen. Typical temperature profiles in the guard and the column for the measurements in helium and nitrogen are plotted in Figure 10. The value of F_g resulting from this guarding should be no more than 2 based on an evaluation of Pyrex using Code 9606 Pyroceram references.

The thermal conductivity of the diatomaceous earth is probably as low as 0.001×10^{-5} Btu/sec-ft-°F in vacuum, 0.4×10^{-5} Btu/sec-ft-°F in nitrogen, and 2.4×10^{-5} Btu/sec-ft-°F in helium. By substituting these values into equation (5) along with the values for the thermal conductivity of the references and specimen and using a value for F_g of 2, the following values are obtained for α:

Pyroceram		Pyrex	
Vacuum α =	0	Vacuum α =	0
Nitrogen α =	-0.05	Nitrogen α =	-0.02
Helium α =	-0.15	Helium α =	-0.08

Note that these results indicate that the data in helium using Pyroceram references may be in error on the high side by as much as 15 percent. The true error, if any, is not accurately known because the value of F_g is not known. Since temperature profiles were matched over portions of the column, F_g may be less than 2.

The theoretical corrections were not applied to the data because of the uncertainty in the value of F_g. The run on the Pyrex specimen using Pyroceram references led us to conclude that F_g was probably less than 2. This conclusion was based on the fact that the thermal conductivity of the Pyrex in vacuum was only about 3.1 percent lower than the value in helium and it should have been 19.5 percent lower if F_g were 2. Thus, it appeared that the Pyrex specimen had a higher conductivity than that assumed in calculating F_g from the helium data. The purpose of investigating the bypass error was to determine the maximum possible uncertainty in the data.

A consideration of the errors involved led to the conclusion that the random uncertainty in the system is about 10 percent with a possible bias error of 15 percent (on the high side). The uncertainties are higher than normal because of the low thermal conductivity of the material.

Data and Results

The data for the char of 0.88 porosity (19 lb/ft^3 virgin density) are presented in Tables 3 and 4 and in Figures 11, 12, and 13. For clarity the data in Figure 11 are presented independently for each gas. Note that the data for Specimen 19-5 were obtained using Pyrex references, and for reasons previously stated, were limited to the 500°F mean temperature level. The thermal conductivity values for Specimen 19-5 were lower than the values for Specimen 19-4 by approximately 20 percent in helium and nitrogen and 10 percent in vacuum. Figure 12 shows the effect of pressure on the effective thermal conductivity of the char in nitrogen at approximately 500°F. Note that while the two specimens had different thermal conductivity values, both exhibited an increase in thermal conductivity (from vacuum to 760 torr) which was more than could be assigned to the conductivity of the gas. In fact, the change was about 4 times the gas conductivity (0.58×10^{-5} Btu/sec-ft-°F). A similar trend is noted in Figure 13 where the data are presented versus pressure for a helium environment. Note that the conductivity was nearly constant between 0.0022 torr and 0.1 torr and then increased with pressure to 760 torr. Note that the change with pressure is most noticeable over the range of mean free paths from 3 microns to 300 microns, which agrees well with the measured range of pore sizes of 5 to 323 microns (see Figure 4).

That there should be a correlation between the pore size distribution and the mean free path may be explained as follows: when the mean free path is much smaller than the distance separating the surfaces between which heat is being exchanged by gas conduction, the conductivity is essentially independent of the separation distance so that heat transfer is dependent upon separation distance. However, when the mean free path is nearly the same as the separation distance, the heat transferred becomes more independent of the separation distance. If the gas density is reduced until the mean free path is longer than the separation distance, the heat transferred is essentially independent of the separation distance. Actually, for a given separation distance, the range of mean free paths over which the thermal conductivity varies extends over a finite range. That is, the change in gas thermal conductivity with pressure does not occur as a discontinuous jump but rather as a smooth change which starts at a mean free path which is lower than the separation distance. However, this range is small, and therefore, it is acceptable to correlate the mean free paths with the pore diameters (separation distances). The fact that the pressure range (range of mean free paths) over which the measurements showed a pressure dependence is broad arises from the distribution of separation distances (pore diameters).

Note in Figure 13 that the change in the conductivity in helium on changing the pressure from 0.002 torr to 760 torr ranged from 2.4 times the gas thermal conductivity (3.4×10^{-5} Btu/sec-ft-°F) for Specimen 19-4 and 3.4 times the gas thermal conductivity for Specimen 19-5.

The data for the char of 0.82 porosity (30 lb/ft^3 virgin density) are presented in Tables 5 and 6 and in Figures 14, 15 and 16. The data are presented separately in Figure 14 for the three different gases. Note that for any given environmental condition there was good agreement among the the data for the two specimens. The data for the thermal conductivity of the char of 0.82 porosity versus pressure in nitrogen at approximately 500°F are shown in Figure 15. Note that the thermal conductivity was constant over the pressure range from 0.0022 torr to approximately 3.5 torr and then increased between 3.5 torr and approximately 300 torr. The range of pressure dependence corresponds to a range of mean free paths from about 0.3 micron to 25 microns, which falls within the measured range of pore diameters from 1 to 250 microns. Note from the pore diameter distribution (Figure 5) that 230 out of 275 pore diameter measurements were less than 20 microns, which closely approximated the mean free path at which the pressure variation essentially ceased. Note that once again the increase in conductivity from vacuum to one atmosphere was more than could be assigned to gas conduction. The data for the thermal conductivity versus pressure in helium are presented in Figure 16. Note that the pressure range of greatest change corresponded to the range of mean free paths from about 2 microns to 200 microns. Once again the increase in thermal conductivity in going from vacuum to 760 torr was greater than could be assigned to gas conduction even for Specimen 30-4, which exhibited the least increase.

The data for the char of 0.79 porosity (42 lb/ft^3 virgin density) are presented in Tables 7 through 11 and in Figures 17, 18 and 19. The data are presented in Figure 17 for each gas separately. Note that Specimen 42-4 had a lower conductivity at 500°F in vacuum and nitrogen than either of the other two specimens. This specimen was found to be badly deteriorated on the rear surface at the termination of the run. This condition may account for the low data. Specimen 42-5 was machined to a thickness of 0.312 inch before it was baked out. Consequently, the gage length for this specimen was only 0.133 inch, or about half the gage length of Specimen 42-3. This specimen was made thin to alleviate the problem of rear surface deterioration, noted previously, during bake out. The data for Specimens 42-3 and 42-5 agreed well at 500°F in vacuum and throughout the temperature range in nitrogen. However, there was a disagreement of approximately 20 percent at 500°F in helium, and this difference increased at the higher

temperatures. Remember that a thin layer of Fiberfrax was inserted between the references and the specimen for the run on Specimen 42-3. A rerun on Specimen 42-3 (without the Fiberfrax) gave good agreement with the first run data at 500°F in both vacuum and nitrogen. Therefore, the differences noted between the conductivities of the two specimen in the helium environment probably represent the true differences between the specimens.

The data for the thermal conductivity of the char of 0.79 porosity versus pressure in nitrogen at approximately 500°F are shown in Figure 18. The conductivity began to increase with pressure at a pressure of 1 torr, which corresponds to a gas mean free path of about 90 microns. Note that this is in fair agreement with the pore diameter measurements shown in Figure 6. The pore diameter measurements indicated that some decrease in thermal conductivity might be noted down to a mean free path of 200 to 300 microns. Note again that the change in thermal conductivity on going from vacuum to 760 torr was more than could be assigned to gas conduction.

The data for the thermal conductivity of the char of 0.79 porosity versus pressure in helium at a temperature of approximately 500°F are presented in Figure 19. This figure shows results of measurements of the variation in thermal conductivity through the specimen. Note that for Specimen 42-3 data are presented for the upper 0.095 inch of the specimen, the middle 0.276 inch of the specimen, and for the lower 0.093 inch of the specimen. During charring, the upper surface was directly exposed to the plasma. These data indicate a definite variation in conductivity across the specimen. However, the data for the upper portion of the specimen are questionable. The surface temperatures (both upper and lower) were measured by spacing bare thermocouple wires on the surface and allowing the specimen to act as the junction. There are local temperature disturbances (distortions of the isotherms) in the vicinity of the interface between the specimen and the references; thus, the surface temperature measurements reflect these disturbances. Further, the disturbances are more severe in vacuum since the heat flow concentrates at the points of solid to solid contact. If there is a gas in the interfacial gap it helps to conduct heat and spread the heat flow more evenly. Since, in vacuum, the temperature difference across the upper portion of the char was considerably smaller than that across the lower portion (8°F versus about 50°F) any errors which resulted from the interfacial problem would have had a greater effect on the conductivity measured for the upper portion of the specimen. It is difficult to explain the large increase in the thermal conductivity of the upper portion of the char with pressure. It is probably most logical to assume that the

values measured in vacuum were low because of the interface problems (and a temperature difference of only 8°F), and that the data at 760 torr were approximately correct. The data obtained for the lower portion of the specimen are less uncertain because of a larger temperature difference (even though the same method of temperature measurement was used). The measurements do indicate an increase in the thermal conductivity of the char from the lower to the upper (exposed) surface; however, because of the uncertainty in the temperature measurements on the upper surface, more data would be required to quantitatively define the variation.

Note that the data in the helium environment for the char of 0.79 porosity indicate that the increase with pressure begins at a mean free path of around 1000 microns for the central portion of the char. This does not correlate with the pore diameter measurements which indicated that the largest pore diameter was 323 microns. The data for the lower portion correlate much better, with the increase beginning at approximately 300 microns.

Summary of Data. - The average conductivities of each porosity of char at 500°F in nitrogen, helium, and vacuum are presented in Table 12. For the char of 0.79 porosity, the data for Specimen 42-4 were neglected in obtaining the average for the reasons previously given.

Note in Table 12 that the most porous char (Specimens 19-4 and 19-5) had the lowest conductivity, as would be expected. However, there was no correlation between the thermal conductivity values for the 0.79 and 0.82 porosities. The porosities for these specimens were nearly identical, and they behaved identically within the data scatter. Prior evaluations on phenolic-nylon char using the radial inflow apparatus yielded values of 12, 16, and 19 x 10^{-5} Btu/sec-ft-°F at 1000°F for specimens with bulk densities of 15.0 lb/ft^3, 22.6 lb/ft^3, and 13.2 lb/ft^3, respectively.[1,2] A helium purge was used for the prior evaluations. However, the specimens were not evacuated prior to the evaluation and consequently the air (nitrogen) which was entrained within the specimens prior to insertion in the furnace probably remained during part of the run. Helium may have replaced the entrained air as the run progressed but it can probably be assumed that the specimens essentially contained nitrogen at the 1000°F point. Correspondingly, the nitrogen data for these evaluations yielded values at 1000°F of 14, 18.8 and 19 x 10^{-5} Btu/sec-ft-°F for bulk densities of 11.9 lb/ft^3, 16.5 lb/ft^3, and 20.0 lb/ft^3, respectively. It was pointed out in Reference 2 that the formulation and processing of the prior material for which the thermal conductivity was 12 x 10^{-5} Btu/sec-ft-°F was less than optimum

for a plastic composition. The formulation was low in volume fraction of phenolic resin and the processing method caused mechanical damage to the Microballoons. The lower thermal conductivity of this material when compared to other formulations of the same basic material was directly correlated with the formulation and processing. The prior values of 16 and 19 x 10^{-5} Btu/sec-ft-°F agree within 19 percent with the values of 18.8 and 19 x 10^{-5} Btu/sec-ft-°F measured in this program on two specimens of similar bulk densities. This represents good agreement between similar specimens and between the two apparatuses used for the evaluations.

Also shown in Table 12 are the absolute changes in the thermal conductivity and the percentage changes in going from vacuum to nitrogen and from vacuum to helium. In each instance the absolute change in thermal conductivity was significantly greater than the thermal conductivity of the gas in question. This indicates either strong dependence on the gas thermal conductivity or convection effects. Radiation, if it were present, would be a constant component.

Recall from the prior discussion that the theoretical analysis of the bias error introduced because of the conductivity mismatch between the specimens and the references predicted a maximum positive error of 25 percent in both helium and nitrogen. This is being recalled because there have been several analyses of porous materials which would predict nearly the total gas thermal conductivity as the contribution of the gas to the measured thermal conductivity for this range of porosities, and one wants to see if this low prediction is probable within the experimental error. The last two columns in Table 12 give the maximum possible percentage change in the measured thermal conductivity which can be attributed to the gas and the difference between this value and the measured value, respectively. In the last column, observe that with one exception the difference in the measured increase in conductivity and the increase obtained by adding the thermal conductivity of the gas exceeded the 25 percent maximum probable error in the measurement. This is important in that it indicates that the thermal conductivity of the gas can have more effect on the "apparent" thermal conductivity of the char than its own value. This effect has appeared in the literature before. Young, Hartwig and Norton[3] presented data for firebrick of 0.82 porosity. The thermal conductivity increased in air (nitrogen) from 1.46 x 10^{-5} Btu/sec-ft-°F at 0.05 torr to 2.52 x 10^{-5} Btu/sec-ft-°F at 760 torr for a change of 73 percent. By assuming that the air contributed its total conductivity, the change would have been only 40 percent (based on a gas conductivity of 0.48 x 10^{-5} Btu/sec-ft-°F). One might argue that convection effects are present. Evidence will be presented

later which indicates that this effect is small. For the range of porosities which have been evaluated, there is small possibility that the matrix is continuous, especially considering the violent birth of the material. Therefore, delaminations and voids exist which offer infinite resistance to heat flow at vacuum but become shorted when a continuum gas is introduced and effectively raise the solid conduction area. It is believed that this accounts for the increase rather than convection currents.

THERMAL ANALYSIS

In order to separate the effects of radiation, solid conduction, gas conduction and convection on the apparent thermal conductivity of the char, a thermal analysis was performed. This analysis also allowed the isolation of one of the important intrinsic properties of the char, the thermal conductivity of the matrix.

In the thermal analysis, each of the aforementioned modes of heat transfer was considered. Before proceeding to the thermal model some work by other authors should be discussed.

Analyses of Porous Materials

Russell[4], Gorring and Churchill[5], Euken (presented in Reference 6), Loeb[7], and many other authors have presented equations for predicting the thermal conductivity of porous materials. In addition, an equation derived by Bruggeman (presented in a paper by Powers[8]) for dispersions may be applied to porous materials. This may be done by treating the pores as the dispersed phase and using the conductivity of the gas within the pores as the conductivity of this phase. The char solid would be treated as the continuous phase. In all of these analyses the authors have assumed that the matrix was continuous (contained no delaminations or irregularities), and most of them give nearly identical results. For completeness, Russell's equation, which has found general acceptance, was applied to the data to ascertain how closely the models for continuous matrices apply. Russell's equation may be written[4]

$$k_a = k_m \frac{k_g P^{2/3} + k_m(1 - P^{2/3})}{k_g P^{2/3} - k_g P + k_m (1 - P^{2/3} + P)} \qquad (6)$$

where

k_a = apparent thermal conductivity
k_m = thermal conductivity of matrix
k_g = thermal conductivity of gas
P = porosity

Russell's equation was applied to the data by reducing k_m (matrix conductivity) from the vacuum data and then predicting the values for nitrogen and helium. Also, k_m was reduced from the nitrogen data, and the vacuum and helium values were predicted. A temperature of 500°F was assumed for these calculations and radiation was neglected. The results of the calculations are shown in Table 13. The vacuum data probably contain the least uncertainty; therefore, for a comparison with the measured data, the predictions based on the vacuum data should be most meaningful. Note that with one exception the predicted values fell below the measured values by a greater percentage than can be attributed to uncertainty in the measurements (maximum of 25 percent), indicating that a continuous model should not be assumed for the highly porous chars.

Development of the Thermal Model

Physical and Thermal Model. - A physical model was assumed which is a first approximation to a noncontinuous matrix. This model is shown in Figure 20(a). It was assumed that the material contained cracks which were parallel to the direction of heat flow. These cracks were assumed to occupy some fraction f of the total area and extend across the thickness of the material. The char does contain these long cracks but obviously they do not extend through the full thickness; some interconnections exist. However, the number of interconnections appeared to be small. It was also assumed that a large number of one-dimensional heat flow channels existed. Note that a heat flow channel consisted of porous material. Some fraction of the total area, (1-f)F, was assumed to consist of continuous (undelaminated) flow channels and the remaining area, (1-f)(1-F), was assumed to contain delaminations (cracks, breaks, or large voids, normal to the heat flow). That these separations do exist is evident from photomicrographs of the char. Observe in Figures 3(b) and 3(d) that voids which separate porous areas are readily visible. The voids shown are perhaps 50 to 100 microns in thickness. Also observe in Figure 3(a) that

areas exist where the pores are not continuous, and delaminations several pore diameters long are apparent. Further note the visible delaminations shown in Figure 21. The view in Figure 21 was obtained by sectioning a specimen along a plane parallel to the direction of heat flow. It is obvious that the char does not consist of well defined delaminated and undelaminated heat flow channels. Further, the heat flow will tend to concentrate in the solid areas adjacent to a delamination and thus somewhat bypass the delamination. However, for purposes of this analysis, bypassing effects were neglected, and the assumption was made that well defined heat flow channels existed.

The thermal conductance network which describes the heat flow through the assumed physical model is shown in Figure 20(b). The separate conductances are outlined below:

K_R = radiant conductance through cracks parallel to the heat flow
K_G = gas conductance through cracks parallel to the heat flow
$K_{m'}$ = solid conductance through undelaminated area
$K_{r'}$ = radiant conductance through undelaminated area
$K_{g'}$ = gas conductance through undelaminated area
K_r = radiant conductance through porous area in the delaminated area
K_m = solid conductance through porous area in the delaminated area
K_g = gas conductance through porous area in the delaminated area
K_{dr} = radiant conductance across delamination
K_{dg} = gas conductance across delamination

Now that the physical model and the thermal conductance network have been defined the equations for the conductances will be explored. Each of the modes of heat transfer, radiation, solid conduction, gas conduction and convection will be discussed under separate headings.

Radiation. - There are three radiation components of concern in porous chars. The first is radiation between the walls of the pores; the second is radiation through the cracks which are parallel to the heat flow; and the third is radiation across any delaminations (separations normal to the heat flow). In his studies of porous materials (not chars), Russell[4] considered radiation across the pores and used the pore diameter as the effective radiation length. His expression has been modified slightly to account for a radiant length which may be longer than one pore diameter because of the somewhat open pore structure. The radiant conductance obtained in this

manner is based on the heat transfer between two parallel plates a finite distance apart. The equation for the radiant conductance through the porous area in a delaminated flow channel may be written

$$K_r = \frac{4\sigma A_r \epsilon T_m^3 x}{(2\rho + \epsilon)x} = \frac{A_r x}{ax} \qquad \left(\begin{array}{l}\text{Radiation through}\\ \text{delaminated flow}\\ \text{channel}\end{array}\right) \qquad (7)$$

where

$$a = \frac{2\rho + \epsilon}{4\sigma \epsilon T_m^3}$$

$$A_r = (1-f)(1-F)P^{2/3}A$$

and

σ = Stefan-Boltzmann constant
ϵ = emittance
ρ = reflectance
x = characteristic radiant length
T_m = absolute temperature
f = fraction of total cross-sectional area, normal to the heat flow, occupied by the cracks which are parallel to the heat flow.
F = fraction of heat flow channels which are undelaminated
A = total area
P = porosity

Note that the radiation term $\sigma(T_1^4 - T_2^4)$ has been written as $4\sigma T_m^3 \Delta T$. By algebraic manipulation it can be shown that these expressions are equivalent within 3 percent error if $\Delta T \leq 0.346 T_m$. This will be true for a reasonable heat flux and char thickness. Note in equation (7) that the term x/x has been introduced where x is some characteristic radiation length which is an unknown for phenolic-nylon chars in general. This term was introduced because K_r is a conductance term and in order to obtain an expression for the radiant conductivity from equation (7) a length term is needed, i.e., $k_r = K_r x/A_r$ where k_r is the radiant conductivity. Thus, an expression for the radiant conductivity would contain x in the numerator

only. If x is thought of as the spacing between parallel plates, it is obvious that the larger the number of plates (in a given length) the smaller x will be and consequently the radiant conductivity will be less.

The term $(2\rho + \epsilon)$ in equation (7) arises from the use of the gray-body shape factor for the heat transfer between the two surfaces with the shape factor being equal to one.

As it is written equation (7) applies to radiation through the porous area in a delaminated flow channel. A similar expression also applies to the radiant conductance of an undelaminated flow channel. This equation may be obtained as follows: Take the reciprocal of the thermal conductance of an element of length x, $(A_r'x/ax)$. This gives the thermal resistance, $ax/A_r'x$, of one element. Then sum all of the resistances over the total length L. In this manner the radiant thermal resistance $aL/A_r'x$ is obtained. Take the reciprocal of the thermal resistance to obtain the thermal conductance

$$K_r' = \frac{A_r'x}{aL} \qquad \left(\begin{array}{l}\text{Radiation through undelaminated} \\ \text{flow channel}\end{array}\right) \qquad (8)$$

where

A_r' = $(1-f)FP^{2/3}A$
L = thickness across which heat is being transferred.

The radiant conductance through the cracks parallel to the heat flow may be written

$$K_R = \frac{4\sigma F_{ir_2} L T_m^3 A_R}{L} \qquad \text{(Radiation through cracks)} \qquad (9)$$

where

$$A_R = fA$$

In equation (9) L represents the length of the crack and F_{ir_2} is a reradiation shape factor. Values of the shape factor may be estimated from curves developed by Jakob[9] for radiation through openings. All that is needed for

the approximation is the ratio of the minimum crack dimension to the crack length. The term L/L was introduced for use later in summing conductances.

The radiant conductance across the delaminations may be written

$$K_{dr} = \frac{4\sigma A_d \epsilon T_m^3 t}{(2\rho + \epsilon)t} = \frac{A_d t}{at} \qquad \left(\begin{array}{l}\text{Radiation across}\\ \text{delaminations}\end{array}\right) \qquad (10)$$

where

t = delamination thickness
$A_d = (1-f)(1-F)A$

Equations (7) through (10) should adequately describe the radiant heat transfer. The two major unknowns in these equations are (1) the radiant length through the porous area, and (2) the delamination thickness. Transparency of the solid was neglected. This aspect requires further study.

Solid Conduction. - Solid conduction through the char accounts for a considerable portion of the heat transfer. The matrix conductance for a delaminated flow channel may be written

$$K_m = \frac{k_m A_m}{x} \qquad \text{(Solid conduction through delaminated flow channel)} \qquad (11)$$

where

k_m = thermal conductivity of the matrix

$A_m = (1-f)(1-F)(1-P^{2/3})A$

In equation (11) the solid conduction length, x, is taken to be equal to the radiant length. This is of no consequence since any length can be used as long as the summing of lengths is properly performed. The determination of the effective cross-sectional area is most important. Some authors have

used (1-P)A as the effective cross-sectional area for isometric pores, where P is the volume pore fraction[6]. Russell[4] and Ribaud (presented in Reference 6) used $(1-P^{2/3})A$ as the effective conduction cross section. The latter expression appears to best describe the effective cross-sectional area. This relation needs experimental verification for these highly porous chars as it has some bearing on reducing the matrix conductivity from experimental measurements of the "apparent" thermal conductivity.

For an undelaminated flow channel the equation for the solid conductance is

$$K_m' = \frac{k_m A_m'}{L} \qquad \left(\begin{array}{l}\text{Solid conduction through}\\ \text{undelaminated flow channel}\end{array}\right) \qquad (12)$$

where

$A_m' = (1-f)F(1-P^{2/3})A$

L = total thickness across which heat is being transferred

Gas Conduction. - There are three gas conduction components in the chars: (1) gas conduction through the porous areas, (2) gas conduction through the cracks parallel to the direction of heat flow, and (3) gas conduction across any delaminations. These conductances may be written as follows:

$$K_g = \frac{k_g A_g}{x} \qquad \left(\begin{array}{l}\text{Gas conduction through}\\ \text{delaminated flow channel}\end{array}\right) \qquad (13)$$

$$K_g' = \frac{k_g A_g'}{L} \qquad \left(\begin{array}{l}\text{Gas conduction through}\\ \text{undelaminated flow channel}\end{array}\right) \qquad (14)$$

$$K_G = \frac{k_g A_R}{L} \qquad \left(\begin{array}{l}\text{Gas conduction through}\\ \text{cracks}\end{array}\right) \qquad (15)$$

$$K_{dg} = \frac{k_g A_d}{t} \qquad \left(\begin{array}{l}\text{Gas conduction across}\\ \text{delamination}\end{array}\right) \qquad (16)$$

where

k_g = thermal conductivity of the gas
A_g = $(1-f)(1-F)P^{2/3}A$
$A_{g'}$ = $(1-f)FP^{2/3}A$
A_R = fA
A_d = $(1-f)(1-F)A$
x = characteristic radiant length
L = total thickness across which heat is being transferred
t = delamination thickness

Convection. - At the outset of the analysis it appeared that gas convection could be neglected because of the minuscule pore sizes. Further, the orientation of the specimen with the heat flowing from top to bottom ruled out convection as stratification occurred. A review of some of the literature essentially confirmed that gas convection was insignificant in small samples having other orientations. Kreith[10] presents the results of DeGraaf and Von der Held and Mull and Reiher for studies of the free convection heat transfer in enclosed air spaces. Based on their results for horizontal layers, heated from below, free convection does not begin until the Grashof number (based on the separation of the heat transfer surfaces) exceeds 1600. The Grashof numbers for the porous char were calculated to be 246 and 0.437 for nitrogen and helium, respectively, based on the total gage length of the char as the characteristic length. Since the Grashof number is based on L cubed, where L represents the separation of the surfaces, the use of total specimen gage lengths would represent the worst case. The calculations were performed for a temperature of 400°F and a temperature difference of 100°F (the upper limit ascertained from the measurements). The highest Grashof number, calculated for nitrogen, is far below the critical Grashof number for the onset of free convection in air. Grashof numbers for helium are much lower than for air. Assuming that the critical Grashof number for helium is probably not much different from the value for air (1600), it is logical to conclude that free convection is also negligible in helium.

Russell[4] said that it appeared that for low temperatures and small pores the conductivity of the pores is that of air alone. Vershoor and Greebler[11] deduced from experimental measurements on glass wool with fiber diameters of 2.58 microns that the free convection of air contributed only 0.145×10^{-5} Btu/sec-ft-°F and 0.049×10^{-5} Btu/sec-ft-°F to total conductivities of 0.915×10^{-5} Btu/sec-ft-°F and 0.570×10^{-5} Btu/sec-ft-°F

for bulk densities of 0.546 and 4.63 lb/ft^3, respectively. Their measurements were made at a mean temperature of 150°F and with a temperature difference of about 120°F. For the least dense material the contribution by free convection was a maximum of 16 percent of the total conductivity of the glass wool which has a very low conductivity. Note that the absolute values of free convection may be neglected with reference to the experimental measurements made in this program since they were less than one percent of the apparent thermal conductivity of the char in nitrogen. Further the fibrous materials on which their measurements were made were more porous than the chars which means that the contribution by free convection would be less in the chars. Thus, these data provide another indication that free convection may be neglected.

It is a well known fact that heat transfer by free convection is dependent on the temperature difference. On some of the specimens data were obtained near 500°F with different temperature differences across the specimens. These measurements did not reveal a consistent dependence on temperature difference. For example, on Specimen 42-3 thermal conductivities at 500°F in nitrogen of 19.6 and 17.5×10^{-5} Btu/sec-ft-°F were measured for temperature differences of 38°F and 72°F, respectively. The thermal conductivity of Specimen 30-4 at 500°F in nitrogen was 17.0×10^{-5} Btu/sec-ft-°F for a temperature difference of 46°F, while the corresponding value for Specimen 30-6 was 18.2×10^{-5} Btu/sec-ft-°F for a temperature difference of 91°F. Specimen 42-4 exhibited a lower thermal conductivity in helium than Specimen 42-5 with the temperature differences being 84°F and 39°F, respectively. All of these differences appeared to be within the data scatter. Therefore, while it may be worthwhile to pursue free convection effects further, it certainly appears that these effects were negligible for the specimen size and orientation to the heat flow used in this program.

Equation for Apparent Thermal Conductivity of Char

The conductances which are shown in Figure 20 and presented in equations (7) through (16) were combined to obtain an expression for the overall conductance, K, of the char. These conductances were combined through the use of the laws of series and parallel electrical conductances. In combining the conductances use was made of the fact that the total thickness of the delaminations in a delaminated flow channel is nt, where n is the total number of delaminations and t is the average thickness of one delamination. Therefore, the length of the porous area in a delaminated

flow channel is (L-nt). The expression for the overall conductance was reduced to an expression for the apparent thermal conductivity of the char through the relation

$$Q = K\Delta T = \frac{k_a A \Delta T}{L} \tag{17}$$

where

K = overall conductance
k_a = apparent thermal conductivity
A = total area
L = total length
ΔT = temperature difference

The expression obtained for the apparent thermal conductivity of the char was

$$k_a = \frac{(1-f)(1-F)(t/a + k_g)\left[\frac{x P^{2/3}}{a} + P^{2/3} k_g + (1 - P^{2/3})k_m\right]}{(1 - c)\left(\frac{t}{a} + k_g\right) + c\left[\frac{x P^{2/3}}{a} + P^{2/3} k_g + (1 - P^{2/3})k_m\right]}$$

$$+ 4 f \sigma F_{ir2} T_m^3 L + f k_g + (1-f) F \left[P^{2/3} k_g\right.$$

$$\left. + (1-P^{2/3}) k_m + \frac{x P^{2/3}}{a}\right] \tag{18}$$

where

$$c = \frac{nt}{L}$$

The details of the derivation of equation (18) are presented in Appendix B. The unknowns in equation (18) are F, x, t, c, and k_m.

Remember that equation (18) is valid only for char thicknesses, L, such that $\Delta T = 0.346\ T_m$. This restriction may be circumvented when such is not the case by segmenting the total thermal model.

Thermal Conductivity of Gases

The apparent thermal conductivity of gases at low densities (free-molecule conduction) depends upon the separation of the surfaces between which heat is being transferred and the gas pressure (density). This results from the fact that the mean free path of the gas at low pressures is of the order of the separation distance. In a continuum gas the mean free path is much shorter than the separation distance, and the gas conductivity is essentially independent of the geometry and pressure. Kennard[12] gives the following equation for the heat transfer per unit area per unit time between flat plates for gases at low densities:

$$H = \left(\frac{a_1 a_2}{a_1 + a_2 - a_1 a_2}\right) \frac{1}{2}(r + 1) \frac{c_v p}{(2\pi RT)^{1/2}} \tag{19}$$

where

H	=	heat transferred per unit area per unit time
a_1, a_2	=	accommodation coefficients for surfaces 1 and 2, respectively
r	=	ratio of specific heat at constant pressure to the specific heat at constant volume
c_v	=	specific heat at constant volume
R	=	gas constant
p	=	pressure
T	=	absolute temperature

Equation (19) yields the following equation for the thermal conductivity of helium at 500°F

$$k_g = 1026 \times 10^{-5}\, p\Delta x \tag{20}$$

where

k_g = thermal conductivity of gas in Btu/sec-ft-°F
p = pressure in torr
Δx = separation of heat transfer surfaces in feet

At 0.010 torr and for a separation of 0.000164 ft (50 microns; approximate pore diameter), the value for the thermal conductivity of helium calculated from equation (20) was 0.00167×10^{-5} Btu/sec-ft-°F. Based on this value the gas conductivity can be considered negligible at vacuum since the continuum value for helium is 3.5×10^{-5} Btu/sec-ft-°F. Note that if a pressure of 760 torr is inserted into equation (20) the calculated value for the same separation is 126×10^{-5} Btu/sec-ft-°F, which is too high and indicates that a continuum exists and the equation does not apply.

Continuum values were used for the thermal conductivities of nitrogen and helium at 760 torr. These curves of the thermal conductivity versus temperature for nitrogen and helium are presented in Figure 22.

Correlation of Thermal Model with Measurements

The first step taken in order to apply equation (18) to the experimental data was to estimate the radiation terms, $xP^{2/3}/a$, t/a, and $4f\sigma F_{ir_2} T_m^3 L$. For a radiant length, x, of 508 microns (approximately 10 pore diameters), a reflectance, ρ, of 0.2, an emittance, ϵ, of 0.8, and a reradiation shape factor, F_{ir_2}, of 0.10 (estimated from approximate measurements of the crack size), the radiation terms were negligible at 500°F. Since the radiation terms were small, the value of t had little influence on the results; therefore, this term was ignored in the low temperature calculations. Only the total delamination thickness, nt, was considered in accounting for gas conduction across the delaminations. Therefore, at the 500°F mean temperature, only three unknowns remain, namely, c, F, and k_m. The fraction of the total area which was occupied by the cracks, f, was estimated to be 0.1.

The experimental data at 500°F were used with equation (18) to determine the values of c, F, and k_m for each specimen. Experimental data were obtained for three different environmental conditions (vacuum,

nitrogen and helium). Thus, the measurements represent the apparent thermal conductivities for three values of k_g (thermal conductivity of gas). One equation in c, F, and k_m was written from equation (18) for each environmental condition. In writing these equations the radiation terms were assumed to be zero since calculations had shown that the values of these terms were negligible at 500°F. Also, the proper values for the char thickness, temperature and porosity, for a given specimen, were substituted into equation (18) along with the values of k_a and k_g for a given environmental condition. Hence, three simultaneous equations were obtained and these equations were solved for c, F and k_m. Only one set of values for c, F and k_m were obtained for each specimen at the given temperature level since there were three experimental conditions and three equations were required for a solution.

The results of these calculations are shown in Table 14. Also shown in Table 14 are the data used in this analysis and the char porosities. The parameter c represents the ratio of the delamination length to the total length; note that the values ranged from 0.6 percent to 7.1 percent of the total length with a mean value of approximately 3 percent. This appears to be a reasonable value and does not represent an excessive amount of cracking. The factor which represented the fraction of the flow channels which were undelaminated, F, ranged from 0.48 to 0.72, which again indicates a reasonable range of values. There was considerable scatter in the matrix conductivity from 127×10^{-5} Btu/sec-ft-°F to 248×10^{-5} Btu/sec-ft-°F. These values are higher than the range of values, 69 to 115×10^{-5} Btu/sec-ft-°F, which is generally accepted for carbon. The data reductions suggest that those specimens having the lowest densities, Specimens 19-4 and 19-5, had the highest matrix conductivity. Note in Table 14 that the matrix conductivity was also reduced using P rather than $P^{2/3}$ in equation (18) and yielded lower values which were still higher than the values normally used for carbon.

Since the range of porosities was small and there was considerable scatter in the parameters, it is hard to evaluate the model for its applicability. The fact that c, F, and k_m varied from specimen to specimen prohibited using one set of values to attempt a correlation of all of the data.

The values reduced from the measurements are reasonable, and there is a possibility that the thermal conductivity of the matrix is higher than the value for carbon because of graphitization. The variation in thermal conductivity through the thickness measured on Specimen 42-3 indicates that

the conductivity increases with charring temperature. That is, the end of the char which was exposed to the hot gases reached the highest temperature level and also had the highest thermal conductivity. Graphitization undoubtedly caused this effect and the degree of graphitization may be a function of time as well as temperature.

One additional check on the model is to see how the predicted variation in the "apparent" thermal conductivity with temperature agrees with the data. The apparent conductivity was calculated using the reduced values of c, F, and k_m, given in Table 14, from 250°F to 1000°F for each specimen. The results of these calculations are given in Figures 23, 24, and 25. Note that the values predicted at the higher temperatures usually agreed with the measured values within the experimental uncertainty with the exception of the vacuum data at the higher temperatures for Specimens 19-4 and 42-3, Figures 23 and 25, respectively. The data for Specimen 19-4 indicate that the value at 500°F in vacuum may be low and that the theoretical curve should be shifted up. The data for Specimen 42-3 at 500°F in vacuum appear erroneous. There is no reasonable explanation for this large increase of thermal conductivity with temperature.

Correlation of Thermal Model with Prior High Temperature Data

Equation (18) contains all of the mechanisms of heat transfer which are essential to the apparent thermal conductivity of the char except for the possibility that the carbon structure might be transparent to thermal radiation at higher temperatures. The thermal conductivity at higher temperatures was computed using equation (18) in order to compare the results with prior high temperature data. The parameters used in the calculations were those given in Table 14 for Specimen 19-4 since the data for this specimen agreed with the prior data at 1000°F. Nitrogen was assumed to be the environmental gas. The average crack thickness was assumed to be 2.5 microns which, for the value of c used, represents 52 delaminations. The calculations were performed for matrix conductivities of 231×10^{-5}, 462×10^{-5} and 693×10^{-5} Btu/sec-ft-°F. The effective radiant length, x, was taken to be 50 microns for one case and 500 microns (about 8 average pore diameters) for the other. The results are presented in Figure 26. The curves for a radiant length of 50 microns are shown as solid lines, and the curves for 500 microns radiant length are shown as the dotted lines. Prior data reported in References 1 and 2 are shown on the

figure for comparison. Note that the measured values at the higher temperatures exceed the predicted values for a matrix conductivity of 231×10^{-5} Btu/sec-ft-°F, even assuming that the effective radiant length is 8 pore diameters. Similar results are presented in Figure 27 for an average crack thickness of 50 microns, which represents only 2 or 3 delaminations (all other parameters used were the same). Notice that the change in the delamination thickness shifted the curves up only slightly.

The first high temperature calculations were based on nitrogen. There is a strong possibility that helium permeates into the pores, which initially contained air, after one or two hours of exposure time in the radial inflow apparatus. Therefore, a family of high temperature curves were generated assuming that helium was in the pores. The results of these calculations are shown in Figure 28. The calculations were performed using the same parameters as were used in developing the other two sets of high temperature curves (See Figures 26 and 27). Notice that the curves were shifted up from the nitrogen predictions and that the slopes were slightly greater. Note that for a matrix conductivity of 231×10^{-5} Btu/sec-ft-°F and a radiant length of 8 pore diameters, 500 microns, the calculated values were only 15 percent lower than the measured value at 5000°F.

The high temperature calculations indicate that the thermal conductivity of porous chars can be explained only by (1) additional graphitization resulting from time exposure at temperature which raises the matrix thermal conductivity; or (2) a radiant length which is several pore diameters; or (3) transparency of the carbon structure to thermal radiation. There is also an indication that the environmental conditions for the high temperature data in the radial inflow apparatus may have changed during the experiment. Helium may have been the predominant gas at high temperatures, whereas nitrogen and the reaction products, CO and CO_2, may have been present at the lower temperatures. This would have given the experimental data a greater slope.

If graphitization is disdained as the cause of the sharp increase in thermal conductivity at high temperatures, then one has to accept the hypothesis that helium replaced nitrogen in the structure and that the radiant length is perhaps 10 average pore diameters or the material is transparent to thermal radiation. It is hard to imagine that the radiant length could be 10 pore diameters long (and still have a geometric shape factor of one). However, transparency of the matrix material to thermal radiation is conceivable at the higher temperatures. Little can be said of transparency effects without some experimentation.

There are two arguments which suggest additional graphitization with time at temperature exposure and subsequently higher matrix thermal conductivity values. The first is our measurements on Specimen 42-3 which indicated that the side of the specimen which was exposed to the highest temperature for the longest period of time had a considerably higher thermal conductivity. The second agrument pertains to some experimental data taken by Neubert, Royal and Van Dyken, which is presented in Reference 13. The material for their experiments consisted of Whiting coke and Barrett No. 30 pitch extruded in long bars and then reimpregnated with pitch. Room temperature measurements were made on heat treated specimens from this material in an axial heat flow apparatus. Separate samples were heated to 3812°F, 4352°F, and 5432°F. The hold times were not specified. The room temperature thermal conductivities of these samples were 485×10^{-5}, 1250×10^{-5}, and 2330×10^{-5} Btu/sec-ft-°F for the heating temperatures of 3812°F, 4352°F, and 5432°F, respectively. Further, they stated that the lowest conductivity specimen was typical of a product for which the graphitization had barely begun. This statement means little quantitatively, and the applicability of these data to phenolic-nylon chars is questionable. However, these results correlate somewhat with the results of the thermal analysis and indicate that "barely begun" graphitization can give high matrix conductivities. If barely begun graphitization means only a slight change in X-ray diffraction patterns from the carbon structure, the results of Neubert, Royal, and Van Dyken may indicate that significant changes in the thermal conductivity can result from seemingly insignificant changes in the lattice parameters.

In summary, it appears that an analysis of the prior thermal conductivity evaluations at high temperatures using the radial inflow apparatus is confounded by an increasing matrix thermal conductivity which results from temperature-time graphitization effects. The matrix conductivity of "in-flight" char may lie below the values reduced from the low temperature measurements on chars exposed for 120 to 150 seconds. Exactly where in-flight values would fall depends on the effects of time at temperature. An in-flight char would most likely not have as high a thermal conductivity as measured in the steady-state apparatus unless graphitization takes place very rapidly once a given temperature level is reached. The measurements on the upper portion of Specimen 42-3 indicate that this effect may be rapid, occurring over a 120 second time interval. A knowledge of the effect of time at temperature is vital to predictions of the in-flight char thermal conductivity. If the time required for graphitization to occur is extremely small, then the thermal conductivity of the char is essentially dependent on the temperature alone. In this event, the thermal conductivity measured in the steady-state apparatus represents the thermal conductivity

of the in-flight char. However, this significant increase in thermal conductivity with temperature would be explained by additional graphitization rather than a large amount of thermal radiation. Later, some possible means of resolving these uncertainties will be presented.

CONCLUSIONS

At low temperatures (100 - 1000°F), the apparent thermal conductivity of phenolic-nylon chars primarily consists of the contributions of solid conduction and gas conduction. At 1000°F the radiation contribution is a minimum of 0.066×10^{-5} Btu/sec-ft-°F (radiant length of one pore diameter) and a maximum (ignoring transparency effects) of 0.66×10^{-5} Btu/sec-ft-°F (radiant length of 8 pore diameters). The higher value represents a maximum contribution to the total conductivity of 6.6 percent (based on the lowest vacuum data and the longest radiant length).

The contributions by the matrix and by the gas are inseparable in that the gas thermally "shorts" the delaminations and increases the effective area for matrix conduction. If this effect is called a contribution by the gas, then the gas can contribute more than twice its own conductivity to the apparent thermal conductivity of the char. It appears that equation (18) adequately describes the effects of the gas conductivity.

The most likely range of values for the thermal conductivity of the matrix (for plasma torch charring conditions) is 155×10^{-5} to 250×10^{-5} Btu/sec-ft-°F for the range of densities investigated. The data suggest that the more dense the virgin material the lower the matrix conductivity for a given exposure time, probably because the denser material reaches lower internal temperatures during the exposure since it has more heat storage capability.

Equation (18) probably will provide a reasonable correlation with the high temperature thermal conductivity data once the matrix conductivity, radiant length, and transparency effects are defined. The heat transfer aspects, the effects of exposure time at temperature, and the radiant transmission characteristics should be further explored in order to refine the analysis.

The apparent thermal conductivity of phenolic-nylon chars varies with porosity. The exact dependence on porosity has not been established because of the small range of porosities investigated and a confounding of the results by apparent differences in the matrix thermal conductivity.

If the value of the matrix conductivity is known accurately, it is possible to use equation (18) with $c = 0$ to predict the apparent thermal conductivity of the char in different gas media (not in vacuum) within about 15 percent uncertainty. Equation (18) gives results similar to Russell's equation when $c = 0$. The utility of this approach is that one would not have to establish statistical values for c and F in order to apply the equation to chars in general. However, if the vacuum values are of concern, one must make enough experiments to statistically establish c and F for a wide range of char conditions.

Southern Research Institute
Birmingham, Alabama
August 7, 1967

APPENDIX A

A COMPARATIVE ROD APPARATUS FOR MEASURING THERMAL CONDUCTIVITY TO 2000°F

Southern Research Institute's comparative rod apparatus is used to measure thermal conductivities of a wide variety of materials from -300°F to 2000°F. This apparatus, shown schematically in Figure A1, consists basically of two cylindrical reference pieces of known thermal conductivity stacked in series with the cylindrical specimen. Heat is introduced to one end of the rod, composed of the references and specimen, by a small electrical heater. A cold sink or heater is employed at the opposite end of the rod as required to maintain the temperature drop through the specimen at the preferred level. Cylinders of zirconia may be inserted in the rod assembly to assist in controlling the temperature drop. Radial losses are minimized by means of radial guard heaters surrounding the rod and consisting of three separate coils of 26-gage Kanthal wire wound on a 2-inch diameter alumina core. The annulus between the rod and the guard heaters is filled with diatomaceous earth. Surrounding the guard is an annulus of diatomaceous earth enclosed in an aluminum shell.

The specimens and references (see Figure A2) are 1-inch diameter by 1-inch long. Thermocouples located $\frac{3}{4}$ inch apart in radially drilled holes measure the axial temperature gradients. Thermocouples located at matching points in each guard heater are used to monitor guard temperatures, which are adjusted to match those at corresponding locations in the test section.

In operation, the apparatus is turned on and allowed to reach steady state. The guard and rod heaters are adjusted to minimize radial temperature gradients between the rod and guard sections consistent with maintaining equivalent functions of thermal conductivity times temperature difference in the references. Temperatures are measured on a Leeds and Northrup Type K-3 potentiometer, and the temperature gradients are calculated. A typical temperature profile in the test section is shown in Figure A3.

The thermal conductivity of the specimen is calculated from the relation

$$k_S = \left(\frac{k_1 \Delta T_1}{\Delta x_1} + \frac{k_2 \Delta T_2}{\Delta x_2} \right) \quad \frac{\Delta x_S}{2 \Delta T_S}$$

where k_1 and k_2 are the thermal conductivities of the upper and lower references; ΔT_1, ΔT_2, and ΔT_S are the temperature gradients in the upper and lower references and specimen, respectively; Δx_S, Δx_1, and Δx_2 are the distances between thermocouples in the specimen, lower reference and upper reference, respectively.

Note that for purely axial heat flow, the products $k_1 \Delta T_1$ and $k_2 \Delta T_2$ should be equal. Due to imperfectly matched guarding and other factors, this condition is seldom attained in practice; therefore, the average of the two values is used in the calculations. Their difference is maintained as small as possible, usually less than 5 percent of the smaller value.

The gage lengths are determined as follows: the depth of the hole is measured by inserting a snugly fitting drill rod in the hole, measuring the projecting length and subtracting it from the total length of the rod. The slope, or angle the hole makes with the perpendicular to the specimen axis, is determined by inserting a drill rod into the hole and measuring the slope of the drill rod with respect to the flat surface of the specimen. The location of the bottom of the holes with respect to the surface of the specimen can then be determined from the measurements of the depth and slope.

For reference materials, Armco iron or copper is used with high conductivity specimens, 316 stainless steel with specimens of intermediate conductivities, and Teflon, Pyroceram 9606, or Pyrex with low conductivity specimens. Extensive calibration of the apparatus, using these reference materials as standards, has yielded accuracies to about 5 percent error, when sufficient care is exercised to maintain closely matched temperatures between the guard and test sections. Even with careless matching, the error is only about 10 percent so the system is not particularly sensitive to minor unbalances.

To establish the accuracy of the apparatus some initial runs were made on 316 stainless steel, using Armco iron as the reference. The data, shown in Figure A4, are somewhat higher than those reported by Lucks, and Deem[14], but agree well with the values reported by several steel manufacturers. Note that the data scatter is less than 5 percent. The data on stainless steel were confirmed by evaluating Armco iron, using 316 stainless steel as reference. These data are shown in Figure A5 in comparison with values reported by Powell[15], who compiled his curve from the data of numerous investigators,

and estimated its accuracy to be within $\pm$ 2 percent over the range from 0° to 1000°C. The comparative rod data for Armco iron, which were computed using the solid curve of Figure A4 for the thermal conductivity of the stainless steel reference, agree with Powell's data within 5 percent, thus comfirming the data obtained for stainless steel.

Some additional data obtained on the comparative rod apparatus are shown in Figures A6 and A7. Figure A6 shows thermal conductivity data for ATJ graphite, with grain, using Armco iron as the reference material. These data show excellent agreement with earlier data obtained here and with those from other sources[16-18]. The maximum scatter of the comparative rod points was about 5 percent.

Figure A7 shows data for thermocouple grade constantan obtained on the comparative rod apparatus using Armco iron references, and on Southern Research Institute's high temperature radial inflow apparatus. Note the excellent agreement. These data also show close agreement with data obtained by Silverman[14] on an alloy of similar composition.

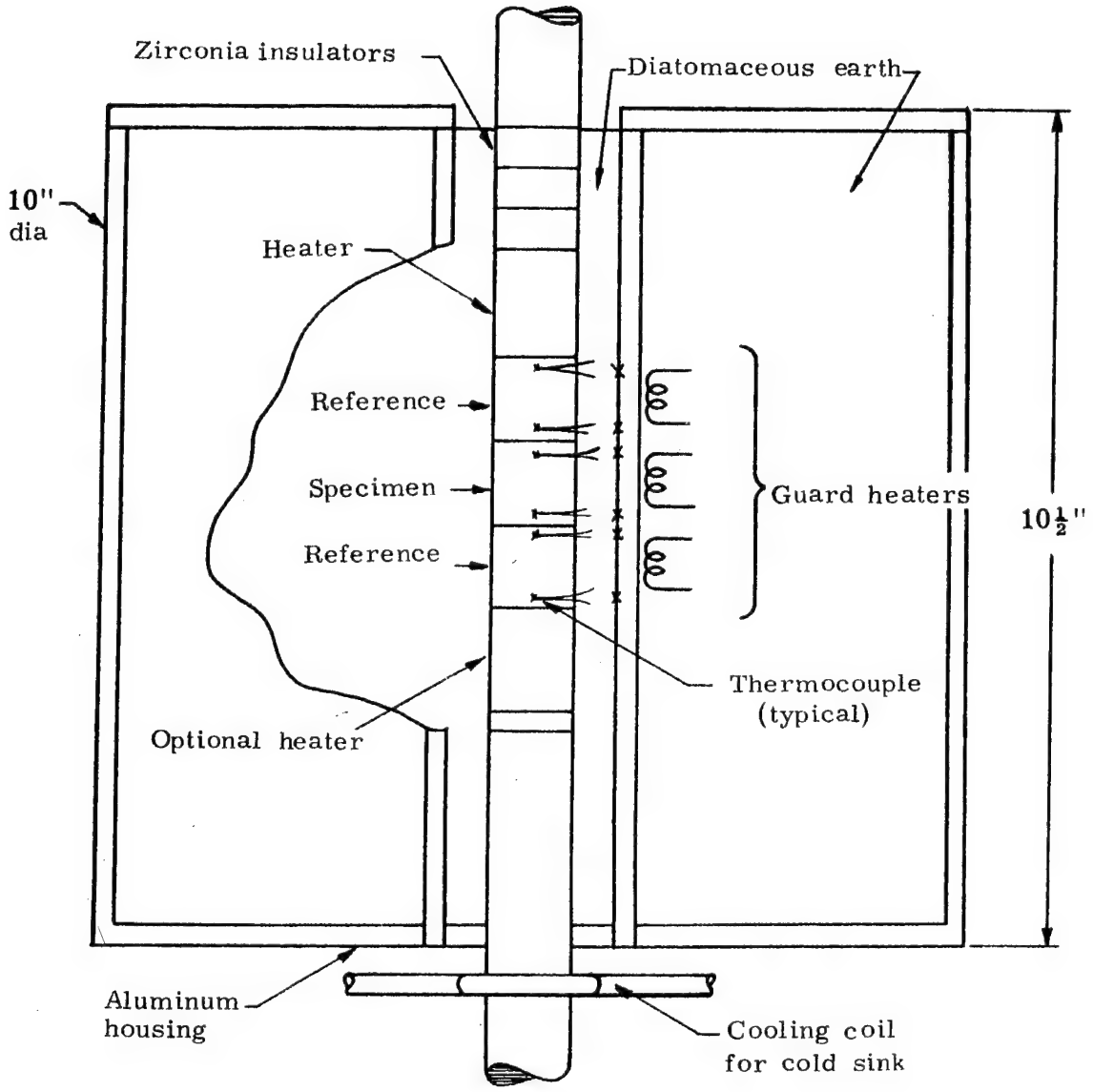

Figure A1. Schematic of comparative rod thermal conductivity apparatus

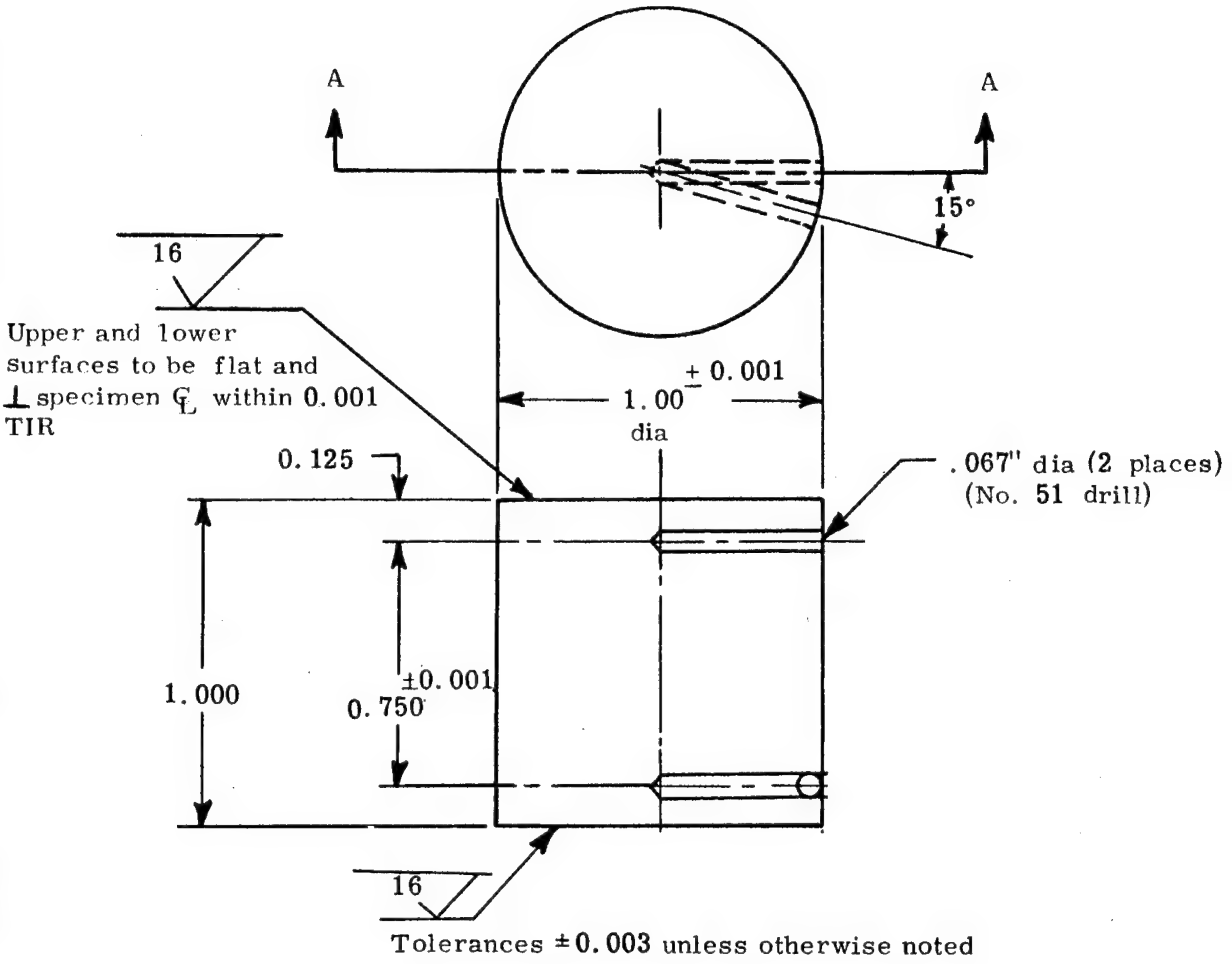

Note: The gage length between holes was less than that shown because the thickness of the char was less than one inch.

Figure A2. Specimen configuration for comparative rod thermal conductivity apparatus

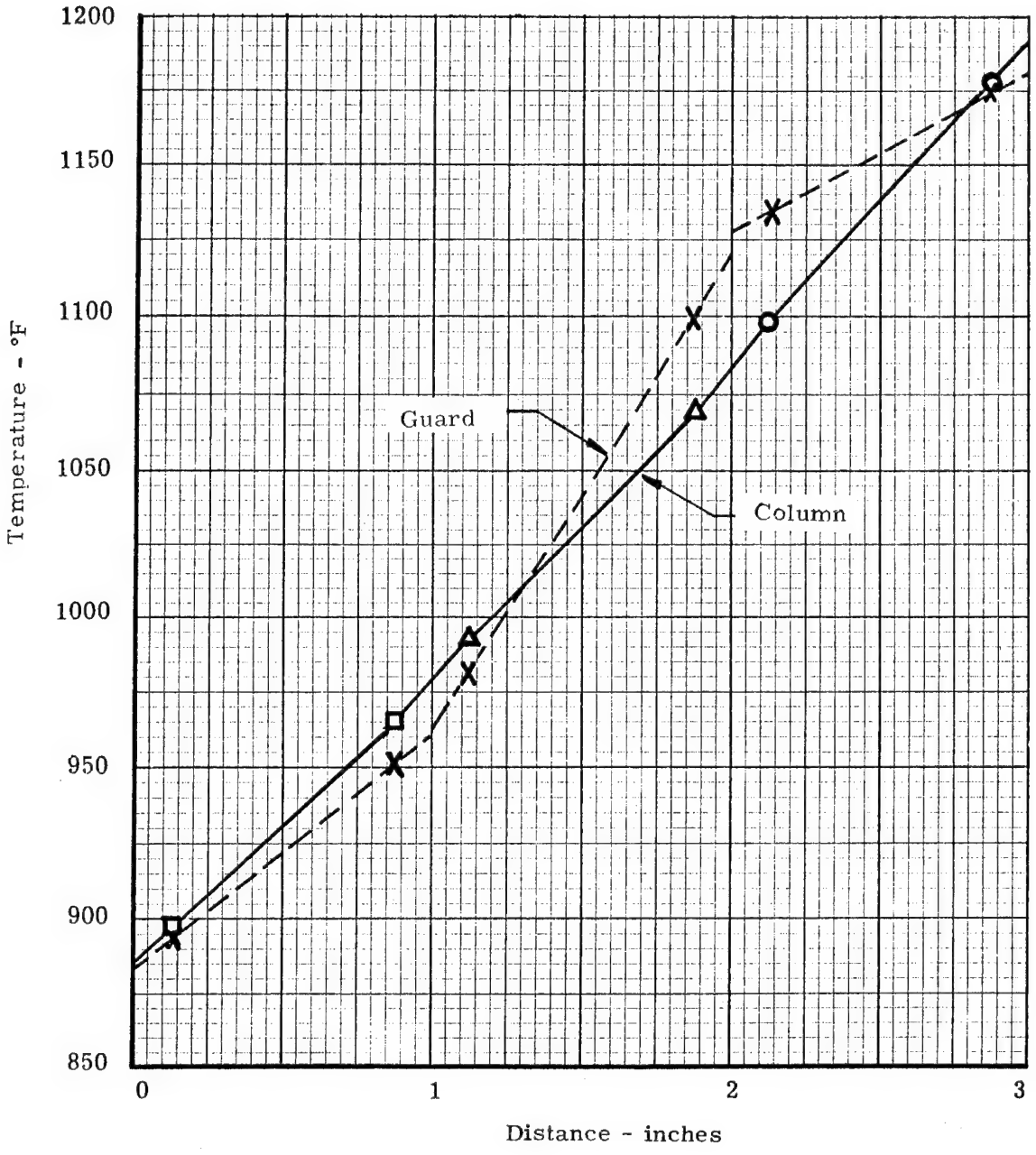

Figure A3. Typical temperature profile in test section

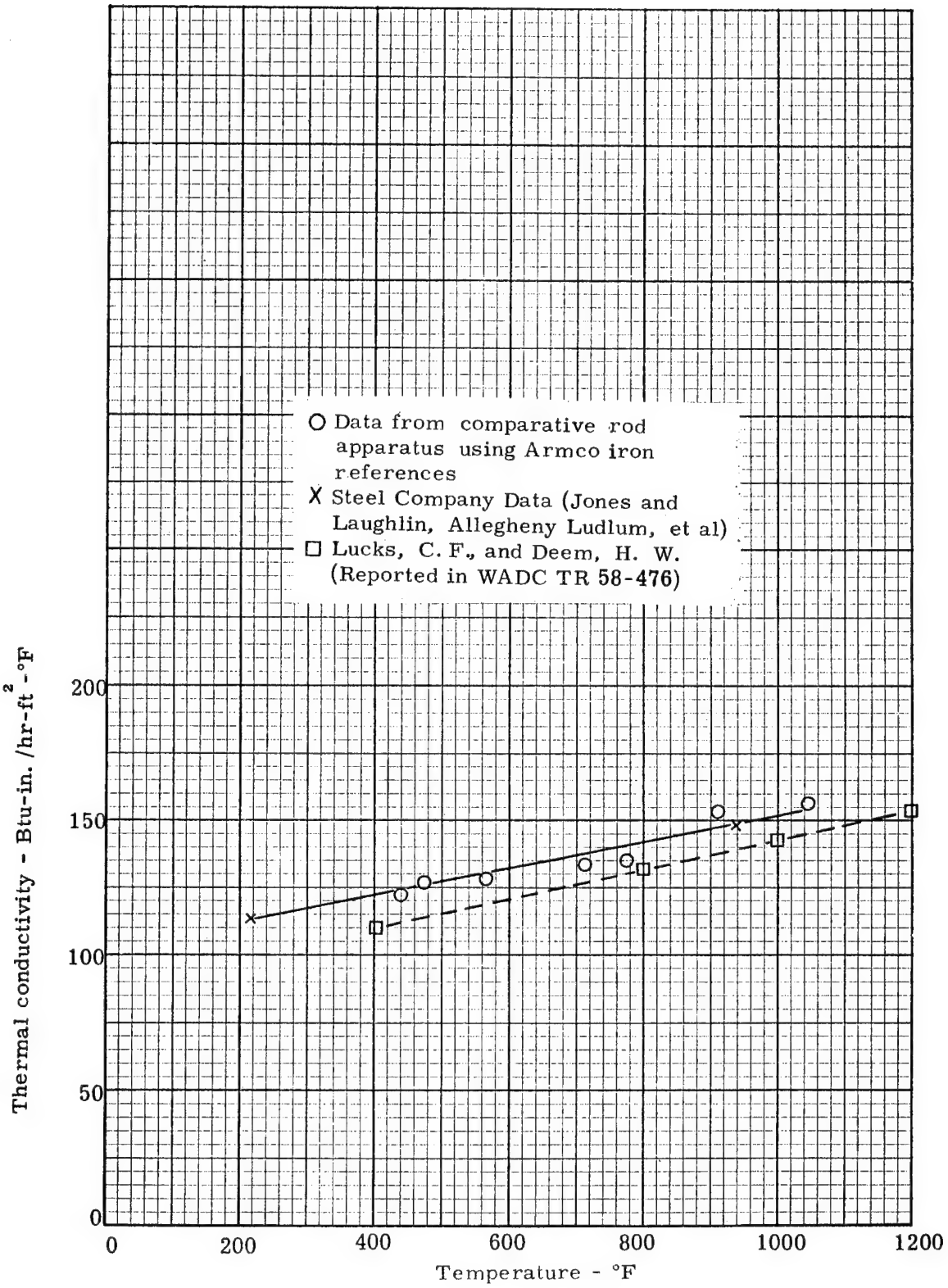

Figure A4. The thermal conductivity of Type 316 stainless steel

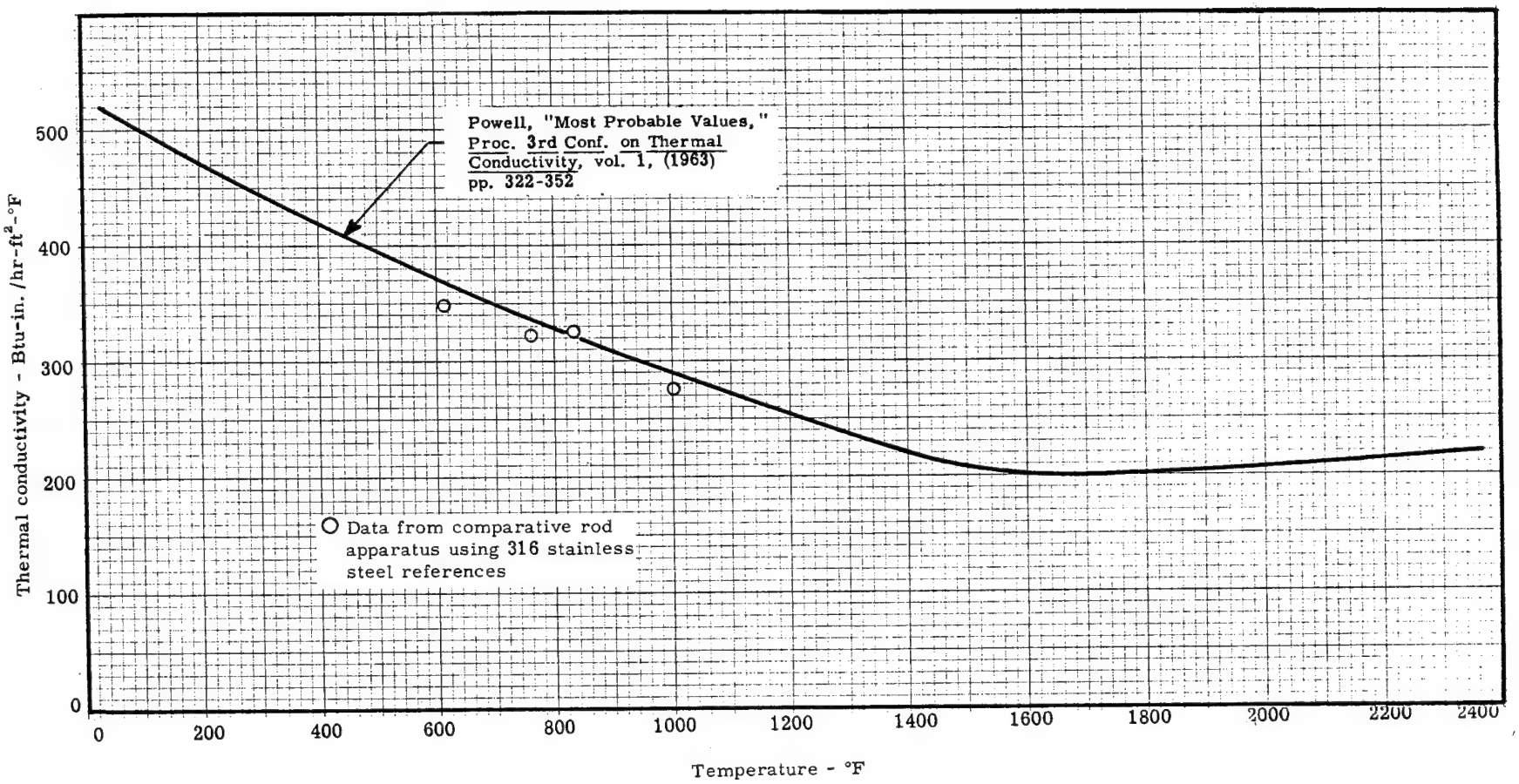

Figure A5. The thermal conductivity of Armco iron

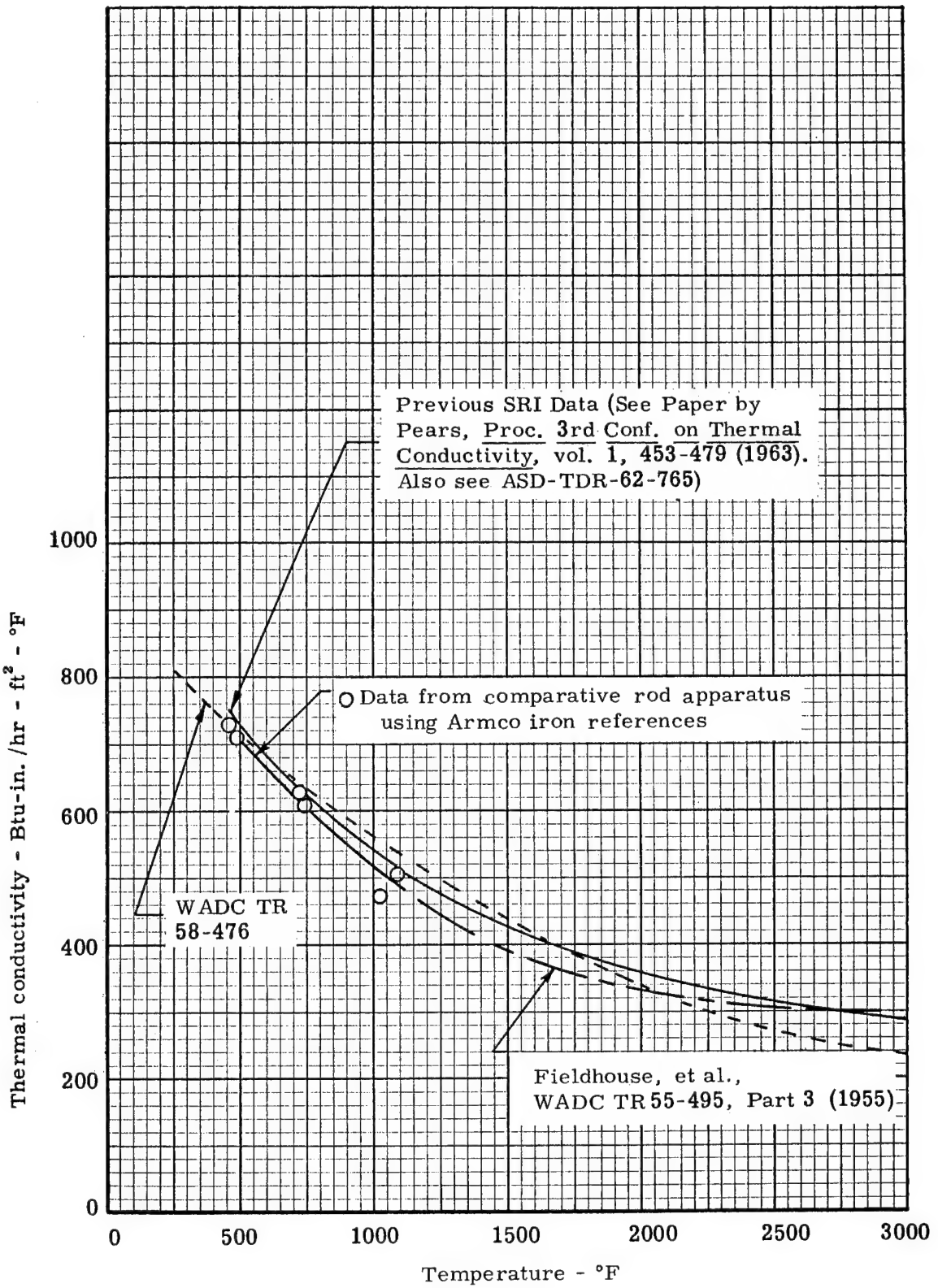

Figure A6. Thermal conductivity of ATJ graphite, with grain

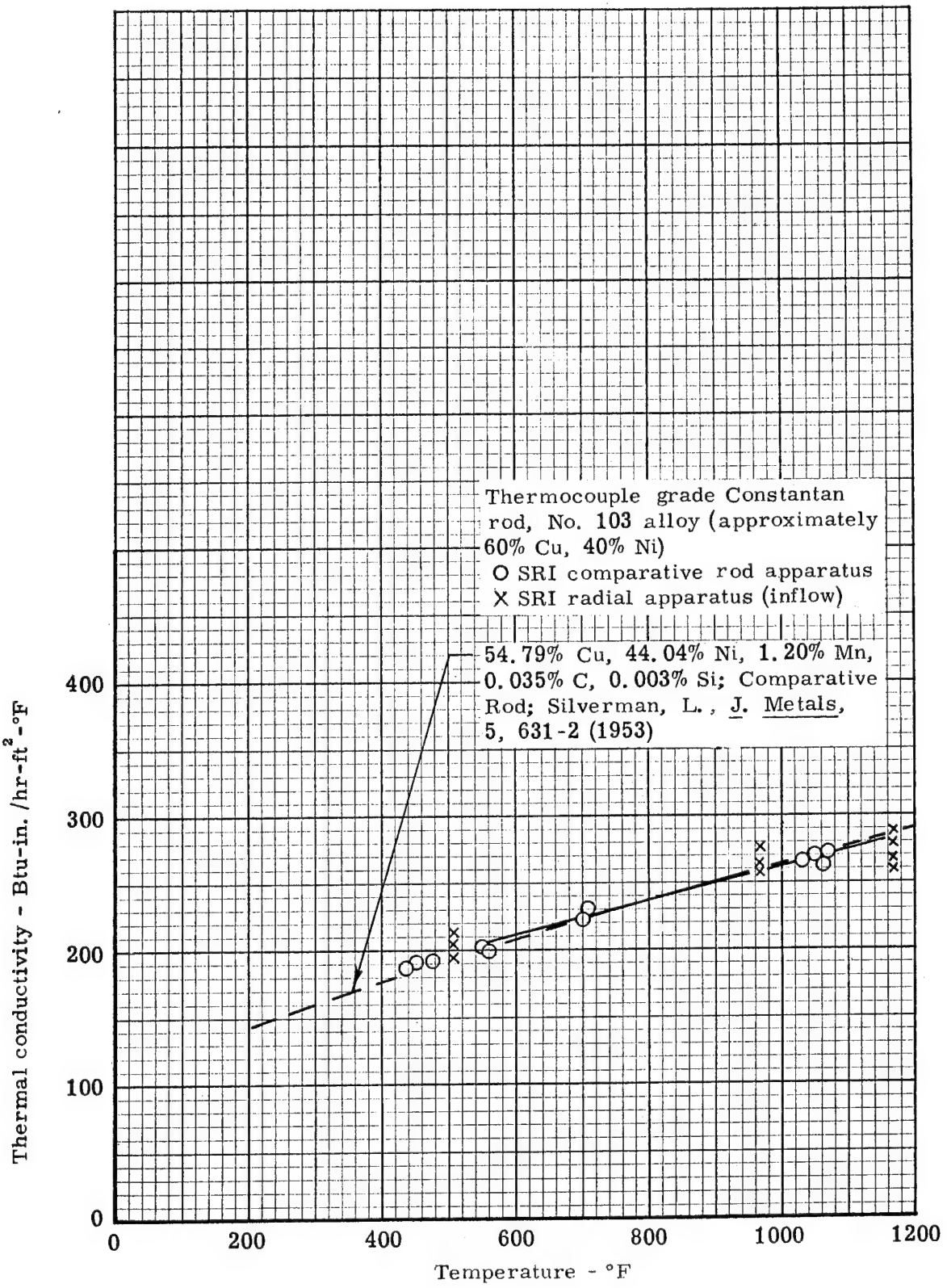

Figure A7. The thermal conductivity of thermocouple grade Constantan rod

APPENDIX B

DETAILS OF DERIVATION OF EQUATION (18) FOR THE APPARENT THERMAL CONDUCTIVITY OF THE CHAR

The thermal conductance network is shown in Figure 20. The thermal conductances shown in that figure are defined in equations (7) through (16). The derivation of equation (18) is presented below.

The first step was to combine the parallel conductances K_{dr} and K_{dg}. Conductances in parallel are combined by addition. Thus one may write

$$K_t = K_{dr} + K_{dg} \tag{B1}$$

Equations (10) and (16) were substituted into equation (B1) and the following expression was obtained for K_t

$$K_t = (1-f)(1-F)A \left[\frac{t}{at} + \frac{k_g}{t}\right] \tag{B2}$$

The conductances K_r, K_m, and K_g shown in Figure 20 were then combined using the relation

$$K_x = K_r + K_m + K_g \tag{B3}$$

The expressions for K_r, K_m, and K_g given in equations (7), (11) and (13), respectively, were substituted into equation (B3) and the following equation was obtained for K_x

$$K_x = \frac{(1-f)(1-F)\,A}{x} \left[\frac{P^{2/3}\,x}{a} + (1 - P^{2/3})\,k_m + P^{2/3}\,k_g\right] \tag{B4}$$

The thermal conductances given by equations (B2) and (B4) were inverted to give the following thermal resistances

$$R_t = \frac{1}{K_t} = \frac{t}{(1-f)(1-F)\,A\left[\frac{t}{a} + k_g\right]} \tag{B5}$$

$$R_x = \frac{1}{K_x} = \frac{x}{(1-f)(1-F)\,A\left[\frac{P^{2/3}x}{a} + (1-P^{2/3})k_m + P^{2/3}k_g\right]} \tag{B6}$$

Equation (B5) is an expression for the thermal resistance of one delamination. If there are on the average n delaminations per delaminated flow channel, the total thermal resistance of the delaminations is

$$R_d = \Sigma R_t = \frac{nt}{(1-f)(1-F)\,A\left[\frac{t}{a} + k_g\right]} \tag{B7}$$

Equation (B6) is an expression for the thermal resistance of an element of porous area of the length x. If all of these elements are summed, the total length is (L - nt). Thus it may be written that

$$R_p = \Sigma R_x = \frac{(L - nt)}{(1-f)(1-F)\,A\left[\frac{P^{2/3}x}{a} + (1-P^{2/3})k_m + P^{2/3}k_g\right]} \tag{B8}$$

The total thermal resistance of the delaminated flow channels is given by

$$R_T = R_d + R_p = \frac{L}{(1-f)(1-F)A}\left\{\frac{\frac{nt}{L}}{\left(\frac{t}{a} + k_g\right)} + \frac{\left(1 - \frac{nt}{L}\right)}{\left[\frac{P^{2/3}x}{a} + (1-P^{2/3})k_m + P^{2/3}k_g\right]}\right\} \tag{B9}$$

The total thermal conductance of the delaminated flow channels may then be written as follows

$$K_T = \frac{1}{R_T} = \frac{A}{L}\left\{\frac{(1-f)(1-F)\left(\frac{t}{a}+k_g\right)\left[\frac{P^{2/3}x}{a}+(1-P^{2/3})k_m+P^{2/3}k_g\right]}{(1-c)\left(\frac{t}{a}+k_g\right)+c\left[\frac{P^{2/3}x}{a}+(1-P^{2/3})k_m+P^{2/3}k_g\right]}\right\} \quad (B10)$$

where

$$c = \frac{nt}{L}$$

Now, K_T may be combined with the other conductances shown in Figure 20, K_m', K_r', K_g', K_R, and K_G, as follows to give the overall thermal conductance of the char.

$$K = K_T + K_r' + K_R + K_m' + K_g' + K_G \quad (B11)$$

The expressions given by equations (B10), (8), (9), (12), (14) and (15) for K_T, K_r', K_R, K_m', K_g', and K_G, respectively, were substituted into equation (B11) and the following equation was obtained

$$K = \frac{A}{L}\left\{\frac{(1-f)(1-F)\left(\frac{t}{a}+k_g\right)\left[\frac{P^{2/3}x}{a}+(1-P^{2/3})k_m+P^{2/3}k_g\right]}{(1-c)\left(\frac{t}{a}+k_g\right)+c\left[\frac{P^{2/3}x}{a}+(1-P^{2/3})k_m+P^{2/3}k_g\right]}\right\}$$

$$+\frac{(1-f)FP^{2/3}Ax}{aL}+\frac{4\sigma F_{ir_2}LT_m^3fA}{L}+\frac{k_m(1-f)F(1-P^{2/3})A}{L}$$

$$+\frac{(1-f)FP^{2/3}Ak_g}{L}+\frac{fAk_g}{L} \quad (B12)$$

The overall thermal conductance is related to the apparent thermal conductivity of the char by the following equation

$$K = \frac{k_a A}{L} \tag{B13}$$

Thus,

$$k_a = K \frac{L}{A} \tag{B14}$$

Equation (B12) was multiplied by L/A and rearranged to yield the following expression for the apparent thermal conductivity of the char

$$k_a = \left\{ \frac{(1-f)(1-F)\left(\frac{t}{a}+k_g\right)\left[\frac{P^{2/3}x}{a} + P^{2/3}k_g + (1-P^{2/3})k_m\right]}{(1-c)\left(\frac{t}{a}+k_g\right) + c\left[\frac{P^{2/3}x}{a} + P^{2/3}k_g + (1-P^{2/3})k_m\right]} \right\}$$

$$+ 4f\sigma F_{ir_2} T_m^3 L + fk_g + (1-f)F\left[P^{2/3}k_g + (1-P^{2/3})k_m + \frac{P^{2/3}x}{a}\right] \tag{B15}$$

Equation (B15) is presented as equation (18) in the text.

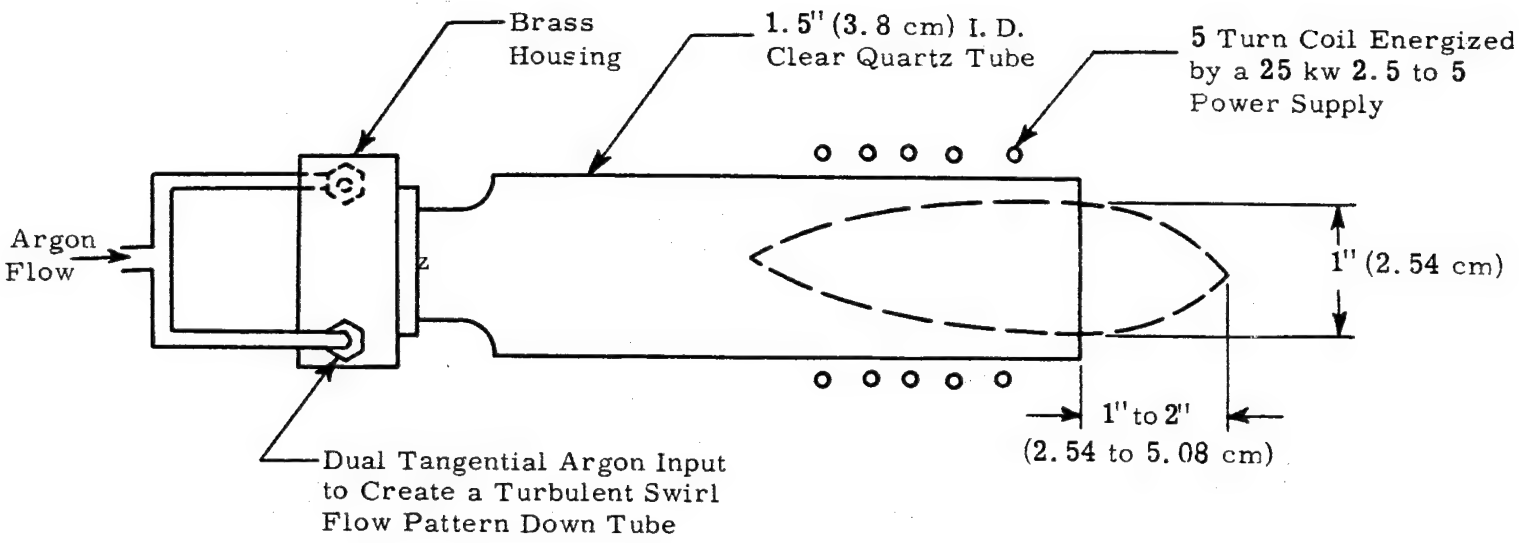

Figure 1. Schematic of Induction Plasma Torch

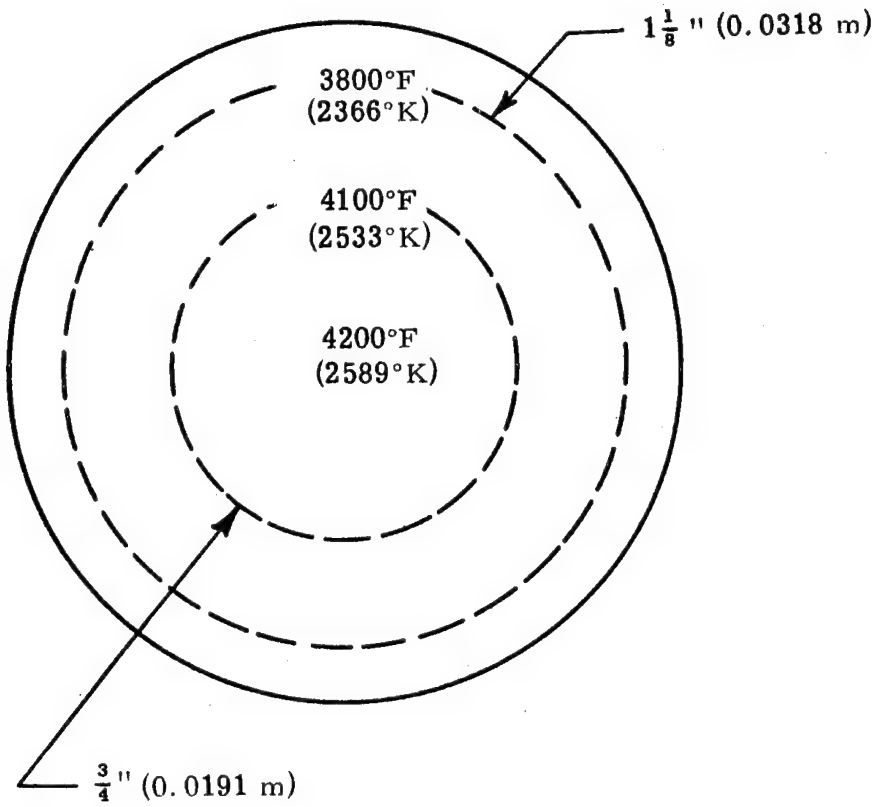

Note: Temperatures were measured with optical pyrometer and were not corrected for effects of emittance or transmittance of the plasma

Figure 2. Typical optically observed temperature profiles of front surface of specimen during exposure to the induction plasma torch

Charring Direction

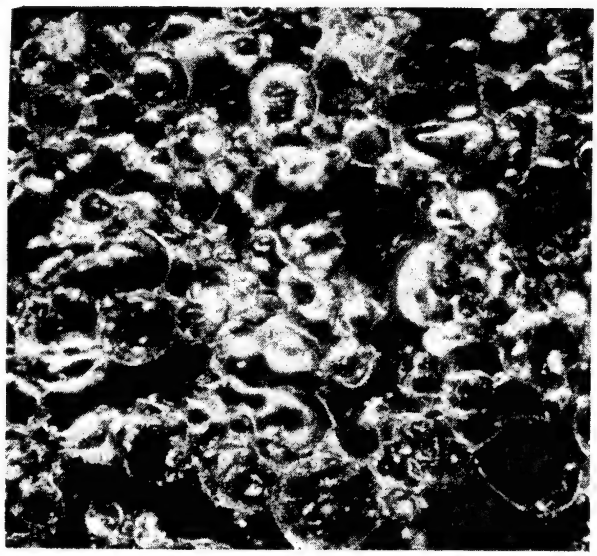

(a) Char of 0.88 porosity
(19 lb/ft^3 virgin density)

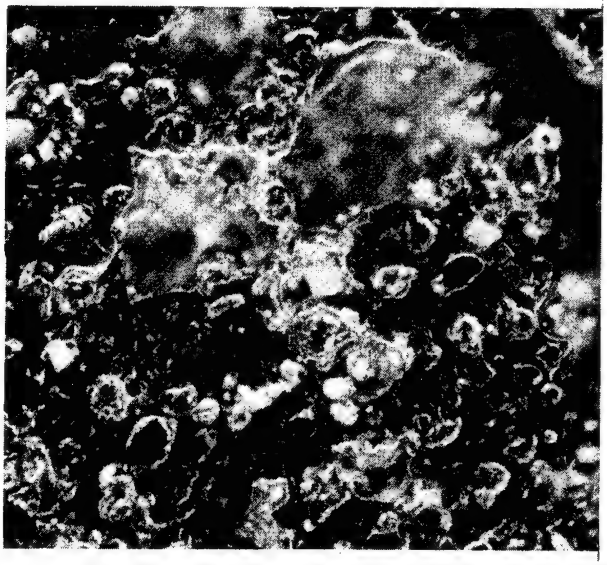

(b) Char of 0.82 porosity
(30 lb/ft^3 virgin density)

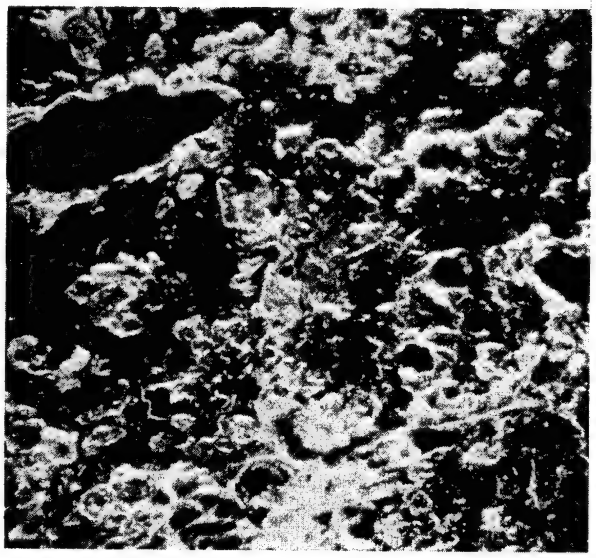

(c) Char of 0.79 porosity
(42 lb/ft^3 virgin density)

(d) Char of 0.79 porosity
(42 lb/ft^3 virgin density)

Figure 3. Photomicrographs at 100X magnification of the three different densities of phenolic-nylon char

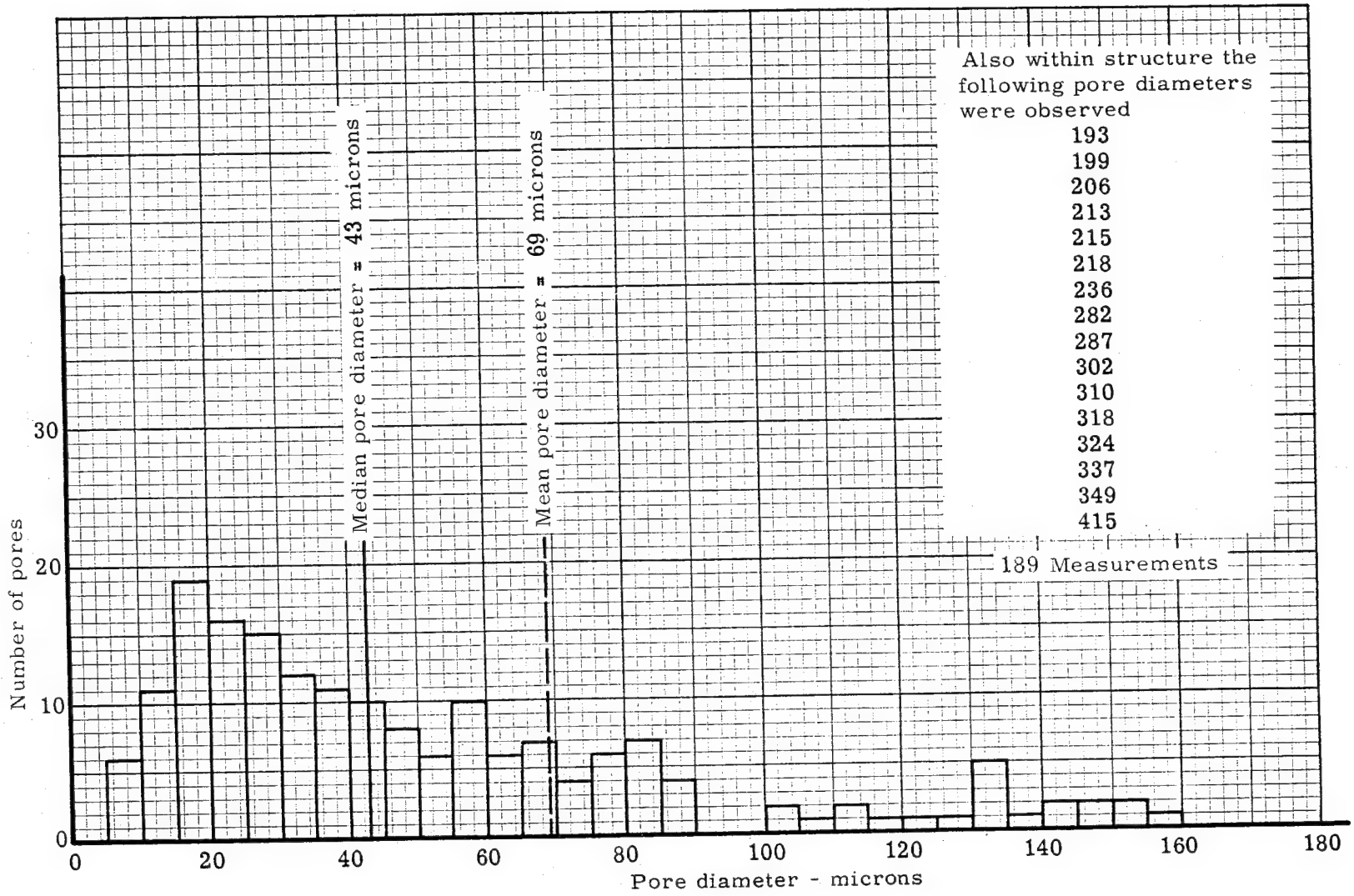

Figure 4. Histogram of pore diameters in the phenolic char of 0.88 porosity (19 lb/ft^3 virgin density)

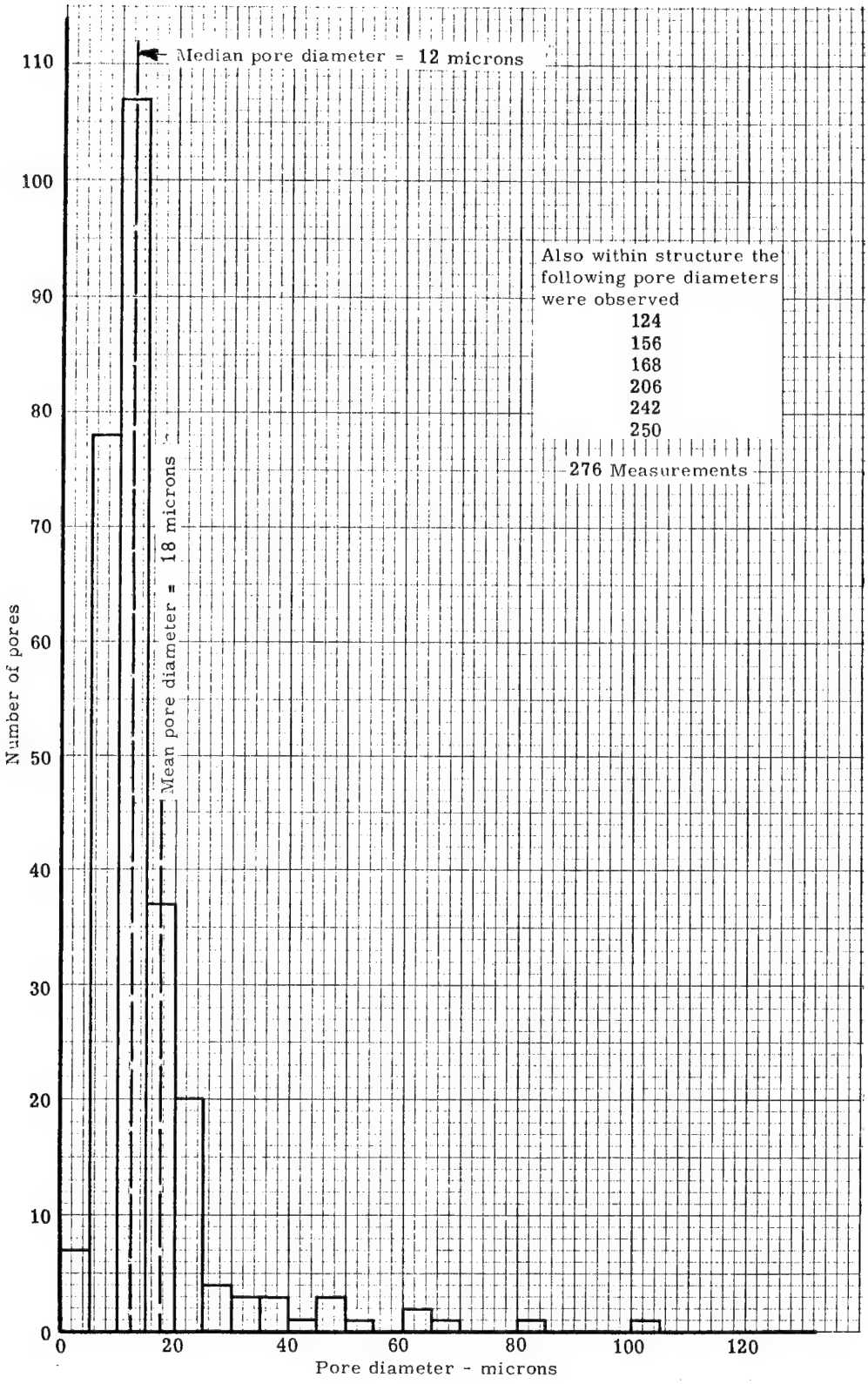

Figure 5. Histogram of pore diameters in the phenolic nylon char of 0.82 porosity (30 lb/ft^3 virgin density)

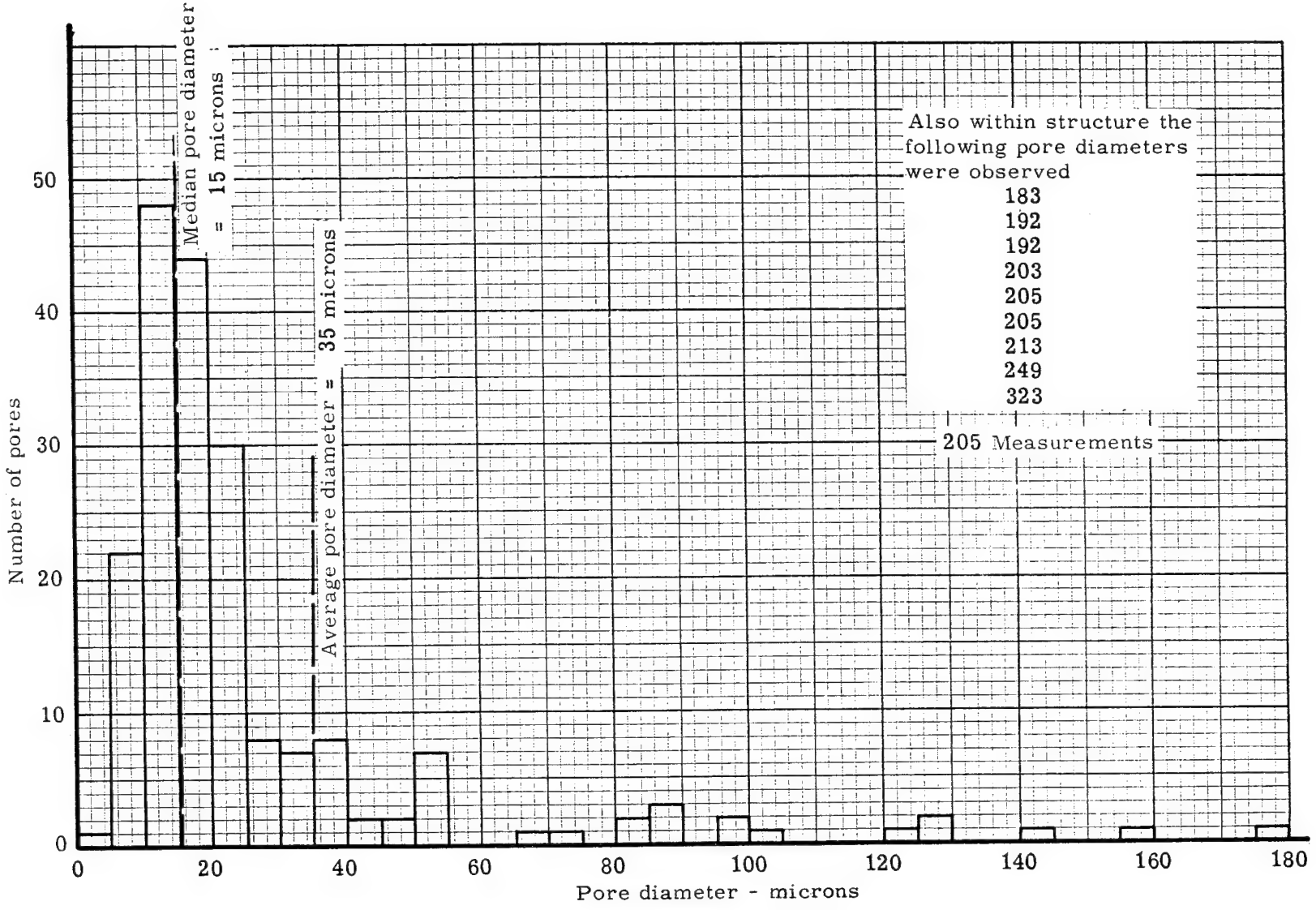

Figure 6. Histogram of pore diameters in the phenolic-nylon char of 0.79 porosity (42 lb/ft^3 virgin density)

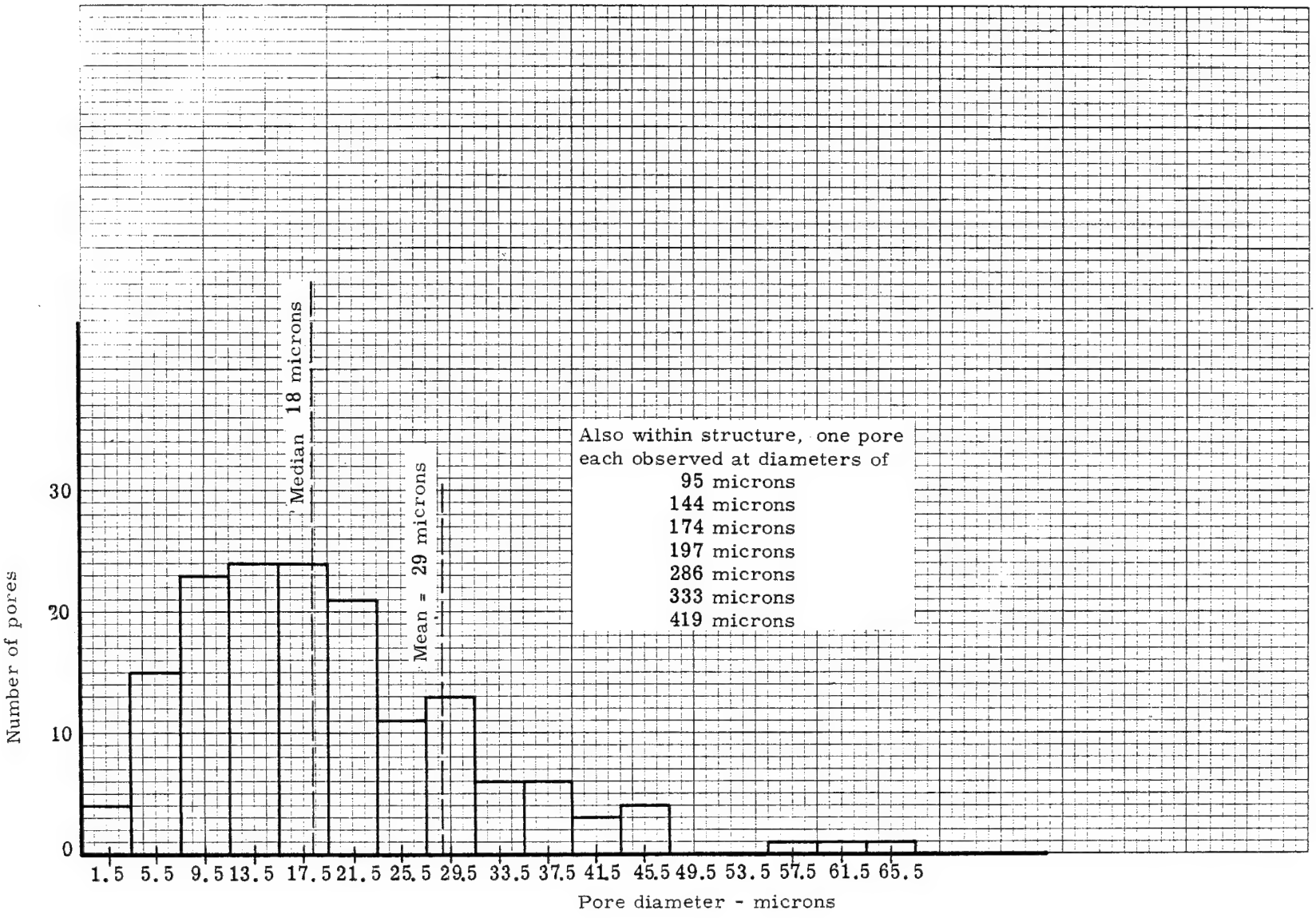

Figure 7. Histogram of pore diameters in the low-density, phenolic-nylon char (36.6 lb/ft^3 virgin density) reported in Reference 2

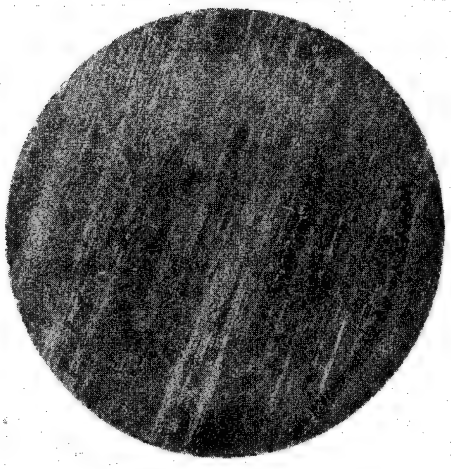

(a) Specimen 30-6 - front surface - impregnated

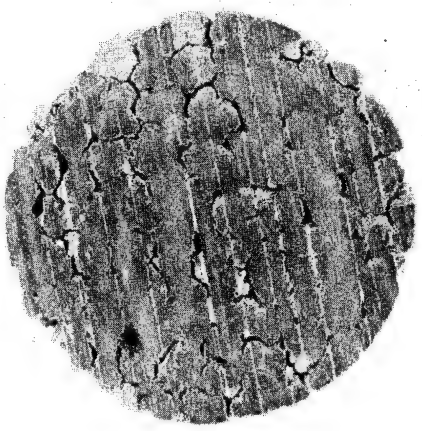

(b) Specimen 30-6 - back surface - impregnated

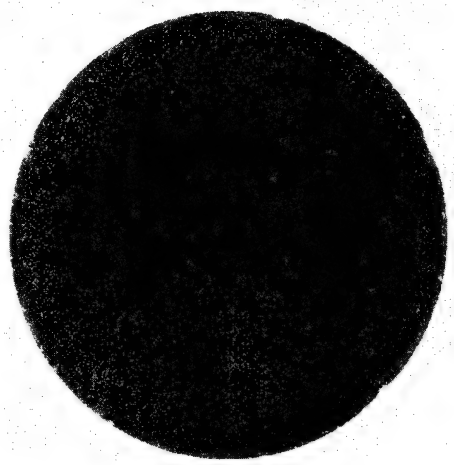

(c) Specimen 30-6 - front surface - after run

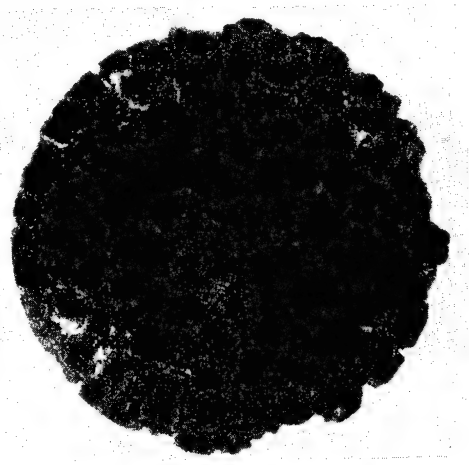

(d) Specimen 30-6 - back surface - after run

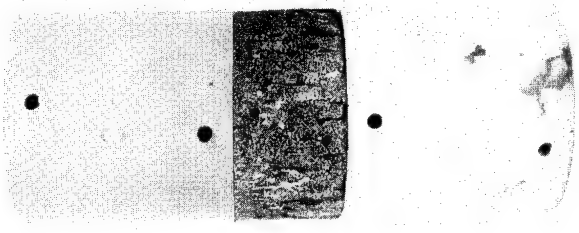

(e) Specimen 30-6 between Pyroceram references - after run

Figure 8. Pictures of specimens before and after runs

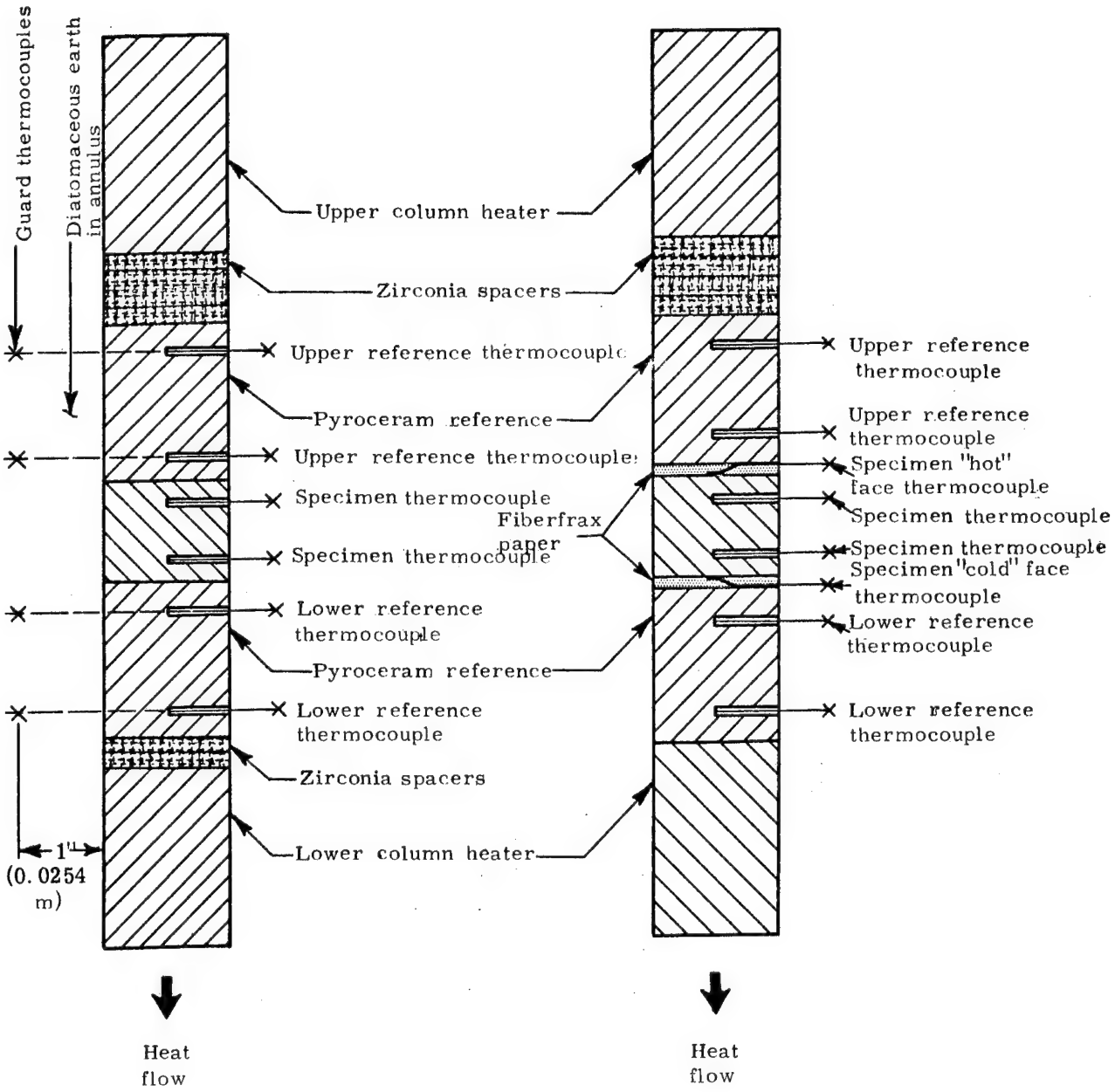

(a) Standard buildup for thermal conductivity evaluations

(b) Buildup for specimen 42-3 (second run) - attempt to measure variation in thermal conductivity across thickness

Figure 9. Schematic diagram of comparative rod apparatus specimen configuration

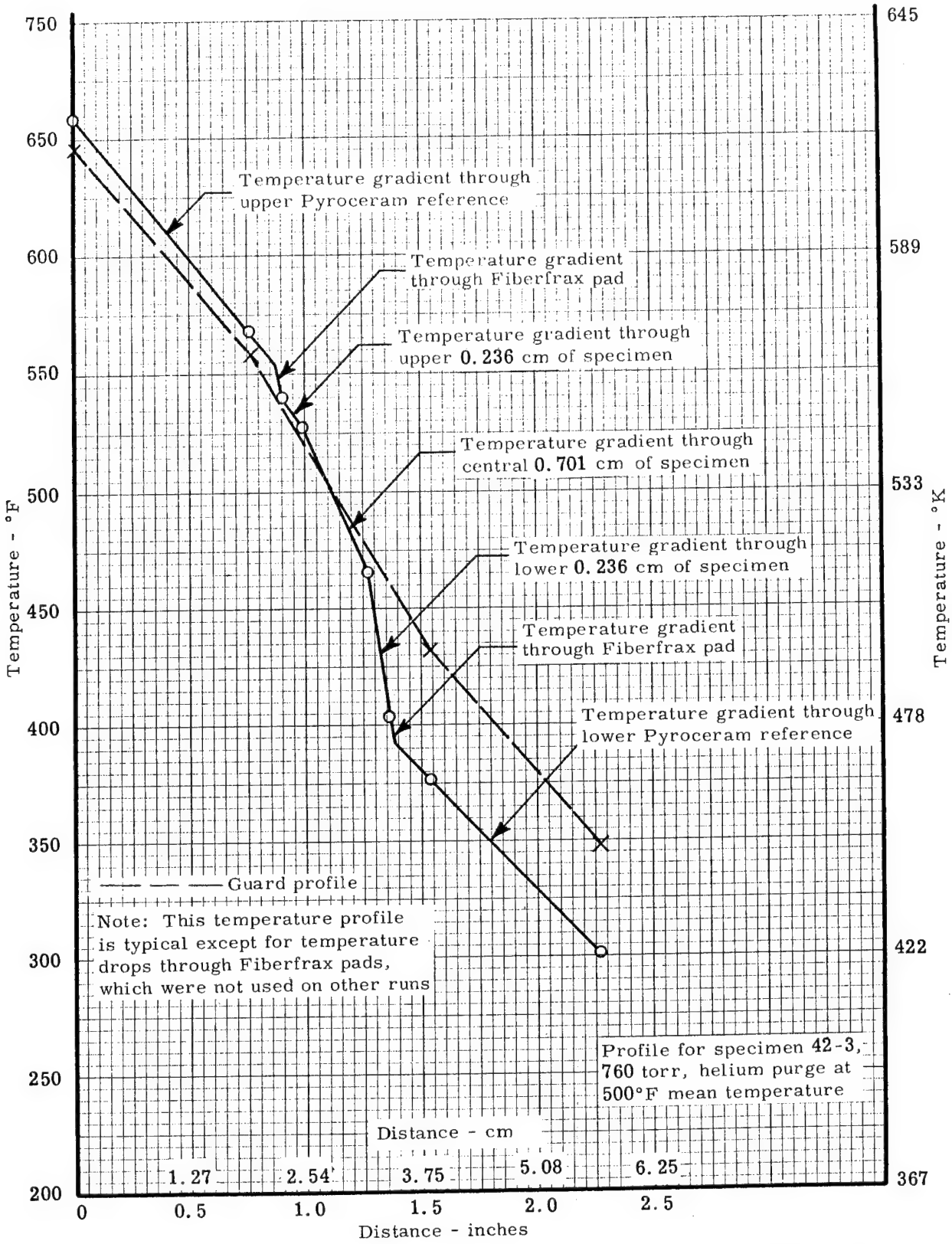

Figure 10. Typical temperature profile for data obtained on comparative rod apparatus using Code 9606 Pyroceram references

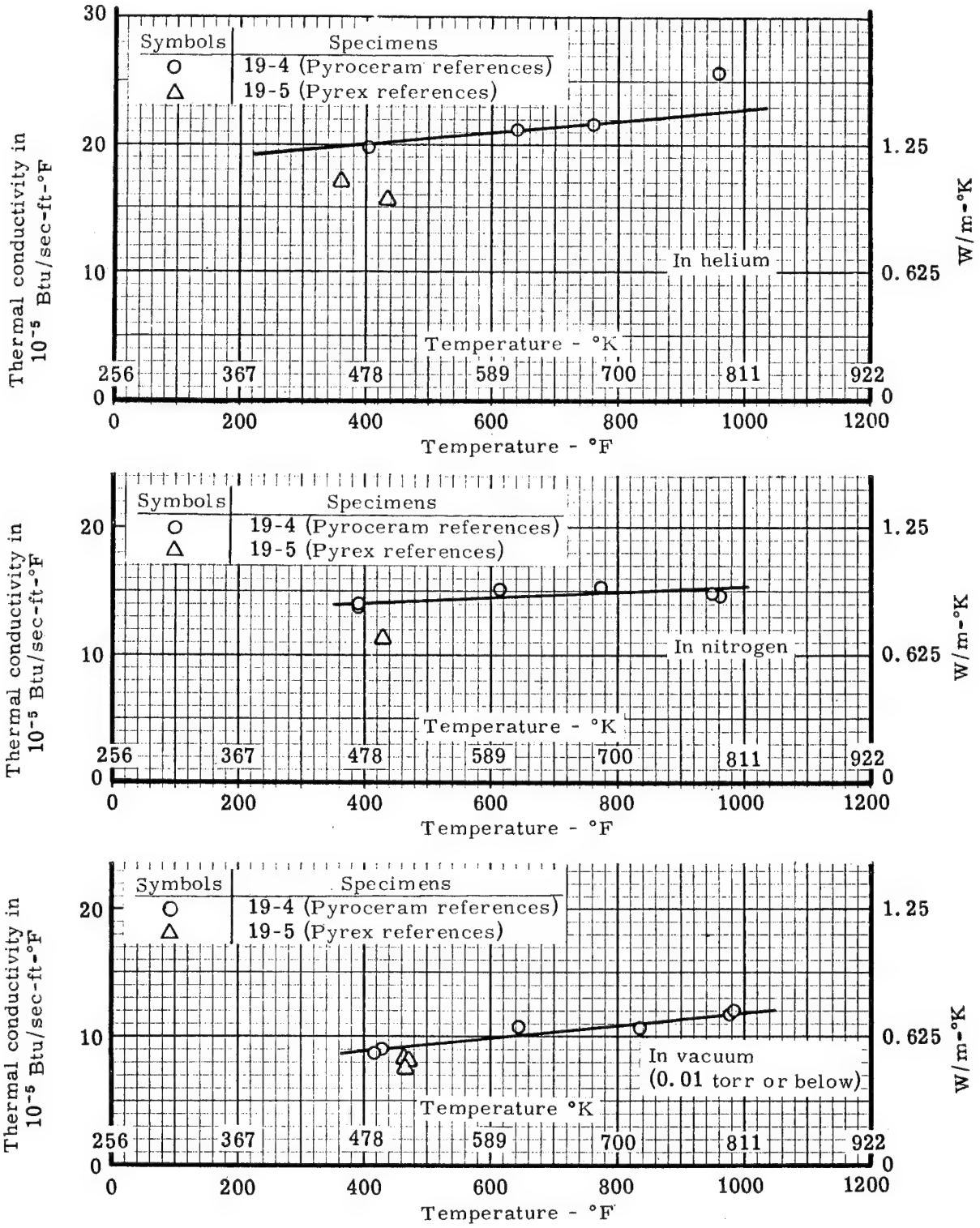

Figure 11. The thermal conductivity of phenolic-nylon char of 0.88 porosity (19 lb/ft^3 virgin density) in vacuum, nitrogen, and helium

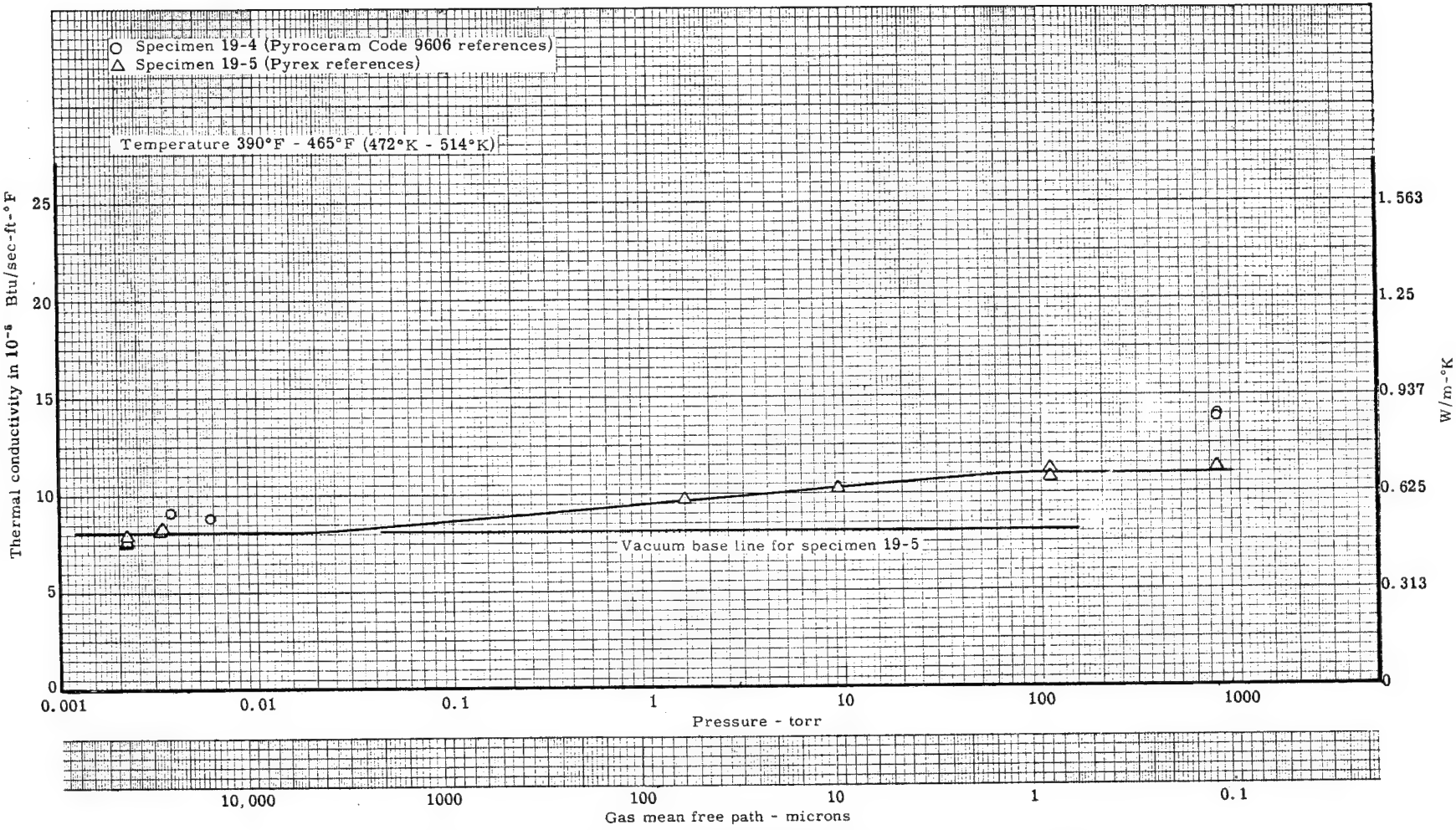

Figure 12. The thermal conductivity of phenolic-nylon char of 0.88 porosity (19 lb/ft^3 virgin density) versus pressure in a nitrogen atmosphere

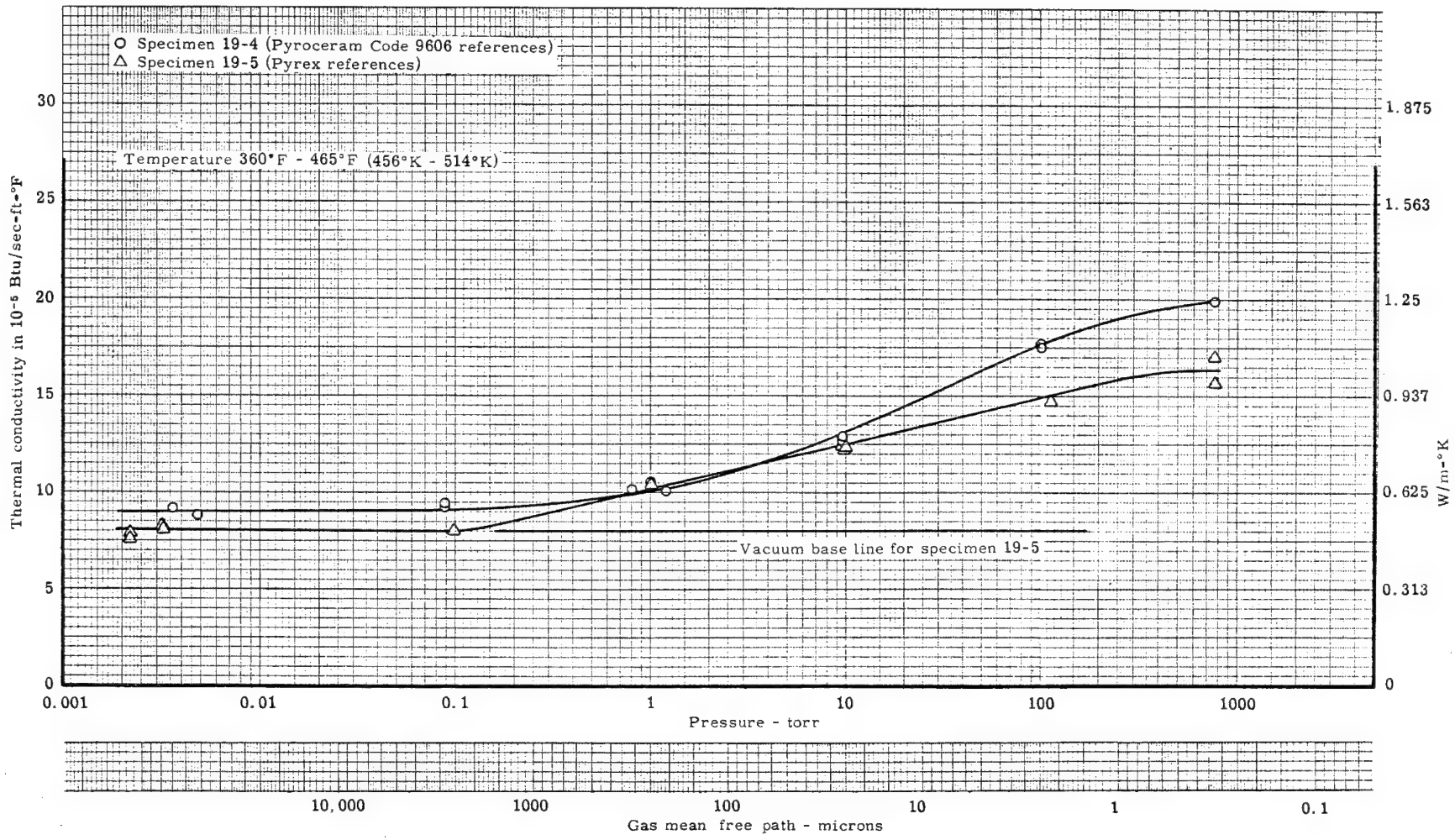

Figure 13. The thermal conductivity of phenolic-nylon char of 0.88 porosity (19 lb/ft^3 virgin density) versus pressure in a helium atmosphere

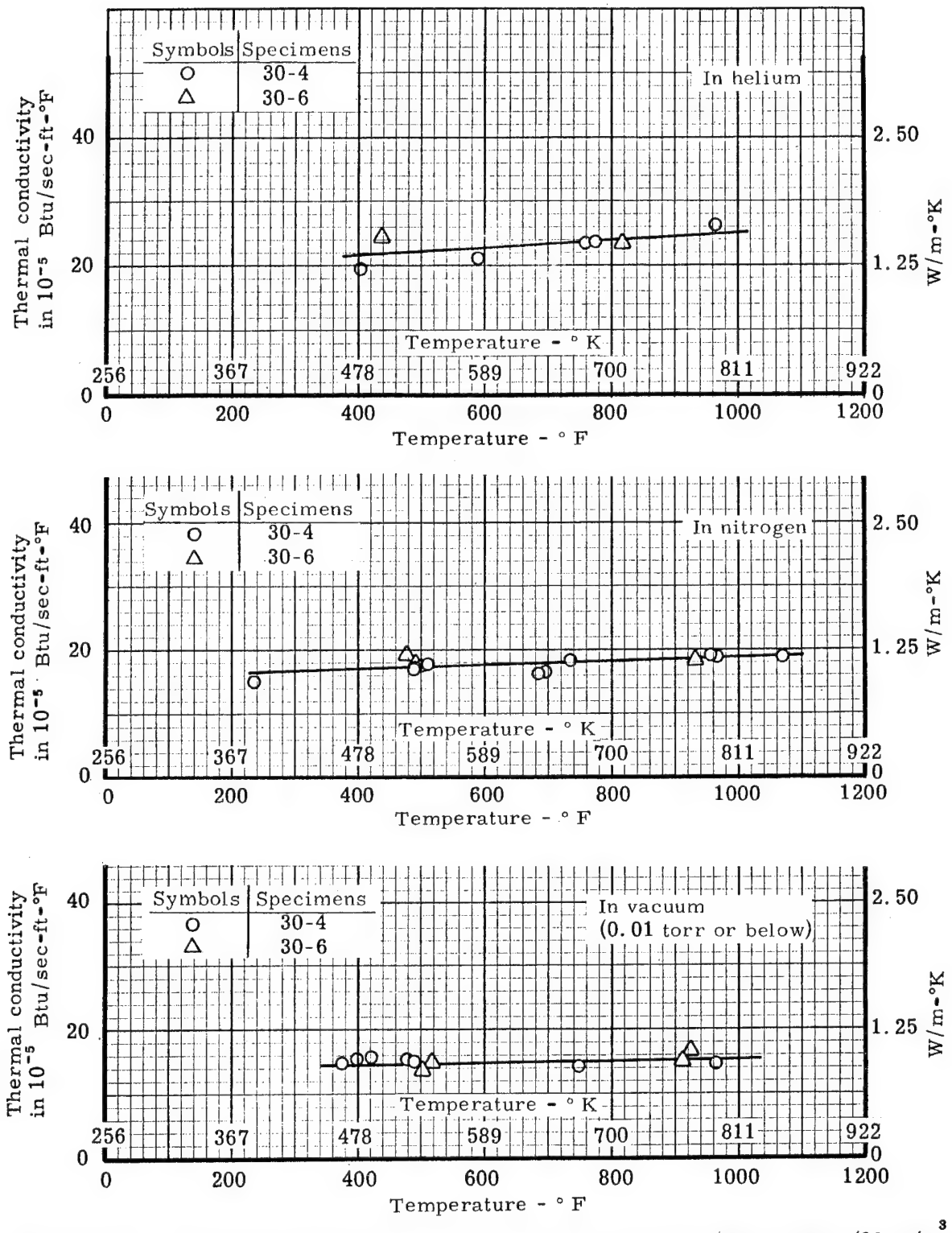

Figure 14. The thermal conductivity of phenolic-nylon char of 0.82 porosity (30 lb/ft^3 virgin density) in vacuum, nitrogen and helium

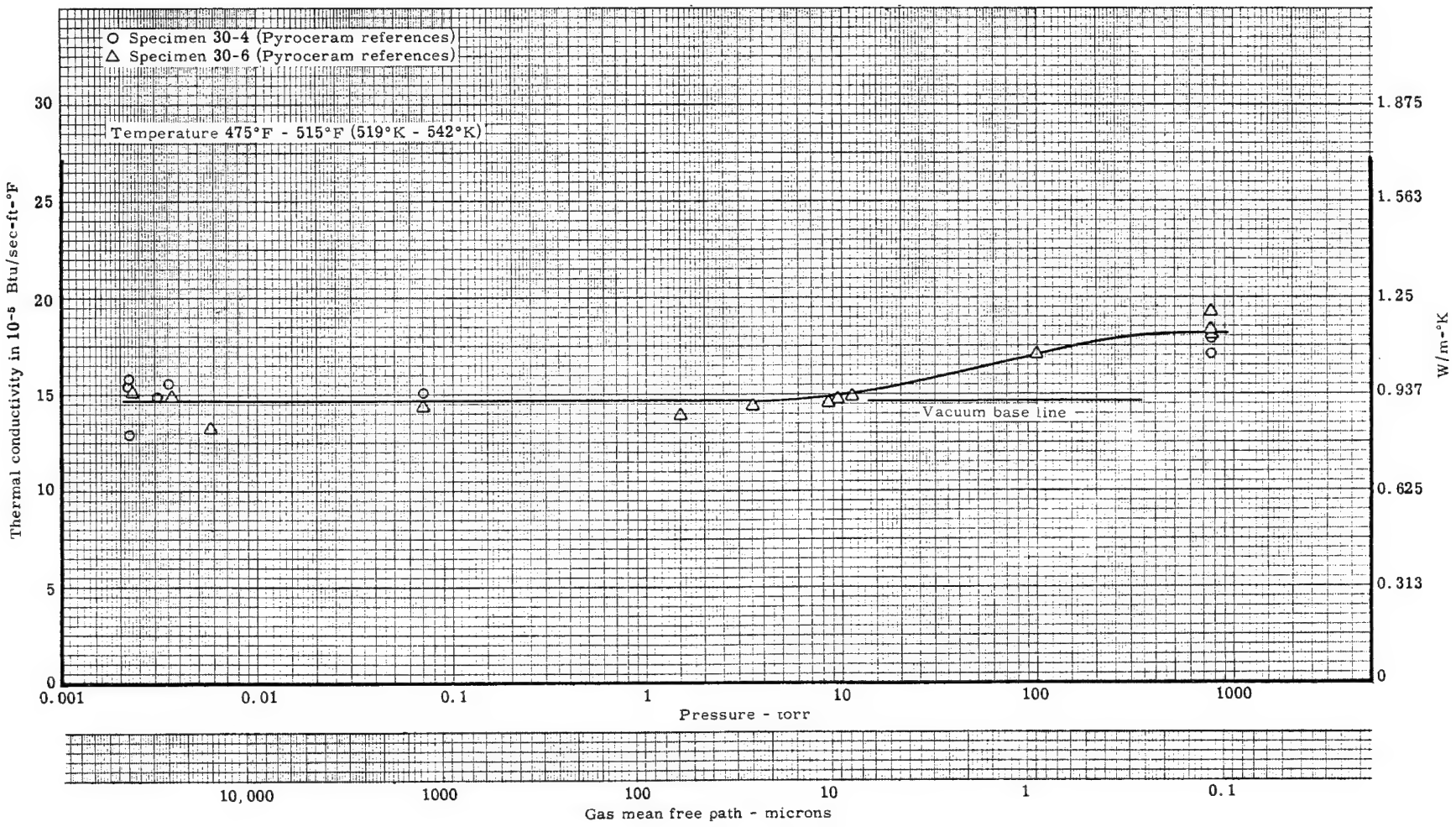

Figure 15. The thermal conductivity of phenolic-nylon char of 0.82 porosity (30 lb/ft^3 virgin density) versus pressure in a nitrogen atmosphere

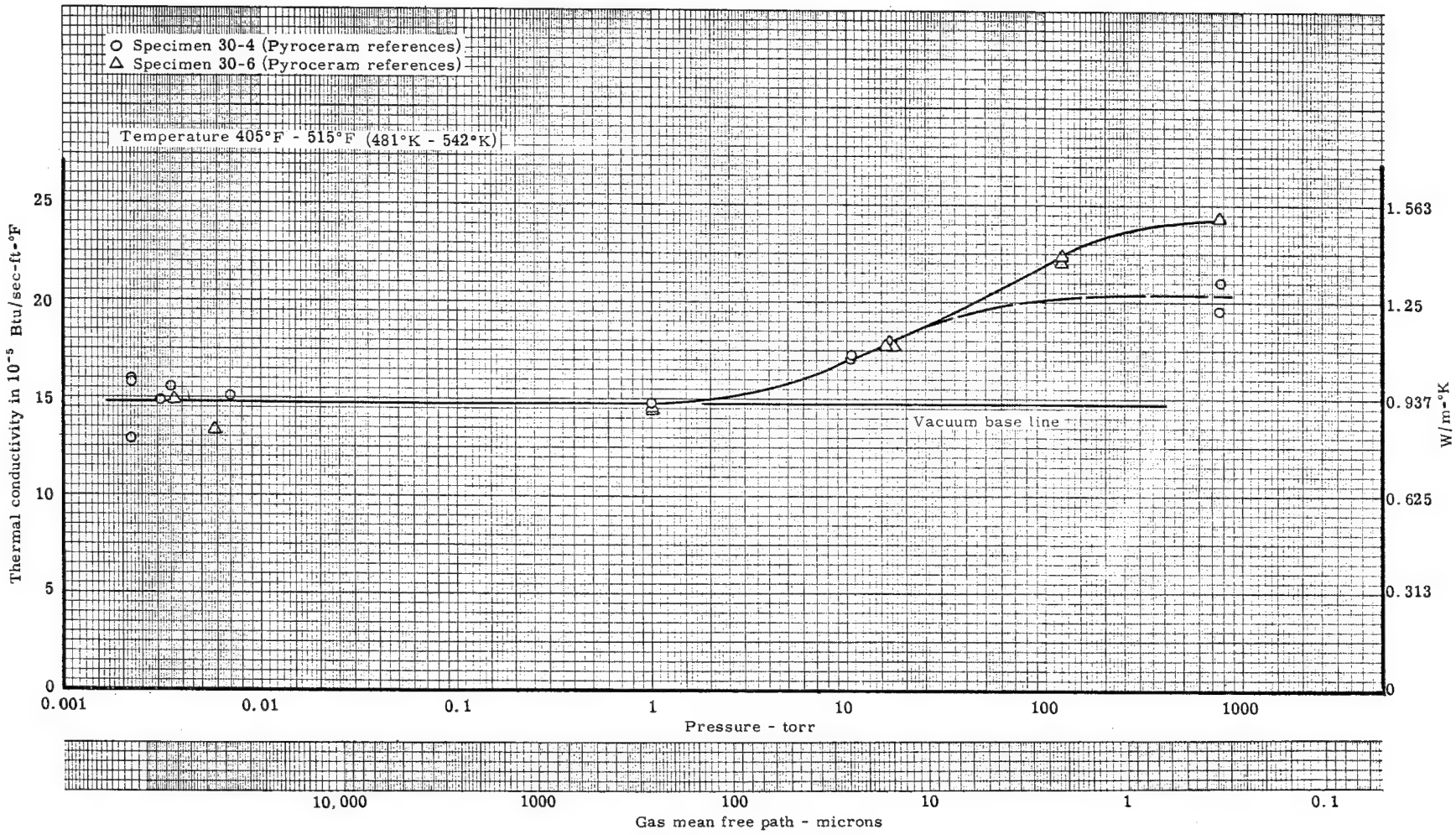

Figure 16. The thermal conductivity of phenolic-nylon char of 0.82 porosity (30 lb/ft^3 virgin density) versus pressure in a helium atmosphere

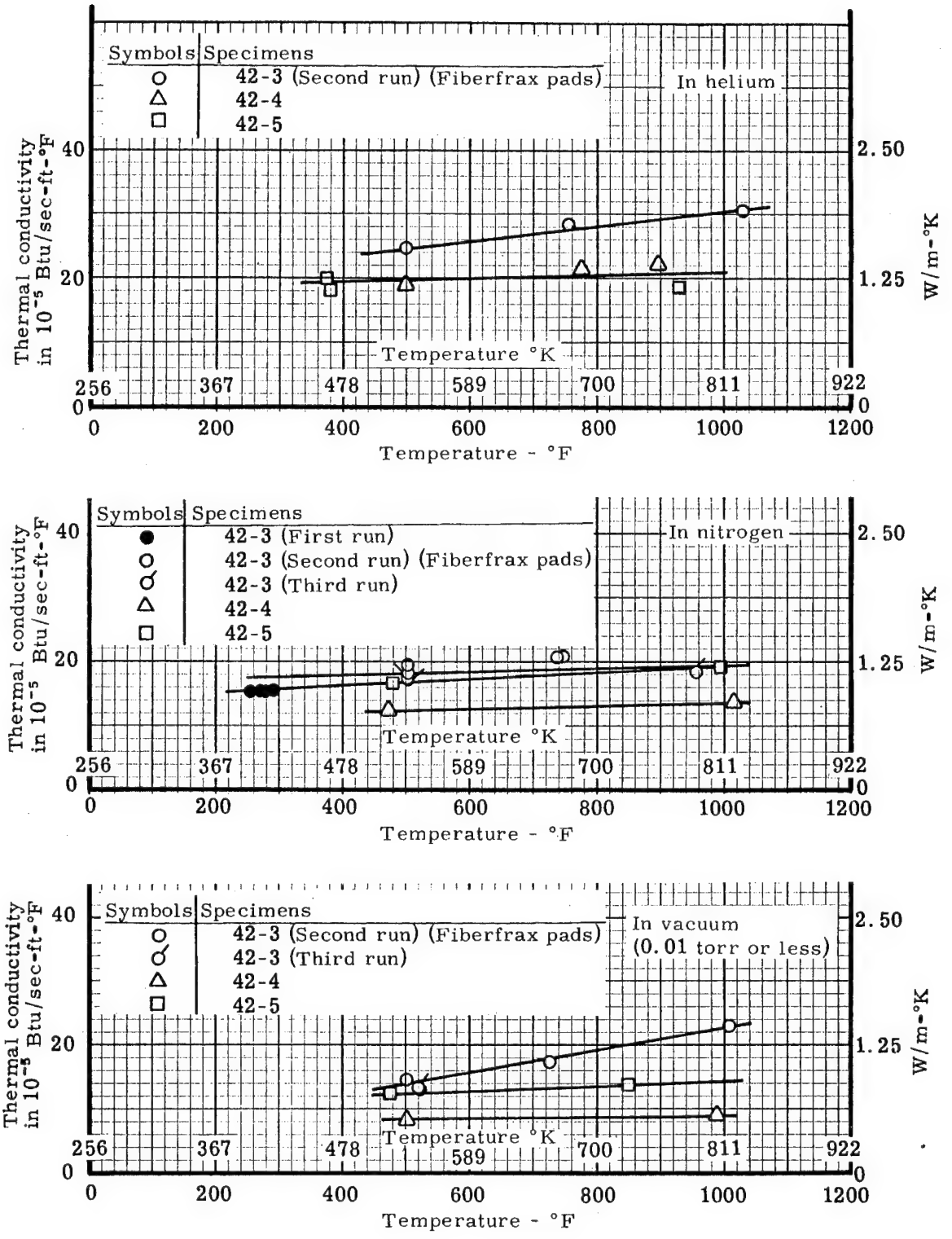

Figure 17. The thermal conductivity of phenolic-nylon char of 0.79 porosity (42 lb/ft^3 virgin density) in vacuum, nitrogen and helium

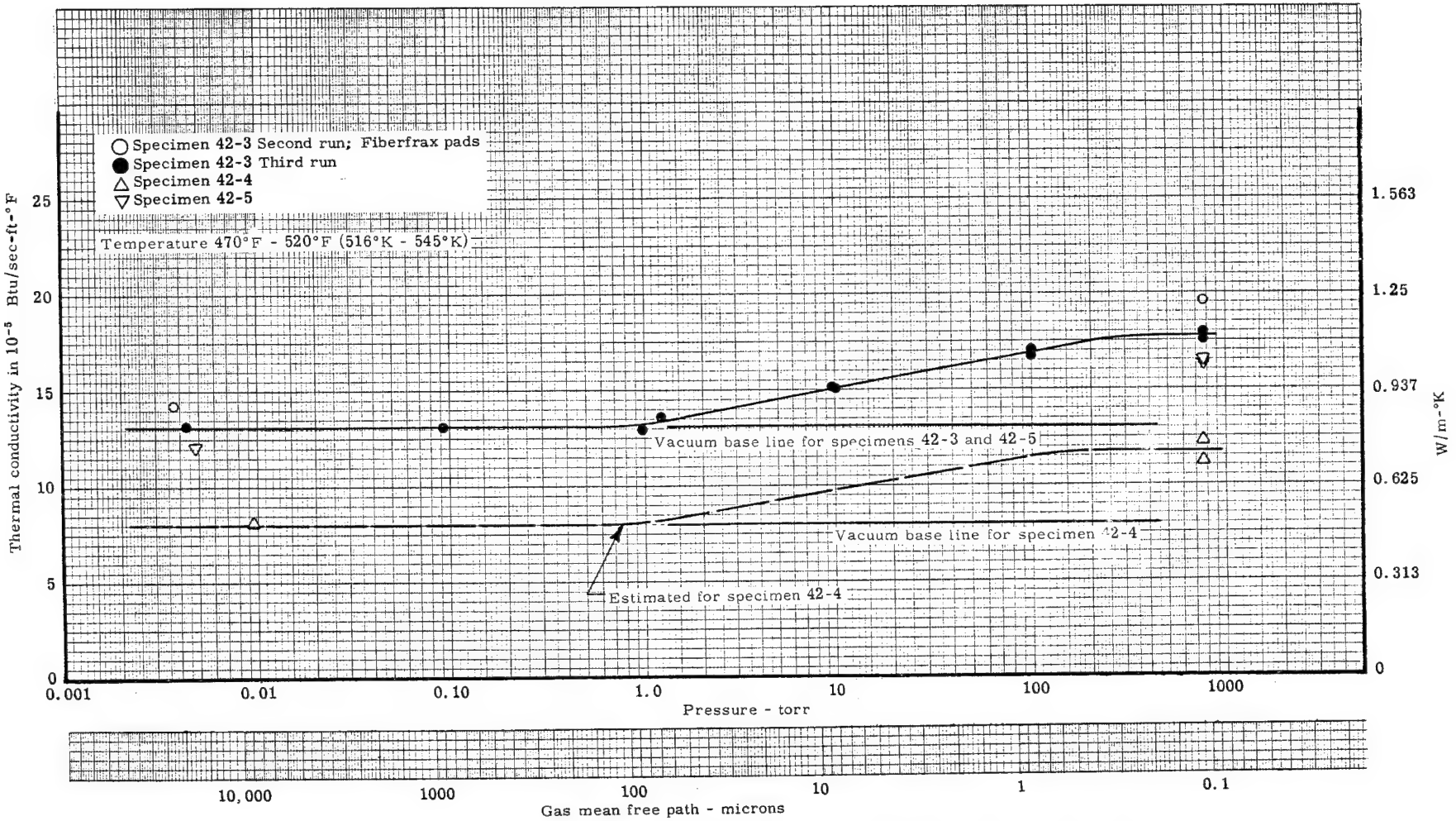

Figure 18. The thermal conductivity of phenolic-nylon char of 0.79 porosity (42 lb/ft^3 virgin density) versus pressure in a nitrogen atmosphere

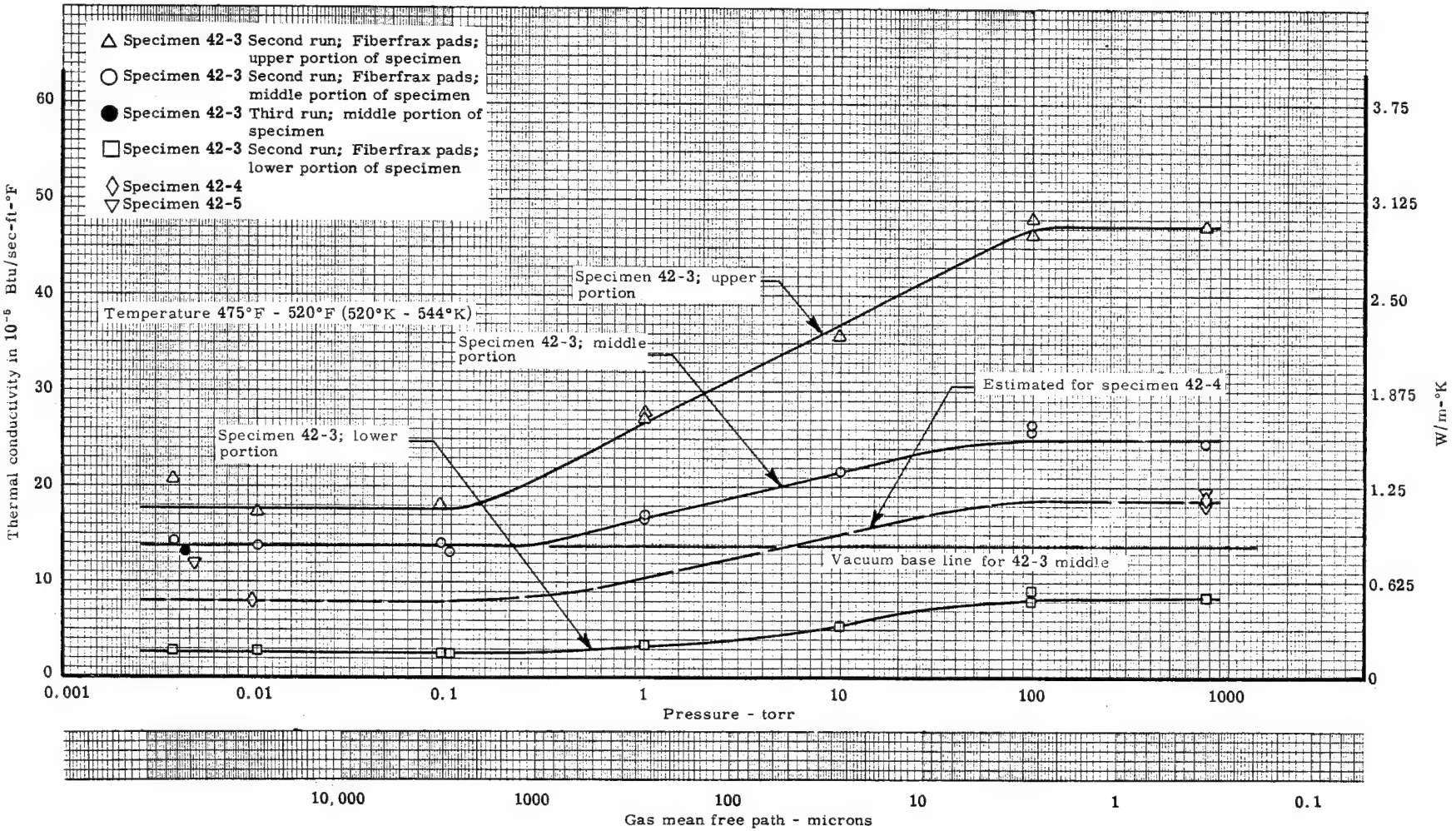

Figure 19. The thermal conductivity of phenolic-nylon char of 0.79 porosity (42 lb/ft^3 virgin density) versus pressure in a helium atmosphere

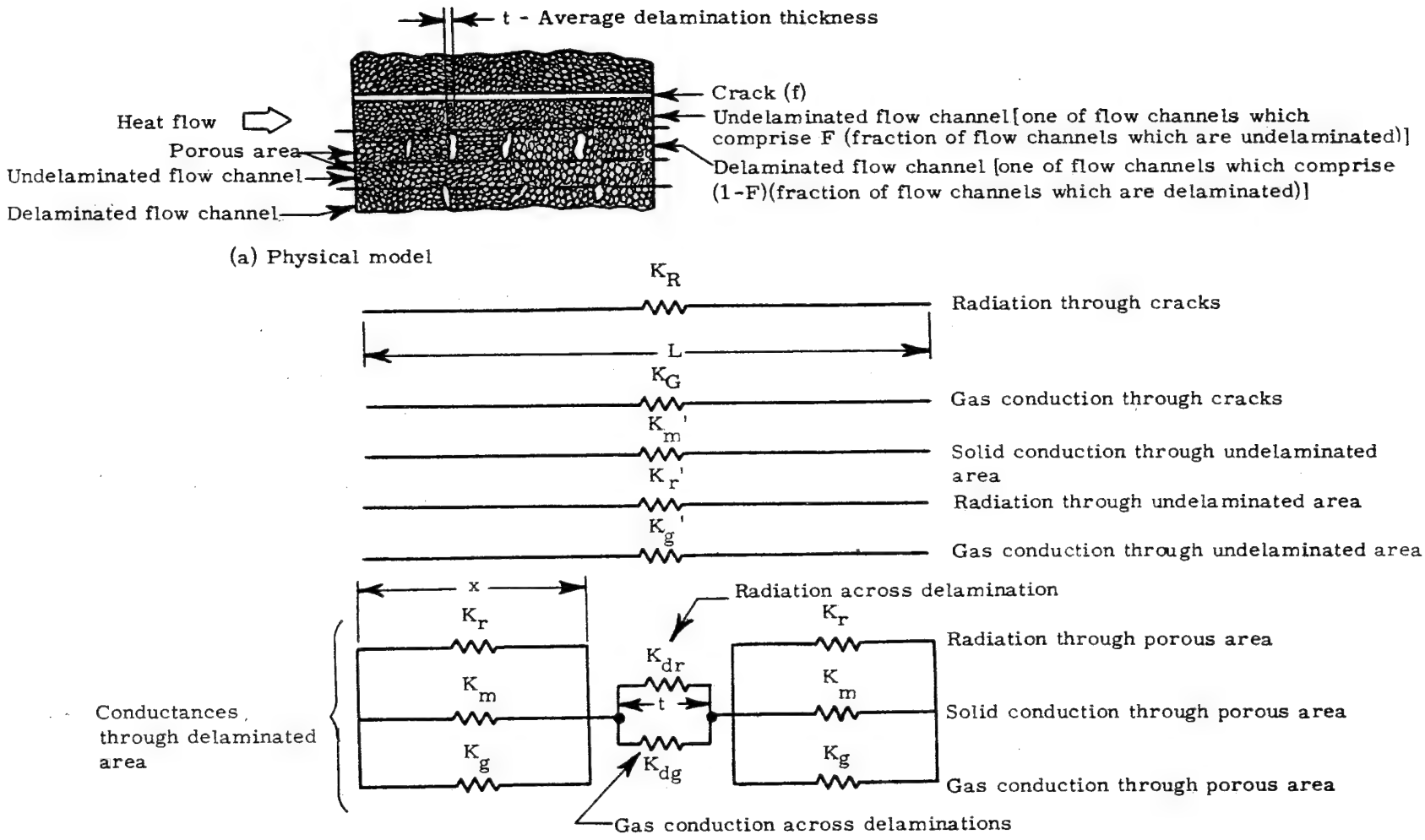

Figure 20. Sketches of physical model and thermal model for porous char

Specimen 42-4
after run

Figure 21. Picture of phenolic-nylon char showing delaminations

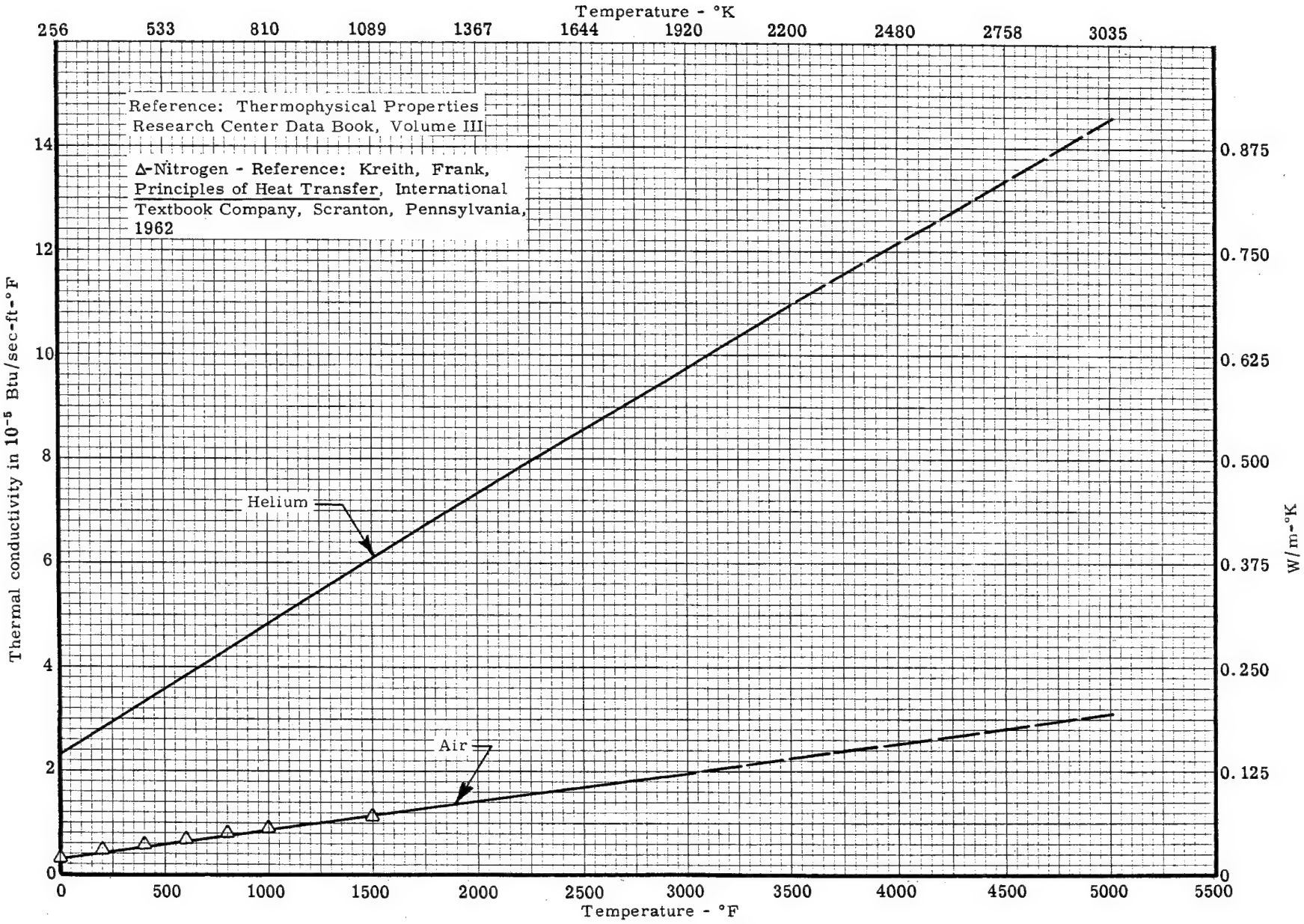

Figure 22. The continuum thermal conductivity of air and helium

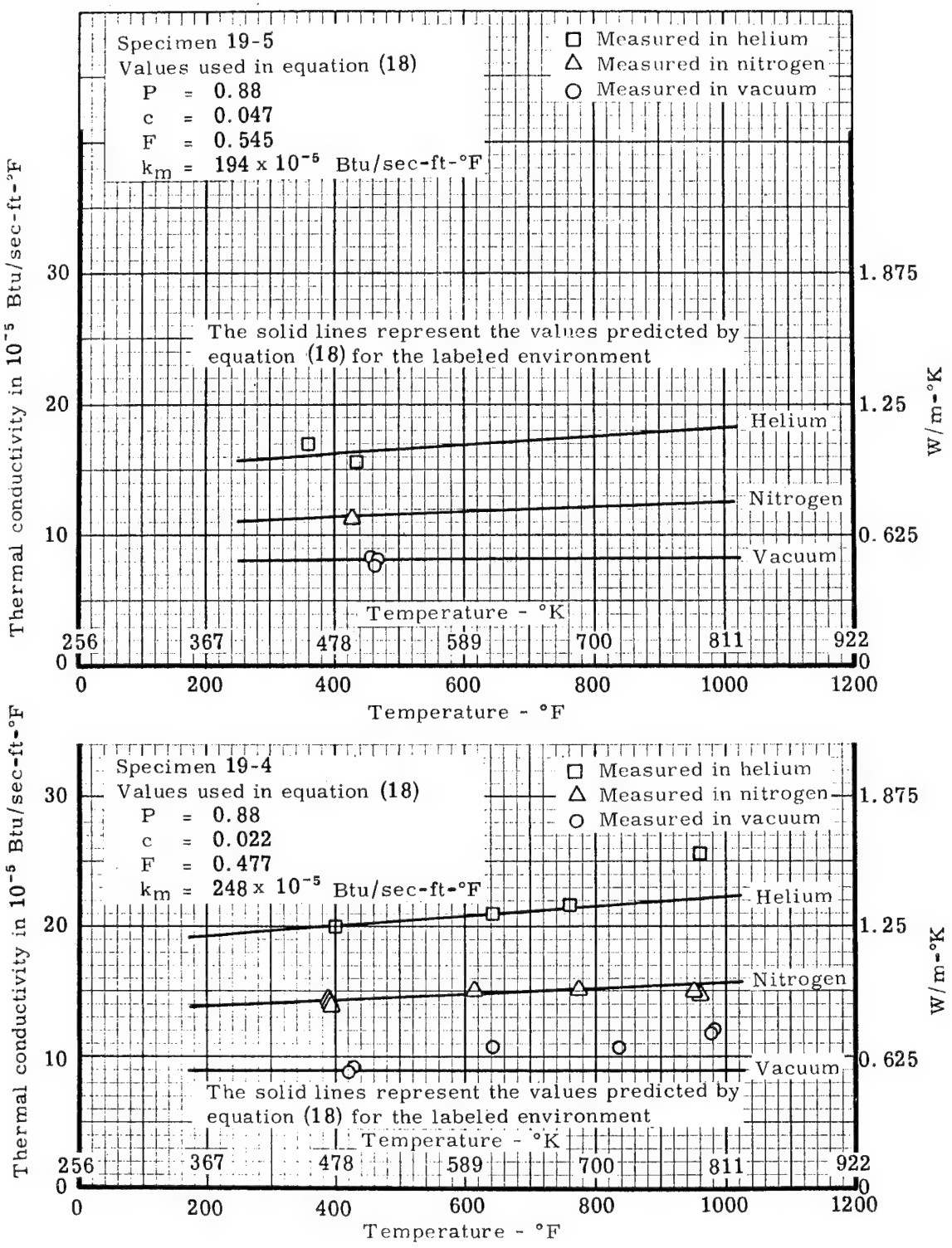

Figure 23. Comparison of the predicted variation in thermal conductivity with temperature with the measured values for specimens 19-4 and 19-5

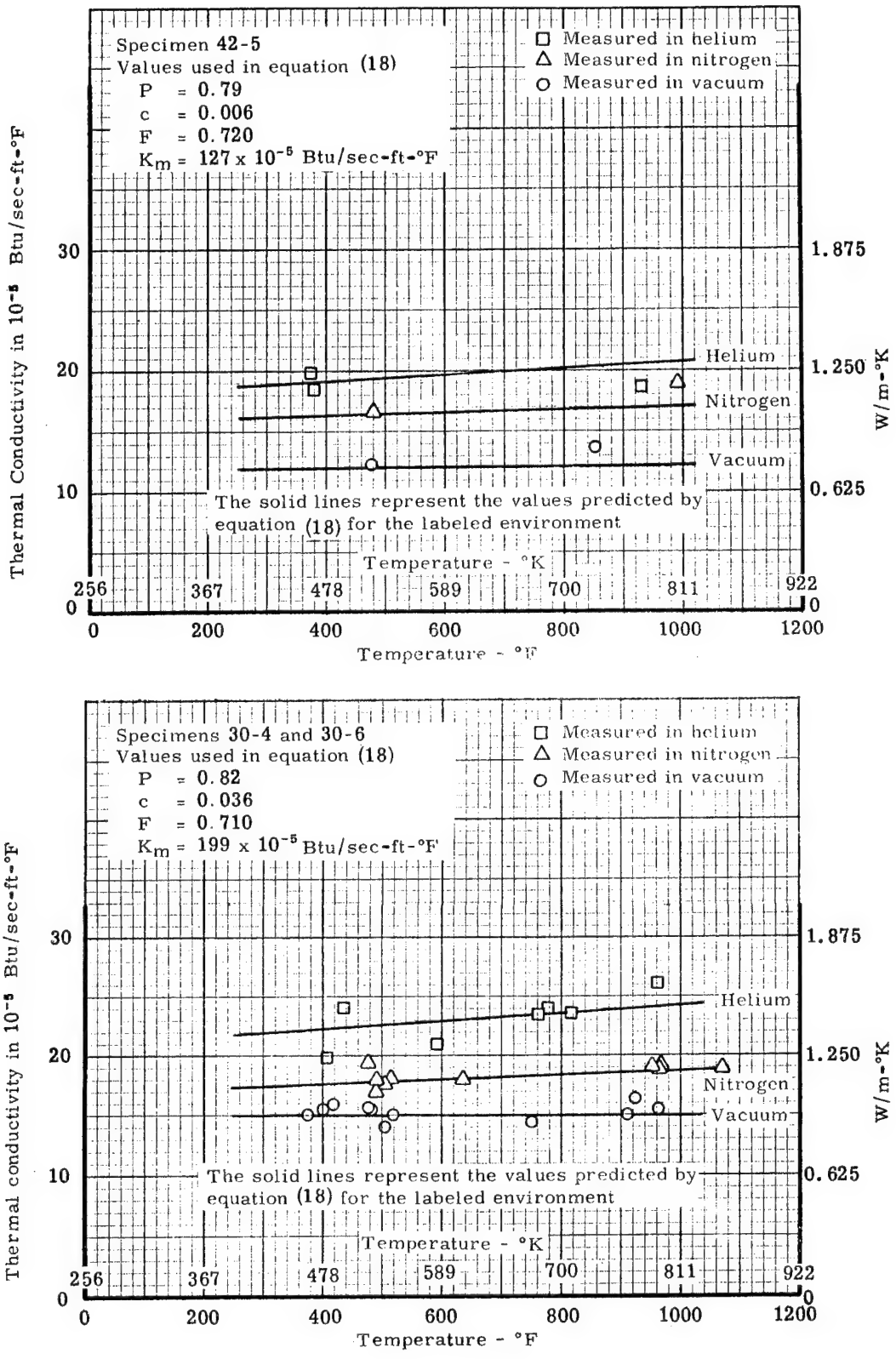

Figure 24. Comparison of the predicted variation in thermal conductivity with temperature with the measured values for specimens 30-4, 30-6, and 42-5

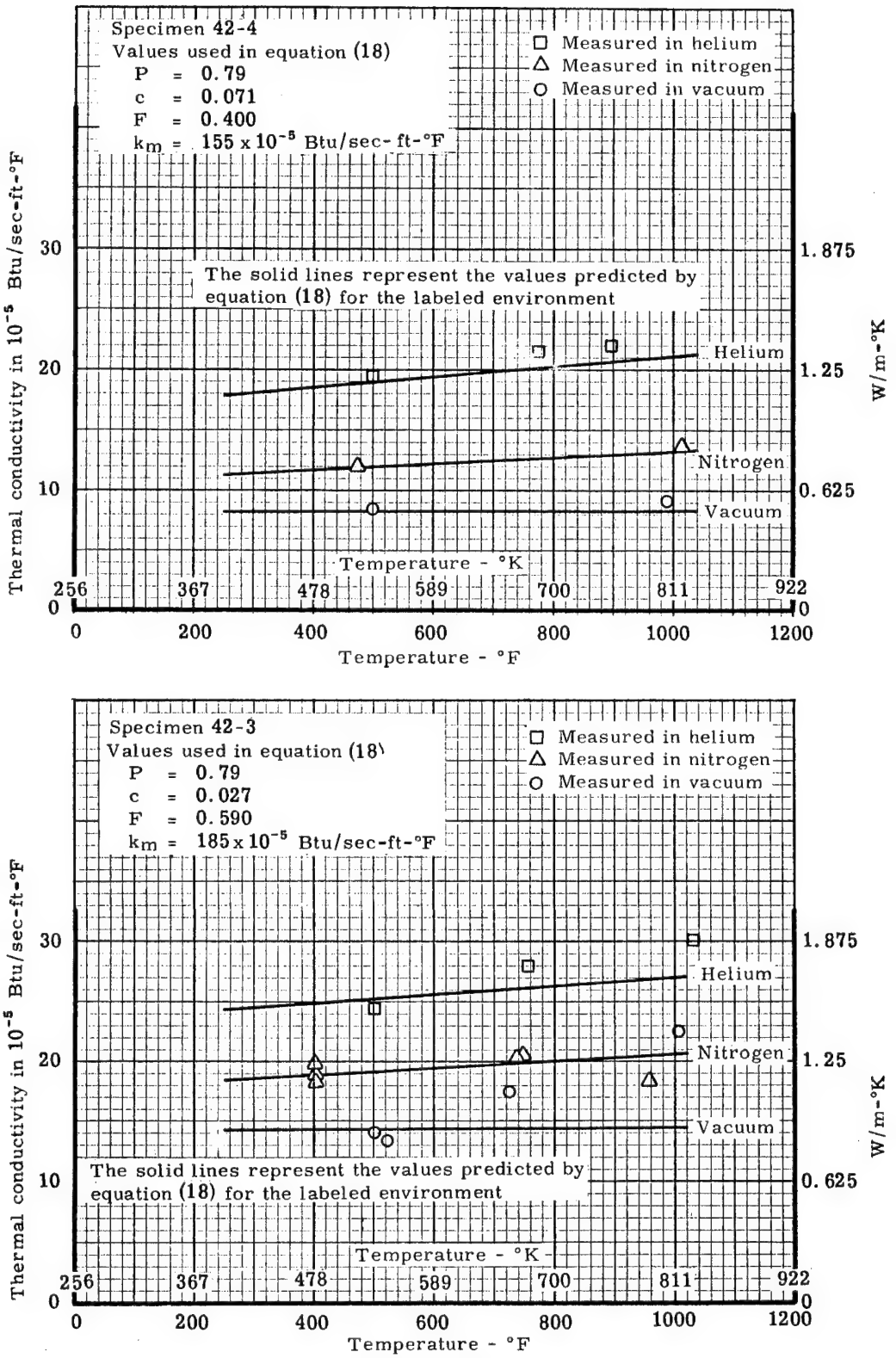

Figure 25. Comparison of the predicted variation in thermal conductivity with temperature with the measured values for specimens 42-3 and 42-4

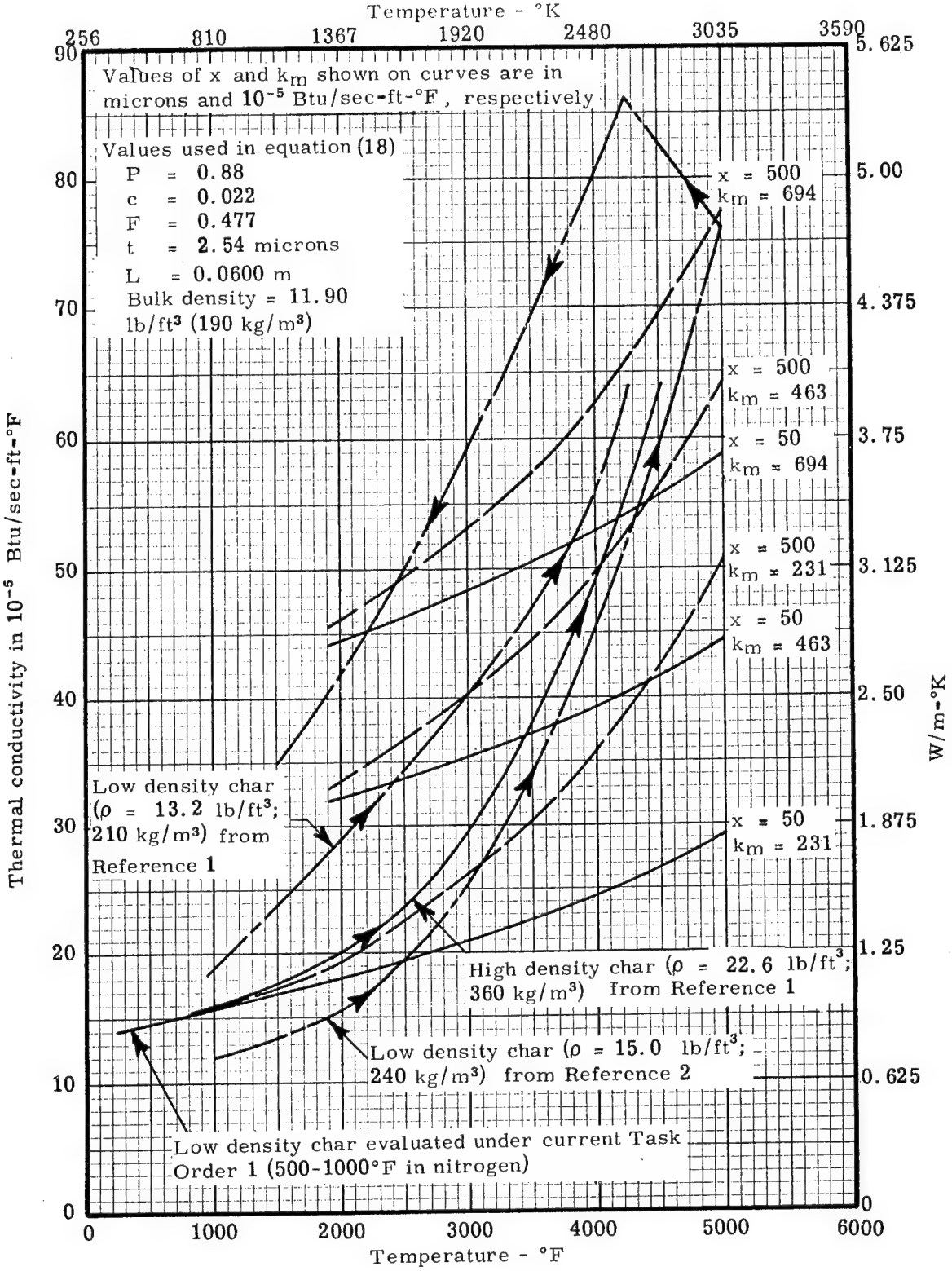

Figure 26. Comparison of the high temperature thermal conductivity predicted by equation (18) for a nitrogen environment with prior data

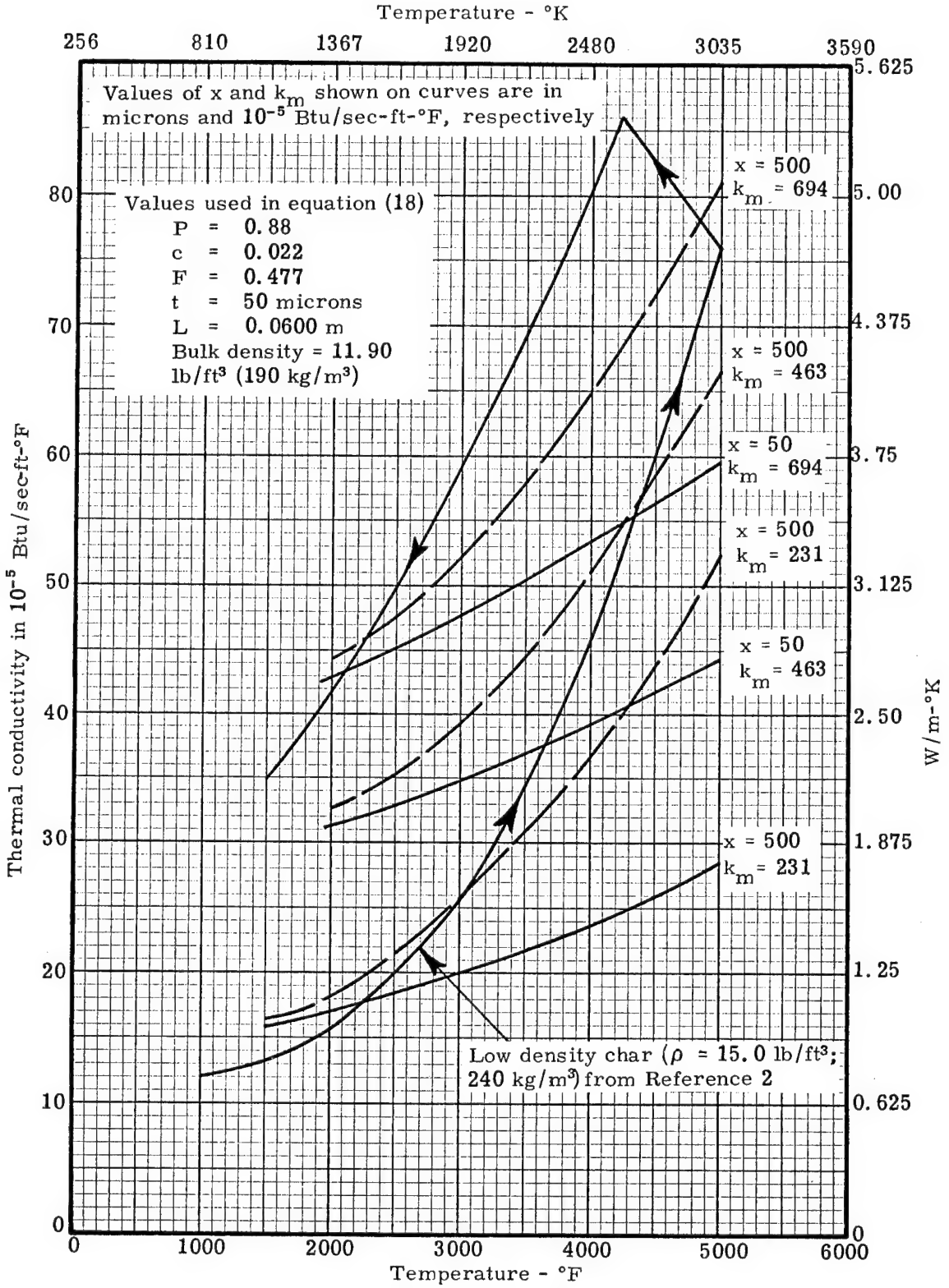

Figure 27. Comparison of the high temperature thermal conductivity predicted by equation (18) for a nitrogen environment with prior data

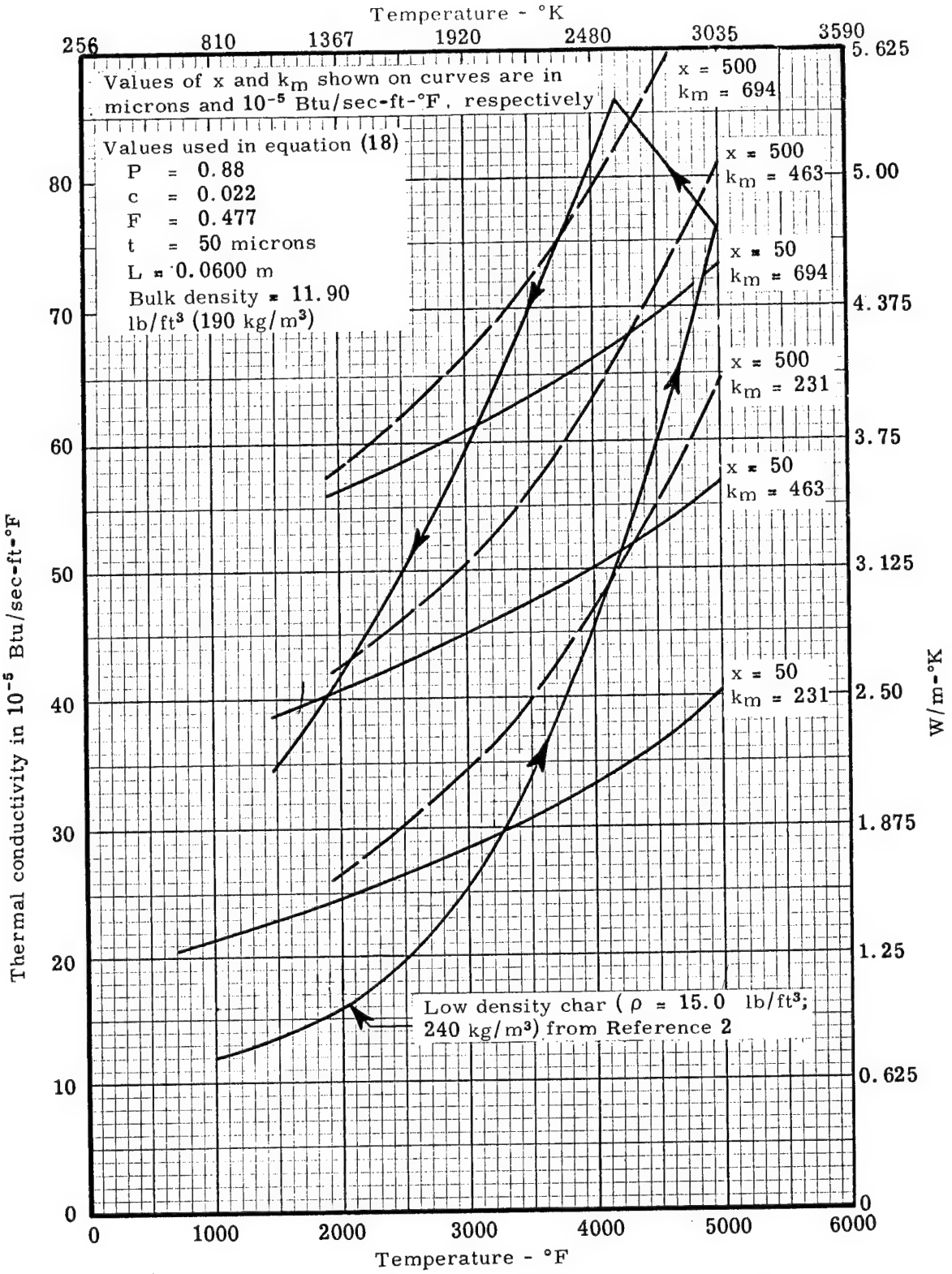

Figure 28. Comparison of the high temperature thermal conductivity predicted by equation (18) for a helium environment with prior data

TABLE 1

RESULTS OF BULK AND TRUE DENSITY MEASUREMENTS
AND POROSITY CALCULATIONS FOR LOW-DENSITY PHENOLIC-NYLON CHARS

Specimen	Bulk densities of chars (kg/m^3)	Bulk densities of chars (lb/ft^3)	True density[1] (kg/m^3)	True density[1] (lb/ft^3)	Porosity[3]	Average porosity for each virgin density	Remarks
19-4	196	12.27	1526[2]	95.60	0.872		Before run
19-4	188	11.78	1526[2]	95.60	0.877	0.876	After run
19-5	186	11.65			0.875/0.811		After run
30-3	282	17.67			0.813/0.823		Not evaluated
30-4	271	16.98	1501[2]	94.03	0.820	0.824	After run
30-6	257	16.10			0.829/0.839		After run
42-3	322	20.17			0.783/0.786		After run
42-4	319	19.98	1479[2]	92.65	0.785	0.786	After run
42-5	315	19.73			0.788/0.790		After run

1. True densities measured on other chars were as follows:
   Char from 19 lb/ft^3 virgin material = 1555 kg/m^3 (97.42 lb/ft^3) (never impregnated)
   Char from 30 lb/ft^3 virgin material = 1588 kg/m^3 (99.48 lb/ft^3) (never impregnated)
   Char from 42 lb/ft^3 virgin material = 1499 kg/m^3 (93.91 lb/ft^3) (never impregnated)

2. Char was ground using mortar and pestle. Particle sizes of powder used in measurements were:
   2 microns or less - 75%
   3-5 microns or less - 20%
   6-12 microns or less - 5%

3. A porosity range is given for those samples on which true density measurements were not made. Range is based on the two different true density measurements made on each virgin density material.

TABLE 2

GAGE LENGTH AND THICKNESS
OF SPECIMENS EVALUATED

Specimen Number	Gage Length		Thickness	
	in.	m	in.	m
19-4	0.2435	0.00618	0.430	0.0109
19-5	0.239	0.00607	0.427	0.0108
30-4	0.2825	0.00718	0.472	0.0120
30-6	0.311	0.00790	0.499	0.0126
42-3	0.276	0.00700	0.465	0.0118
42-4	0.2625	0.00667	0.450	0.0114
42-5	0.133	0.00338	0.312	0.00793

TABLE 3

THE THERMAL CONDUCTIVITY OF PHENOLIC-NYLON CHAR SPECIMEN 19-4 AS MEASURED USING THE COMPARATIVE ROD APPARATUS WITH CODE 9606 PYROCERAM REFERENCES

Specimen and run number	Time	Mean temperature of specimen °F	ΔT through specimen °F	Thermal conductivity Btu-in./hr-ft²-°F	Thermal conductivity in 10^{-5} Btu/sec-ft-°F	Thermal conductivity W/m-°K	Mean temperature of lower reference °F	Thermal conductivity of lower reference K_1 Btu-in./hr-ft²-°F	ΔT through lower reference ΔT_1 °F	Mean temperature of upper reference °F	Thermal conductivity of upper reference K_2 Btu-in./hr-ft²-°F	ΔT through upper reference ΔT_2 °F	Pressure and environment
Specimen 19-4 Run 4491-38	Specimen thickness: 0.430 in. (0.0109 m); specimen gage length: 0.2435 in. (0.00618 m); initial weight: 0.001087 kg; final weight 0.001043 kg; bulk density: 190 kg/m³ Pulled vacuum to 0.5 torr; backfilled with nitrogen												
	12-27-66												
	4:05 am	391	59.84	5.97	13.82	0.86	253	25.38	41.28	466	23.90	48.75	760 torr - nitrogen purge
	4:45 am	392	61.67	6.05	14.00	0.87	250	25.39	42.28	471	23.88	51.90	760 torr - nigrogen purge
	5:15 am	393	62.18	6.04	13.98	0.87	250	25.38	42.24	472	23.87	52.60	760 torr - nigrogen purge
	8:30 am	614	98.65	6.51	15.07	0.94	386	24.37	76.64	748	22.62	95.52	760 torr - nitrogen purge
	11:45 am	776	120.75	6.58	15.23	0.95	500	23.70	98.09	942	21.90	118.61	760 torr - nigrogen purge
	4:45 pm	951	157.03	6.46	14.95	0.93	603	23.22	131.58	1165	21.14	153.00	760 torr - nitrogen purge
	6:00 pm	963	154.50	6.33	14.65	0.91	618	23.17	133.95	1169	21.13	139.80	760 torr - nigrogen purge
	Pumped down to (0.01 torr<) backfilled with helium												
	12-28-66												
	7:15 pm	406	67.32	8.62	19.95	1.24	265	25.26	69.59	504	23.70	77.70	760 torr - helium purge
	11:15 pm	402	67.24	7.62	17.64	1.10	262	25.25	62.77	495	23.74	66.99	100 torr - helium leak
	11:45 pm	402	68.45	7.55	17.48	1.09	260	25.29	67.37	496	23.72	63.21	100 torr - helium leak
	12-29-66												
	5:05 am	397	71.45	5.45	12.62	0.79	248	25.40	48.56	484	23.80	49.63	9.5 torr - helium leak
	5:37 am	393	69.88	5.57	12.89	0.80	245	25.40	48.62	478	23.82	49.37	9.5 torr - helium leak
	7:10 am	451	77.89	4.37	10.12	0.63	272	25.19	37.42	540	23.51	49.53	0.8 torr - helium leak
	10:15 am	375	58.27	4.57	10.58	0.66	234	25.45	33.36	440	24.00	33.36	1.0 torr - helium leak
	12:30 pm	381	61.86	4.34	10.05	0.63	238	25.42	32.04	450	23.96	35.41	1.2 torr - helium leak
	5:35 pm	430	71.05	4.04	9.35	0.58	259	25.30	32.68	507	23.68	40.25	0.089 torr - helium leak
	6:15 pm	438	70.90	4.08	9.44	0.59	264	25.27	32.45	515	23.63	41.13	0.089 torr - helium leak
	9:15 pm	416	63.67	3.82	8.84	0.55	259	25.31	29.50	483	23.80	32.03	0.0058 torr - residual helium
	12-30-66												
	2:25 am	430	63.65	3.95	9.14	0.57	268	25.21	31.58	498	23.72	32.08	0.036 torr - residual helium
	10:30 am	643	97.10	4.17	10.88	0.60	398	24.28	50.86	754	22.60	56.48	0.0024 torr - residual helium
	2:15 pm	834	120.96	4.63	10.72	0.67	534	23.55	72.61	979	21.79	80.63	0.0027 torr - residual helium
	6:30 pm	978	129.97	5.11	11.83	0.74	665	22.97	91.83	1139	21.23	94.57	0.0033 torr - residual helium
	7:15 pm	984	127.46	5.23	12.11	0.75	679	22.90	92.30	1144	21.22	95.07	0.0033 torr - residual helium
	Backfilled with helium												
	12-31-66												
	8:00 am	960	102.4	11.12	25.74	1.60	727	22.69	154.5	1147	21.20	167.5	760 torr - helium purge
	7:50 pm	761	92.59	9.41	21.78	1.36	576	23.34	92.26	927	21.94	148.02	760 torr - helium purge
	1-2-67												
	6:00 pm	641	95.58	9.14	21.16	1.32	439	24.08	107.49	794	22.44	125.91	760 torr - helium purge

Note: The thermal conductivity was calculated from the equation $K = \frac{0.2435}{0.754}\left(\frac{K_1\Delta T_1 + K_2\Delta T_2}{2\Delta T_s}\right)$, where the gage length of the references was 0.754 in. (0.01915 m)

TABLE 4

THE THERMAL CONDUCTIVITY OF PHENOLIC-NYLON CHAR SPECIMEN 19-5 AS MEASURED USING THE COMPARATIVE ROD APPARATUS WITH PYREX REFERENCES

Specimen and run number	Time	Mean temperature of specimen °F	ΔT through specimen °F	Thermal conductivity Btu-in./hr-ft²-°F	Thermal conductivity in 10^{-5} Btu/sec-ft-°F	Thermal conductivity W/m-°K	Mean temperature of lower reference °F	Thermal conductivity of lower reference K_1 Btu-in./hr-ft²-°F	ΔT through lower reference ΔT_1 °F	Mean temperature of upper reference °F	Thermal conductivity of upper reference K_2 Btu-in./hr-ft²-°F	ΔT through upper reference ΔT_2 °F	Pressure and environment
Specimen 19-5 Run 4491-32	Specimen thickness: 0.427 in. (0.0108 m); specimen gage length: 0.239 in. (0.00607 m); final weight: 0.001017 kg; final bulk density: 190 kg/m³ pumped down to 0.050 torr; backfilled with nitrogen; pumped down to vacuum												
	12-19-66												
	9:45 am												
	10:30 pm	462	42.39	3.60	8.33	0.52	335	8.80	42.05	535	9.60	63.78	0.0033 torr - residual nitrogen
	12:15 am	468	43.50	3.53	8.17	0.51	339	8.80	42.80	542	9.65	63.32	0.0032 torr - residual nitrogen
	5:45 am	458	47.80	4.18	9.68	0.60	317	8.74	71.50	541	9.65	68.85	1.5 torr - nitrogen leak
	7:10 am	443	47.75	4.45	10.30	0.64	309	8.70	75.90	528	9.60	73.85	9.4 torr - nitrogen leak
	12:50 pm	425	42.35	4.63	10.72	0.67	308	8.70	73.40	498	9.50	66.05	110 torr - nitrogen leak
	1:35 pm	424	41.75	4.83	11.18	0.70	308	8.70	73.15	499	9.50	70.05	110 torr - nitrogen leak
	5:00 pm	428	44.65	4.88	11.30	0.70	307	8.65	80.51	508	9.50	74.80	760 torr - nitrogen purge
		Pulled vacuum											
	12-20-66												
	3:50 am	467	46.26	3.26	7.55	0.47	336	8.75	47.10	541	9.60	58.35	0.0022 torr - residual nitrogen
	4:30 am	458	42.40	3.30	7.64	0.48	335	8.75	44.97	527	9.50	53.55	0.0022 torr - residual nitrogen
	5:35 am	461	43.13	3.41	7.89	0.49	338	8.80	45.99	533	9.60	56.53	0.0022 torr - residual nitrogen
	12:05 pm	417	34.81	3.48	8.06	0.50	317	8.70	42.37	475	9.40	43.88	0.098 torr - helium leak
	4:20 pm	402	36.76	4.50	10.42	0.65	298	8.60	54.88	473	9.45	63.04	1 torr - helium leak
	6:40 pm	362	38.96	5.59	12.94	0.81	256	8.50	71.03	446	9.25	86.43	10 torr - helium leak
	12-22-66												
	3:00 am	374	42.15	5.32	12.31	0.77	262	8.50	75.62	461	9.30	86.37	9.9 torr - helium leak
	3:30 am	376	42.00	5.38	12.45	0.78	263	8.50	76.90	462	9.30	86.35	9.5 torr - helium leak
	5:15 am	368	39.85	6.35	14.70	0.92	257	8.50	90.07	456	9.25	93.65	114 torr - helium leak
	5:45 am	371	39.40	6.38	14.77	0.92	207	8.40	90.98	458	9.30	92.05	115 torr - helium leak
	7:05 am	362	37.63	7.35	17.01	1.06	251	8.50	96.55	455	9.25	104.03	760 torr - helium purge
	11:30 am	435	39.55	6.77	15.67	0.98	321	8.70	100.13	522	9.55	89.73	760 torr - helium purge

Note: The thermal conductivity was calculated from the equation

$$K_S = \frac{\Delta x_S}{2\Delta T_S A_S}\left(\frac{A_1 \Delta T_1 K_1}{\Delta x_1} + \frac{A_2 \Delta T_2 K_2}{\Delta x_2}\right) = \frac{0.154\ \Delta T_1 K_1 + 0.156\ \Delta T_2 K_2}{\Delta T_S}$$

where the area of the upper reference was 0.759 in.² (4.900×10^{-4} m²),
the area of the lower reference was 0.762 in.² (4.920×10^{-4} m²),
the gage length of the upper reference was 0.739 in. (0.0188 m)
and the gage length of the lower reference was 0.750 in. (0.01905 m)
The specimen area was 0.785 in.² (5.07×10^{-4} m²).

TABLE 5

THE THERMAL CONDUCTIVITY OF PHENOLIC-NYLON CHAR SPECIMEN 30-4 AS MEASURED USING THE COMPARATIVE ROD APPARATUS WITH CODE 9606 PYROCERAM REFERENCES

Specimen and run number	Time	Mean temperature of specimen °F	ΔT through specimen °F	Thermal conductivity Btu-in./hr-ft²-°F	Thermal conductivity in 10^{-5} Btu/sec-ft-°F	Thermal conductivity W/m-°K	Mean temperature of lower reference °F	Thermal conductivity of lower reference K_1 Btu-in./hr-ft²-°F	ΔT through lower reference ΔT_1 °F	Mean temperature of upper reference °F	Thermal conductivity of upper reference K_2 Btu-in./hr-ft²-°F	ΔT through upper reference ΔT_2 °F	Pressure and environment
Specimen 30-4 Run 4491-11	Specimen thickness: 0.472 in. (0.0120 m); specimen gage length: 0.283 in. (0.00718 m); final weight: 0.001581 kg; bulk density: 271 kg/m³												
	11-23-66												
	4:00 pm	237	39.06	6.47	14.98	0.93	143	26.56	25.10	281	25.08	27.21	760 torr - nitrogen purge
	4:30 pm	238	39.24	6.57	15.21	0.95	144	26.56	25.31	282	25.08	28.04	760 torr - nitrogen purge
		506	88.22	7.71	17.85	1.11	285	25.06	71.99	617	23.18	78.75	760 torr - nitrogen purge
	5:30 am	509	89.48	7.76	17.96	1.12	286	25.06	72.77	623	23.12	81.47	760 torr - nitrogen purge
		736	85.90	7.84	18.15	1.13	534	23.54	67.42	852	22.25	90.35	760 torr - nitrogen purge
	8:00 am	684	50.42	7.03	16.27	1.01	568	23.39	37.60	748	22.60	44.71	760 torr - nitrogen purge
	3:30 pm	698	51.83	7.08	16.39	1.02	577	23.32	39.57	764	22.55	45.99	760 torr - nitrogen purge
		965	60.95	8.17	18.91	1.18	827	22.31	54.90	1051	21.52	66.60	760 torr - nitrogen purge
	10:00 pm	959	60.24	8.30	19.21	1.20	826	21.51	49.90	1048	22.20	71.46	760 torr - nitrogen purge
	3:00 am	1073	71.94	8.16	18.89	1.18	906	22.35	70.13	1172	21.11	74.17	760 torr - nitrogen purge
	4:00 pm	486	45.68	7.36	17.04	1.06	381	24.40	33.65	543	23.50	41.42	760 torr - nitrogen purge
	11-28-66												
	5:20	487	47.04	6.53	15.11	0.94	329	24.74	29.74	555	23.44	38.59	0.007 torr - residual nitrogen
	6:30 pm	484	47.02	6.48	15.00	0.93	328	24.73	28.79	552	23.46	39.00	0.007 torr - residual nitrogen
	3:30 am	747	38.83	6.07	14.05	0.88	628	23.10	26.01	806	22.40	29.38	0.007 torr - residual nitrogen
	4:45 am	743	38.96	6.25	14.47	0.90	627	23.10	25.04	800	22.41	28.71	0.007 torr - residual nitrogen
	11:15 am	962	79.66	6.39	14.79	0.92	720	22.71	60.25	1075	21.42	63.04	0.0055 torr-residual nitrogen
	7:45 pm	396	38.58	6.76	15.65	0.97	266	25.23	23.78	448	23.98	33.04	0.0035 torr-residual nitrogen
	10:34 pm	374	38.94	6.46	14.95	0.93	243	25.41	21.72	426	24.11	32.80	0.0031 torr-residual nitrogen
	12-5-66												
		502	76.70	5.60	12.96	0.81	302	24.90	40.60	603	23.20	55.40	0.0022 torr-residual nitrogen
	10:00 am	476	54.52	6.68	15.46	0.96	287	25.03	34.70	553	23.46	45.92	0.0022 torr-residual nitrogen
		Backfilled with helium and pulled vacuum											
	4:00 pm	428	46.26	6.83	15.81	0.98	281	25.09	30.67	490	23.75	38.61	0.0022 torr-residual helium
	4:30 pm	421	43.82	6.88	15.93	0.99	281	25.09	28.48	480	23.81	37.58	0.0022 torr-residual helium
	12:30 am	411	46.26	6.40	14.81	0.92	288	24.07	27.57	474	23.85	38.42	1 torr - residual helium
	12-7-66												
	10:00 am	380	43.22	7.39	17.11	1.07	280	25.10	31.55	440	24.04	38.04	10.5 torr - residual helium
	10:30 am	380	42.10	7.44	17.22	1.07	281	25.10	31.07	437	24.05	37.13	10.5 torr - residual helium
	7:05 pm	402	38.34	8.47	19.61	1.22	325	24.78	36.71	451	23.98	34.39	760 torr - helium purge
	7:45 pm	402	37.98	8.49	19.65	1.22	326	24.77	36.85	451	23.98	33.69	760 torr - helium purge
	11:25 pm	590	56.76	9.08	21.02	1.31	474	23.86	59.53	668	22.95	37.99	760 torr - helium purge
	12:20 am	591	56.22	9.12	21.11	1.32	476	23.83	58.53	668	22.95	58.40	760 torr - helium purge
	9:00 am	774	84.27	10.31	23.86	1.49	605	23.22	88.21	909	22.00	117.83	760 torr - helium purge
	11:00	759	78.36	9.84	22.78	1.42	600	23.22	83.12	881	21.12	103.61	760 torr - helium purge
	6:30 pm	964	109.10	11.30	26.16	1.63	726	22.70	147.23	1139	21.22	152.65	760 torr - helium purge
	8:00 pm	959	107.58	11.24	26.02	1.62	724	22.70	145.32	1131	21.25	148.55	760 torr - helium purge

Note: The thermal conductivity was calculated from the equation $K_S = \frac{0.276}{0.754}\left(\frac{K_1\Delta T_1 + K_2\Delta T_2}{2\Delta T_S}\right)$, where the gage length of the references was 0.754 in. (0.01915 m)

TABLE 6

THE THERMAL CONDUCTIVITY OF PHENOLIC-NYLON CHAR SPECIMEN 30-6 AS MEASURED USING THE COMPARATIVE ROD APPARATUS WITH CODE 9606 PYROCERAM REFERENCES

Specimen and run number	Time	Mean temperature of specimen °F	ΔT through specimen °F	Thermal conductivity			Mean temperature of lower reference °F	Thermal conductivity of lower reference K_1 Btu-in./hr-ft²-°F	ΔT through lower reference ΔT_1 °F	Mean temperature of upper reference °F	Thermal conductivity of upper reference K_2 Btu-in./hr-ft²-°F	ΔT through upper reference ΔT_2 °F	Pressure and environment
				Btu-in./hr-ft²-°F	in 10^{-5} Btu/sec-ft-°F	W/m-°K							
Specimen 30-6 Run 4491-23	Specimen thickness: 0.499 in. (0.0126 m); specimen gage length: 0.311 in. (0.00790 m): final weight 0.00164 kg; bulk density: 257 kg/m³												
	10:45	505	60.50	5.80	13.43	0.84	327	24.73	31.61	576	23.33	39.52	0.0058 torr - residual nitrogen
	3:50 am	474	72.47	6.25	14.47	0.90	288	25.05	41.90	560	23.40	49.07	3.5 torr - residual nitrogen
	5:50 am	476	65.20	6.04	13.98	0.87	306	24.90	34.50	554	23.44	44.92	1.5 torr - residual nitrogen
	7:15 am	447	67.83	6.28	14.54	0.91	283	25.10	39.87	525	23.43	45.55	8.5 torr - residual nitrogen
	8:50 am	423	64.35	6.43	14.88	0.93	270	25.20	37.58	498	23.73	44.70	10.25 torr - residual nitrogen
	9:08 am	421	63.76	6.37	14.74	0.92	267	25.21	37.07	494	23.74	43.73	9.5 torr - residual nitrogen
	1:45 pm	535	62.46	6.25	14.47	0.90	334	24.70	39.72	616	23.17	39.47	0.07 torr - residual nitrogen
	4:30 pm	435	73.29	7.39	17.11	1.07	264	25.24	49.35	522	23.59	58.71	100 torr - residual nitrogen
		441	76.68	7.38	17.08	1.06	266	25.25	49.59	534	23.54	63.60	100 torr - residual nitrogen
	9:20 pm	476	93.62	8.34	19.30	1.20	268	25.23	60.26	598	23.23	97.70	760 torr - nitrogen purge
	3:15 am	489	91.15	7.85	18.17	1.13	279	25.11	65.75	599	23.24	78.44	760 torr - nitrogen purge
	3:45 am	485	88.40	7.90	18.29	1.14	280	25.11	65.60	592	23.27	74.93	760 torr - nitrogen purge
	6:50 am	934	46.87	7.83	18.12	1.13	829	22.30	41.42	992	21.75	39.43	760 torr - nitrogen purge
	8:25 am	Pulled vacuum to 40 microns; backfilled with helium; pulled second vacuum											
	5:10 pm	519	66.55	6.44	14.91	0.93	308	24.90	39.55	609	23.19	47.22	0.0036 torr - residual helium
	7:40 pm	472	72.06	6.31	14.61	0.91	285	25.06	43.05	560	23.41	48.27	1 torr - residual helium
	8:30 pm	464	71.99	6.24	14.44	0.90	277	25.13	41.99	553	23.44	48.05	1 torr - residual helium
	3:00 am	487	86.07	7.67	17.75	1.11	294	24.99	58.90	597	23.25	74.47	15.8 torr - residual helium
	4:00 am	502	88.60	7.73	17.89	1.11	303	24.92	62.50	616	23.18	76.05	16.5 torr - residual helium
	5:10 am	511	89.80	7.65	17.71	1.10	308	24.90	64.35	625	23.12	75.02	17.2 torr - residual helium
	9:25 am	515	100.10	9.70	22.45	1.40	309	24.85	88.62	655	22.98	109.32	120 torr - residual helium
	10:00 am	520	93.89	9.56	22.13	1.39	325	24.75	84.81	648	23.00	98.18	120 torr - residual helium
	12:30 pm	439	77.41	10.52	24.35	1.52	285	25.10	75.62	547	23.49	87.47	760 torr - helium purge
	5:10 pm	819	148.32	10.14	23.47	1.46	519	23.60	160.37	1029	21.60	162.87	760 torr - helium purge
	9:45 pm	909	58.76	6.52	15.09	0.94	762	22.57	34.91	986	21.74	49.29	0.0023 torr - residual helium
	3:15 pm	904	57.50	6.82	15.79	0.98	755	22.60	36.80	980	21.76	49.30	0.0021 torr - residual helium
	4:45 pm	923	61.00	7.22	16.71	1.04	763	22.56	40.40	1003	21.69	52.30	0.0021 torr - residual helium

Note: The thermal conductivity was calculated from the equation $K_S = \frac{0.311}{0.754}\left(\frac{K_1\Delta T_1 + K_2\Delta T_2}{2\Delta T_S}\right)$, where the gage length of the references was 0.754 in. (0.01915 m)

TABLE 7

THE THERMAL CONDUCTIVITY OF PHENOLIC-NYLON CHAR SPECIMEN 42-3 AS MEASURED USING THE COMPARATIVE ROD APPARATUS WITH CODE 9606 PYROCERAM REFERENCES

Specimen and run number	Time	Mean temperature of specimen °F	ΔT through specimen °F	Thermal conductivity			Mean temperature of lower reference °F	Thermal conductivity of lower reference K_1 Btu-in./hr-ft²-°F	ΔT through lower reference ΔT_1 °F	Mean temperature of upper reference °F	Thermal conductivity of upper reference K_2 Btu-in./hr-ft²-°F	ΔT through upper reference ΔT_2 °F	Pressure and environment
				Btu-in./hr-ft²-°F	in 10^{-5} Btu/sec-ft-°F	W/m-°K							
Specimen 42-3 Run 4491-3 (First Run)	Specimen thickness: 0.465 in. (0.0118 m); specimen gage length: 0.276 in. (0.00700 m); final weight: 0.001925 kg; bulk density: 322 kg/m³												
	10-11-66												
	10:30 am	Began run											
	2:15 pm	271	38.28	6.73	15.58	0.97	178	26.13	24.47	319	24.80	30.97	760 torr - nitrogen purge
	3:00 pm	274	38.08	6.76	15.65	0.97	188	26.00	25.17	321	24.77	30.36	760 torr - nitrogen purge
	6:00 pm	289	36.70	6.75	15.62	0.97	201	25.88	24.87	335	24.70	28.73	760 torr - nitrogen purge
	10:15 pm	282	34.25	6.63	15.35	0.96	201	25.88	23.47	324	24.77	25.57	760 torr - nitrogen purge
	10-12-66												
	10:15 pm	277	22.65	5.34	12.36	0.77	206	25.88	11.89	309	24.91	16.55	0.20 torr - residual nitrogen
	10-13-66												
	4:15 pm	299	19.92	5.76	13.33	0.83	233	25.55	12.27	326	24.76	12.64	0.20 torr - residual nitrogen
	5:30 pm	270	16.08	5.47	12.66	0.79	217	25.70	9.67	291	25.03	9.27	0.18 torr - residual nitrogen
		Could not achieve vacuum level desired: backfilled with nitrogen											
	10:30 pm	256	27.87	6.63	15.35	0.96	189	26.00	19.21	289	25.05	20.39	760 torr - nitrogen purge
		Terminated run; removed specimen from rig; built same specimen up using Fiberfrax pads between specimen and references; began second run 11-1-66; pumped down; backfilled with helium; pumped down for second time											
Specimen 42-3 Run 4491-5 (Second Run)	11-1-66	502	29.22	6.15	44.24	0.89	354	24.56	19.58	612	23.17	21.64	0.0037 torr - residual helium
		517	31.12	6.03	13.96	0.87	357	24.52	19.94	637	23.08	23.22	0.010 torr - residual helium
	11-2-66												
	1:35 am	508	28.96	6.10	14.12	0.88	348	24.62	19.60	622	23.13	20.91	0.088 torr - residual helium
	4:55 am	503	27.80	5.67	13.12	0.82	352	24.60	16.56	613	23.18	19.58	0.098 torr - residual helium
		499	31.95	7.24	16.76	1.04	335	24.70	24.84	620	23.06	28.21	1.0 torr - residual helium
		496	31.53	7.36	17.04	1.06	336	24.69	24.21	615	23.18	28.07	1.0 torr - residual helium
	11-4-66												
	8:25	479	39.50	9.38	21.71	1.35	330	24.71	39.50	590	23.28	45.00	9.9 torr - residual helium
		506	63.66	11.20	25.92	1.62	335	24.71	75.30	630	23.10	88.05	100 torr - residual helium
	7:20 am	497	63.08	11.57	26.78	1.67	339	24.69	76.30	614	23.19	90.68	100 torr - residual helium
		498	41.53	10.63	24.61	1.53	396	24.30	47.62	572	23.34	53.82	760 torr - helium purge
		Pumped down below 0.1 torr and backfilled with nitrogen											
	12:30 pm	503	37.95	8.47	19.61	1.22	383	24.49	35.30	577	23.32	38.27	760 torr - nitrogen purge
	3:45 pm	498	37.64	8.43	19.51	1.22	381	24.40	34.50	572	23.35	38.17	760 torr - nitrogen purge

TABLE 7 - Concluded

THE THERMAL CONDUCTIVITY OF PHENOLIC-NYLON CHAR SPECIMEN 42-3 AS MEASURED USING THE COMPARATIVE ROD APPARATUS WITH CODE 9606 PYROCERAM REFERENCES

Specimen and run number	Time	Mean temperature of specimen °F	ΔT through specimen °F	Thermal conductivity			Mean temperature of lower reference °F	Thermal conductivity of lower reference K_1 Btu-in./hr-ft²-°F	ΔT through lower reference ΔT_1 °F	Mean temperature of upper reference °F	Thermal conductivity of upper reference K_2 Btu-in./hr-ft²-°F	ΔT through upper reference ΔT_2 °F	Pressure and environment
				Btu-in./hr-ft²-°F	in 10^{-5} Btu/sec-ft-°F	W/m-°K							
Specimen 42-3 Run 4491-5 (Second Run) Continued	11-7-66 3:10 am	738	43.32	8.82	20.42	1.27	609	23.20	38.73	829	22.30	53.13	760 torr - nitrogen purge
	9:30 am	746	40.41	8.84	20.46	1.27	612	23.19	41.99	826	22.33	43.83	760 torr - nitrogen purge
	11-8-66 12:55 pm	725	34.94	7.52	17.41	1.08	563	23.40	31.89	857	22.21	31.05	0.0037 torr - residual nitrogen
	3:20 pm	729	37.87	7.41	17.15	1.07	559	23.42	29.24	876	22.14	38.30	0.0037 torr - residual nitrogen
		Backfilled with helium											
	11-9-66 6:00 am	756	30.68	12.12	28.05	1.75	678	22.91	42.56	816	22.37	47.26	760 torr - helium purge
	1:20 pm	1029	89.28	13.07	30.25	1.88	800	22.42	139.31	1212	20.98	154.99	760 torr - helium purge
	2:20 pm	1031	89.46	13.07	30.25	1.88	801	22.40	139.98	1213	20.99	155.10	760 torr - helium purge
		1008	32.97	9.84	22.78	1.42	870	22.15	38.27	1136	21.27	43.53	0.0037 torr - residual helium
Sepcimen 42-3 Run 4491-51 (Third Run)	1-11-67 8:10 am	520	66.61	5.75	13.31	0.83	297	24.95	38.44	590	23.27	48.70	0.0043 torr - residual nitrogen
	9:30 am	525	69.83	5.70	13.19	0.82	300	24.90	39.86	602	23.25	50.83	0.092 torr - nitrogen bleed
	1:15 pm	466	69.40	5.60	12.96	0.81	259	25.28	38.91	544	23.48	48.64	0.98 torr - nitrogen bleed
	2:15 pm	471	70.12	5.88	13.61	0.85	260	25.28	41.14	553	23.45	51.91	1.2 torr - nitrogen bleed
	6:15 pm	467	81.26	6.51	15.07	0.94	254	25.34	53.81	567	23.39	65.27	10.0 torr - nitrogen bleed
	7:07 pm	480	83.33	6.54	15.14	0.94	259	25.29	56.12	584	23.30	66.93	9.75 torr - nitrogen bleed
	11:15 pm	465	69.24	7.22	16.71	1.04	291	24.99	54.46	552	23.45	58.45	100 torr - nitrogen bleed
	11:30 pm	470	69.79	7.37	17.06	1.06	294	24.98	56.12	558	23.42	60.20	100 torr - nitrogen bleed
	1-12-67 12:00 am	502	72.04	7.59	17.57	1.09	326	24.75	58.43	593	23.25	66.39	760 torr - nitrogen purge
	1:15 pm	502	70.70	7.75	17.94	1.12	325	24.75	58.00	593	23.35	66.99	760 torr - nitrogen purge
		Reduced ΔT through specimen to 20°F; could not obtain good data because ΔT was too low in references											
	1-13-67 1:15 pm	955	122.9	7.86	18.19	1.13	644	23.03	108.93	1126	21.27	130.91	760 torr - nitrogen purge

Note: The thermal conductivity was calculated from the equation $K_S = \frac{0.276}{0.754}\left(\frac{K_1\Delta T_1 + K_2\Delta T_2}{2\Delta T_S}\right)$, where the gage length of the references was 0.754 in. (0.01915 m)

TABLE 8

THE THERMAL CONDUCTIVITY OF THE UPPER PORTION OF PHENOLIC-NYLON CHAR SPECIMEN 42-3
AS MEASURED USING THE COMPARATIVE ROD APPARATUS WITH CODE 9606 PYROCERAM REFERENCES

Specimen and run number	Time	Mean temperature of specimen °F	ΔT through specimen °F	Thermal conductivity			Mean temperature of lower reference °F	Thermal conductivity of lower reference K_1 Btu-in./hr-ft²-°F	ΔT through lower reference ΔT_1 °F	Mean temperature of upper reference °F	Thermal conductivity of upper reference K_2 Btu-in./hr-ft²-°F	ΔT through upper reference ΔT_2 °F	Pressure and environment
				Btu-in./hr-ft²-°F	in 10^{-5} Btu/sec-ft-°F	W/m-°K							
Specimen 42-3 Run 4491-5 (Second Run)		Gage length: 0.095 in. (0.00241 m)											
	11-1-66												
		521	6.88	8.99	20.81	1.29	354	24.56	19.58	612	23.17	21.64	0.0037 torr - residual helium
		537	8.67	7.44	17.22	1.07	357	24.52	19.94	637	23.08	23.22	0.010 torr - helium bleed
	11-2-66												
	1:35 am	526	7.78	7.81	18.08	1.12	348	24.62	19.60	622	23.13	20.91	0.088 torr - helium bleed
	4:55 am	521	7.01	7.73	17.89	1.11	352	24.60	16.56	613	23.18	19.58	0.098 torr - helium bleed
		519	6.79	11.71	27.11	1.69	335	24.70	24.84	620	23.06	28.21	1.0 torr - helium bleed
		515	6.71	11.89	27.53	1.71	336	24.69	24.21	615	23.18	28.07	1.0 torr - helium bleed
	11-4-66												
	8:25	553	8.21	15.52	35.93	2.23	330	24.71	39.50	590	23.28	45.00	9.9 torr - helium bleed
		544	12.22	20.07	46.46	2.89	335	24.71	75.30	630	23.10	88.05	100 torr - helium bleed
	7:20 am	534	12.08	20.78	48.11	2.99	339	24.69	76.30	614	29.19	90.68	100 torr - helium bleed
		523	7.43	20.43	47.30	2.94	396	24.30	47.62	572	23.34	53.82	760 torr - helium purge

Note: The thermal conductivity was calculated from the equation $K_S = \frac{0.095}{0.754}\left(\frac{K_1\Delta T_1 + K_2\Delta T_2}{2\Delta T_S}\right)$, where the gage length of the reference was 0.754 in. (0.01915 m)

TABLE 9

THE THERMAL CONDUCTIVITY OF THE LOWER PORTION OF PHENOLIC-NYLON CHAR SPECIMEN 42-3
AS MEASURED USING THE COMPARATIVE ROD APPARATUS WITH CODE 9606 PYROCERAM REFERENCES

Specimen and run number	Time	Mean temperature of specimen °F	ΔT through specimen °F	Thermal conductivity			Mean temperature of lower reference °F	Thermal conductivity of lower reference K_1 Btu-in./hr-ft²-°F	ΔT through lower reference ΔT_1 °F	Mean temperature of upper reference °F	Thermal conductivity of upper reference K_2 Btu-in/hr-ft²-°F	ΔT through of upper reference ΔT_2 °F	Pressure and environment
				Btu-in./hr-ft²-°F	in 10^{-5} Btu/sec-ft-°F	W/m-°K							
Specimen 42-3 Run 4491-5 (Second Run)		Gage length: 0.093 in. (0.00236 m)											
	11-1-66												
		464	48.19	1.27	2.94	0.182	354	24.56	19.58	612	23.17	21.64	0.0037 torr - residual helium
		476	50.73	1.26	2.92	0.181	357	24.52	19.94	637	23.08	23.22	0.010 torr - helium bleed
	11-2-66												
	1:35 am	467	51.70	1.17	2.71	0.168	348	24.62	19.60	622	23.13	20.91	0.088 torr - helium bleed
	4:55 am	464	49.70	1.08	2.50	0.155	352	24.60	16.56	613	23.18	19.58	0.098 torr - helium bleed
		457	52.25	1.51	3.50	0.217	335	24.70	24.84	620	23.06	28.21	1.0 torr - helium bleed
		455	50.50	1.56	3.61	0.225	336	24.69	24.21	615	23.18	28.07	1.0 torr - helium bleed
	11-4-66												
	8:25	432	54.14	2.33	5.39	0.335	330	24.71	39.50	590	23.28	45.00	9.9 torr - helium bleed
		440	68.42	3.55	8.22	0.511	335	24.71	75.30	630	23.10	88.05	100 torr - helium bleed
	7:20 am	434	62.26	3.99	9.24	0.575	339	24.69	76.30	614	23.19	90.68	100 torr - helium bleed
		457	41.29	3.64	8.43	0.524	396	24.30	47.62	572	23.34	53.82	760 torr - helium purge

Note: The thermal conductivity was calculated from the equation $K_s = \frac{0.093}{0.754}\left(\frac{K_1\Delta T_1 + K_2\Delta T_2}{2\Delta T_s}\right)$, where the gage length of the references was 0.754 in. (0.01915 m)

TABLE 10

THE THERMAL CONDUCTIVITY OF PHENOLIC-NYLON CHAR SPECIMEN 42-4 AS MEASURED USING THE COMPARATIVE ROD APPARATUS WITH CODE 9606 PYROCERAM REFERENCES

Specimen and run number	Time	Mean temperature of specimen °F	ΔT through specimen °F	Thermal conductivity			Mean temperature of lower reference °F	Thermal conductivity of lower reference K_1 Btu-in./hr-ft²-°F	ΔT through lower reference ΔT_1 °F	Mean temperature of upper reference °F	Thermal conductivity of upper reference K_2 Btu-in./hr-ft²-°F	ΔT through of upper reference ΔT_2 °F	Pressure and environment
				Btu-in./hr-ft²-°F	in 10^{-5} Btu/sec-ft-°F	W/m-°K							
Specimen 42-4 Run 4491-19	Specimen thickness: 0.450 in. (0.0114 m); specimen gage length: 0.263 in. (0.00667 m); final weight: 0.001613 kg; bulk density: 320 kg/m³												
	12-8-66												
	2:30 pm	473	43.72	4.85	11.23	0.70	395	24.30	23.22	523	23.60	27.75	760 torr - nitrogen purge
	2:45 pm	470	40.84	4.95	11.46	0.71	396	24.30	22.00	516	23.62	26.50	760 torr - nitrogen purge
	3:00 pm	468	40.38	5.31	12.29	0.77	396	24.30	21.82	514	23.64	26.29	760 torr - nitrogen purge
	10:00 pm	1017	125.97	5.97	13.82	0.86	790	22.47	89.00	1180	21.09	109.94	760 torr - nitrogen purge
	10:50 pm	1018	126.55	5.91	13.68	0.85	791	22.47	88.10	1180	21.09	109.78	760 torr - nitrogen purge
	Turned power off at 11:00 pm; pulled vacuum												
	12-9-66												
	6:00 pm	502	68.79	3.50	8.10	0.50	342	24.64	23.31	563	23.40	34.51	0.0095 torr - residual nitrogen
	12-11-66												
	4:45 am	1317	206.10	4.10	9.49	0.59	870	22.15	116.00	1638	20.00	114.30	0.0077 torr - residual nitrogen
	Backfilled with helium at 6:00 am on 12-11-66												
	12-12-66												
	5:15 am	498	84.10	8.18	18.93	1.18	359	24.56	73.50	621	23.14	92.95	760 torr - helium purge
	5:45 am	499	84.25	8.18	18.93	1.18	360	24.56	73.88	622	23.14	92.62	760 torr - helium purge
	10:00 am	777	89.47	9.34	21.62	1.35	622	23.15	91.51	921	22.72	118.15	760 torr - helium purge
	1:15 pm	898	117.61	9.55	22.11	1.38	688	22.85	132.66	1092	21.50	159.26	760 torr - helium purge
	Turned power off 3:10 pm; pulled vacuum												
	12-13-66												
	4:50 am	989	75.77	3.91	9:05	0.56	831	22.30	35.13	1078	21.44	42.83	0.0053 torr - residual helium

Note: The thermal conductivity was calculated from the equation $K_S = \frac{0.263}{0.754}\left(\frac{K_1\Delta T_1 + K_2\Delta T_2}{2\Delta T_S}\right)$, where the gage length of the references was 0.754 in. (0.01915 m)

TABLE 11

THE THERMAL CONDUCTIVITY OF PHENOLIC-NYLON CHAR SPECIMEN 42-5 AS MEASURED USING THE COMPARATIVE ROD APPARATUS WITH CODE 9606 PYROCERAM REFERENCES

Specimen and run number	Time	Mean temperature of specimen °F	ΔT through specimen °F	Thermal conductivity			Mean temperature of lower reference °F	Thermal conductivity of lower reference K_1 Btu-in./hr-ft²-°F	ΔT through lower reference ΔT_1 °F	Mean temperature of upper reference °F	Thermal conductivity of upper reference K_2 Btu-in/hr-ft²-°F	ΔT through upper reference ΔT_2 °F	Pressure and environment
				Btu-in./hr-ft²-°F	in 10^{-5} Btu/sec-ft-°F	W/m-°K							
Specimen 42-5 Run 4491-46	Specimen thickness: 0.312 in. (0.00793 m); specimen gage length: 0.133 in. (0.00338 m); final weight: 0.001265 kg; final bulk density: 320 kg/m³												
	1-3-67												
	8:50 pm	480	47.72	7.10	16.43	1.02	353	24.58	76.25	585	23.30	84.56	760 torr - nitrogen purge
	9:25 pm	485	48.21	7.14	16.53	1.03	357	24.56	78.12	590	23.28	85.45	760 torr - nitrogen purge
	1-4-67												
	8:05 am	994	67.52	8.22	19.03	1.19	802	22.42	131.79	1165	21.14	158.30	760 torr - nitrogen purge
	7:30 pm	476	48.69	5.20	12.04	0.75	325	24.77	55.40	563	23.40	64.21	0.00475 torr - residual nitrogen
	11:15 pm	850	73.60	6.00	13.89	0.87	610	23.19	100.83	1018	21.64	123.60	0.0043 torr - residual nitrogen
	Backfilled with helium; pumped down below 0.1 torr; backfilled with helium												
	1-5-67												
	2:30 pm	381	42.05	7.83	18.12	1.13	274	25.20	65.11	478	23.82	88.03	760 torr - helium purge
	3:05 pm	379	39.32	8.46	19.58	1.22	272	25.20	67.16	475	23.80	87.46	760 torr - helium purge
	10:00 pm	931	85.08	8.11	18.77	1.17	704	22.80	169.64	1133	21.24	186.60	760 torr - helium purge

Note: The thermal conductivity was calculated from the equation $K_S = \frac{0.133}{0.754}\left(\frac{K_1\Delta T_1 + K_2\Delta T_2}{2\Delta T_S}\right)$, where the gage length of the references was 0.754 in. (0.01915 m)

TABLE 12

COMPARISON OF THE EXPERIMENTAL DATA AT APPROXIMATELY 500°F FOR THE THREE CHAR DENSITIES

Specimen number	Average bulk density kg/m³	Average porosity	Average thermal conductivity in vacuum		Average thermal conductivity in nitrogen		Absolute change in thermal conductivity going from vacuum to nitrogen		Percent change in going from vacuum to nitrogen[1]	Average thermal conductivity in helium		Absolute change in thermal conductivity going from vacuum to helium		Percent change in thermal conductivity going from vacuum to helium[1]	Maximum possible percent change due to gas conduction[2]		Difference between measured percent change and maximum possible percent change due to gas conduction	
			in 10^{-5} Btu/sec-ft-°F	W/m-°K	in 10^{-5} Btu/sec-ft-°F	W/m-°K	in 10^{-5} Btu/sec-ft-°F	W/m-°K		in 10^{-5} Btu/sec-ft-°F	W/m-°K	in 10^{-5} Btu/sec-ft-°F	W/m-°K		Nitrogen	Helium	Nitrogen	Helium
19-4 and 19-5	187	0.88	9.0	0.561	12.5	0.779	3.5	0.218	38.8	18.8	1.171	9.8	0.611	108.8	6.5	39	32.3	69.8
30-4 and 30-6	264	0.82	14.5	0.905	17.5	1.090	3.0	0.187	20.6	22.0	1.370	7.5	0.467	51.7	4.1	25	16.5	26.7
42-3 and 42-5	318	0.79	13.0	0.810	17.5	1.090	4.5	0.281	34.6	22.0	1.370	9.0	0.561	69.2	4.5	27	30.1	32.2

Notes:

1. Percent change = $\frac{\text{Thermal conductivity in gas} - \text{thermal conductivity in vacuum}}{\text{thermal conductivity in vacuum}}$

2. This value obtained by adding the thermal conductivity of the gas to the thermal conductivity measured in vacuum

3. The thermal conductivities of nitrogen and helium at 500°F are:

   Nitrogen – 0.58×10^{-5} Btu/sec-ft-°F (0.0362 W/m-°K)
   Helium – 3.5×10^{-5} Btu/sec-ft-°F (0.218 W/m-°K)

TABLE 13

RESULTS OBTAINED BY APPLYING RUSSELL' S EQUATION TO EXPERIMENTAL DATA AT 500°F

Specimen number	Units for thermal conductivity	Reduced k_m	Thermal conductivity predicted by Russell's equation using value of matrix conductivity reduced from vacuum data: In vacuum at 500°F (532°K) Measured	In nitrogen at 500°F (532°K) Predicted	In nitrogen at 500°F (532°K) Measured	In nitrogen at 500°F (532°K) Percent[1] Difference	In helium at 500°F (532°K) Predicted	In helium at 500°F (532°K) Measured	In helium at 500°F (532°K) Percent[1] Difference
19-4	Btu-in/hr-ft²-°F 10^{-5} Btu/sec-ft-°F W/m-°K	44.3 103 6.38	3.9 9.0 0.56	4.1 9.5 0.59	6.2 14.4 0.89	51.2	5.3 12.3 0.76	8.7 20.1 1.25	64.1
19-5	Btu-in/hr-ft²-°F 10^{-5} Btu/sec-ft-°F W/m-°K	39.8 92 5.73	3.5 8.1 0.50	3.7 8.6 0.52	4.9 11.3 0.71	32.4	4.9 11.3 0.71	7.0 16.2 1.01	42.8
30-4 and 30-6	Btu-in/hr-ft²-°F 10^{-5} Btu/sec-ft-°F W/m-°K	50.0 116 7.2	6.4 14.8 0.92	6.8 15.7 0.98	7.5 17.3 1.08	10.2	7.8 18.1 1.12	9.5 21.9 1.37	21.7
42-3	Btu-in. /hr-ft²-°F 10^{-5} Btu/sec-ft-°F W/m-°K	38.0 88 5.47	6.0 13.9 0.86	6.4 14.8 0.92	8.0 18.5 1.15	25.0	7.4 17.1 1.07	10.5 24.3 1.51	41.8
42-4	Btu-in. /hr-ft²-°F 10^{-5} Btu/sec-ft-°F W/m-°K	22.2 51 3.20	3.5 8.1 0.50	3.7 8.6 0.53	5.0 11.6 0.72	35.1	4.9 11.3 0.71	8.0 18.5 1.15	63.2
42-5	Btu-in. /hr-ft²-°F 10^{-5} Btu/sec-ft-°F W/m-°K	32.9 76 4.74	5.2 12.0 0.75	5.4 12.5 0.78	7.1 16.4 1.02	31.4	6.6 15.3 0.95	8.2 18.9 1.18	24.2

Specimen number	Units for thermal conductivity	Reduced k_m	Thermal conductivity predicted by Russell's equation using value of matrix conductivity reduced from nitrogen data: In nitrogen at 500°F (532°K) Measured	In vacuum at 500°F (532°K) Predicted	In vacuum at 500°F (532°K) Measured	In vacuum at 500°F (532°K) Percent[1] Difference	In helium at 500°F (532°K) Predicted	In helium at 500°F (532°K) Measured	In helium at 500°F (532°K) Percent[1] Difference
19-4	Btu-in. /hr-ft²-°F 10^{-5} Btu/sec-ft-°F W/m-°K	67.8 157 9.76	6.2 14.4 0.89	6.0 13.9 0.86	3.9 9.0 0.56	-35.0	7.4 17.1 1.07	8.7 20.1 1.25	17.5
19-5	Btu-in. /hr-ft²-°F 10^{-5} Btu/sec-ft-°F W/m-°K	53.0 123 7.63	4.9 11.3 0.71	4.7 10.8 0.68	3.5 8.1 0.50	-25.5	6.1 14.2 0.88	7.0 16.2 1.01	14.7
30-4 and 30-6	Btu-in. /hr-ft²-°F 10^{-5} Btu/sec-ft-°F W/m-°K	56.8 131 8.18	7.5 17.3 1.08	7.3 16.9 1.05	6.4 14.8 0.92	-12.3	8.7 20.1 1.25	9.5 21.9 1.37	9.1
42-3	Btu-in. /hr-ft²-°F 10^{-5} Btu/sec-ft-°F W/m-°K	49.2 114 7.08	8.0 18.5 1.15	7.8 18.1 1.12	6.0 13.9 0.86	-23.0	9.1 21.1 1.31	10.5 24.3 1.51	15.3
42-4	Btu-in. /hr-ft²-°F 10^{-5} Btu/sec-ft-°F W/m-°K	30.2 69 4.35	5.0 11.6 0.72	4.8 11.1 0.69	3.5 8.1 0.50	-27.0	6.1 14.1 0.88	8.0 18.5 1.15	31.1
42-5	Btu-in. /hr-ft²-°F 10^{-5} Btu/sec-ft-°F W/m-°K	43.5 101 6.26	7.1 16.4 1.02	6.9 15.8 0.99	5.2 12.0 0.75	-24.6	8.2 18.9 1.18	8.2 18.9 1.18	0

[1]Percent difference = $\left[\frac{\text{measured conductivity} - \text{predicted conductivity}}{\text{predicted conductivity}}\right] \times 100\%$

TABLE 14

RESULTS OF REDUCING THE PARAMETERS c, F, AND k_m IN EQUATION (18) FROM THE EXPERIMENTAL DATA

Specimen No.	Porosity	Thermal conductivity measured at 500°F (532°K)								
		Btu-in. /hr-ft²-°F			10^{-5} Btu/sec-ft-°F			W/m-°K		
		Vacuum	Nitrogen	Helium	Vacuum	Nitrogen	Helium	Vacuum	Nitrogen	Helium
19-4	0.877	3.9	6.2	8.7	9.02	14.35	20.13	0.56	0.89	1.25
19-5	0.878	3.5	4.9	7.0	8.10	11.34	16.20	0.50	0.71	1.01
30-4 30-6	0.827	6.4	7.5	9.5	14.81	17.36	21.98	0.92	1.08	1.37
42-3	0.785	6.0	8.0	10.5	13.88	18.51	24.30	0.86	1.15	1.51
42-4	0.785	3.5	5.0	8.0	8.10	11.57	18.51	0.50	0.72	1.15
42-5	0.789	5.2	7.1	8.2	12.03	16.43	18.97	0.75	1.02	1.18

Specimen No.	Porosity	Value of c, F, and k_m in equation (19) obtained by fitting data at 500°F (532°K)					Value obtained for k_m by using P rather than $P^{2/3}$ in equation (19)		
				k_m					
		c	F	$\frac{\text{Btu-in.}}{\text{hr-ft}^2\text{-°F}}$	$10^{-5}\ \frac{\text{Btu}}{\text{sec-ft-°F}}$	$\frac{\text{W}}{\text{m-°K}}$	$\frac{\text{Btu-in.}}{\text{hr-ft}^2\text{-°F}}$	$10^{-5}\ \frac{\text{Btu}}{\text{sec-ft-°F}}$	$\frac{\text{W}}{\text{m-°K}}$
19-4	0.877	0.022	0.477	107	248	15.41	73	169	10.51
19-5	0.878	0.047	0.545	84	194	12.10	57	132	8.21
30-4 30-6	0.827	0.036	0.710	86	199	12.38	59	137	8.50
42-3	0.785	0.027	0.590	80	185	11.52	54	125	7.78
42-4	0.785	0.071	0.400	67	155	9.65	46	106	6.62
42-5	0.789	0.006	0.720	55	127	7.92	38	88	5.47

REFERENCES

1. Wilson, R. Gale: Thermophysical Properties of Six Charring Ablators from 140° to 700°K and Two Chars from 800° to 3000°K. NASA TN D-2991, October 1965.

2. Engelke, W. T.; Pyron, C. M., Jr.; and Pears, C. D.: Thermophysical Properties of a Low-Density Phenolic-Nylon Ablation Material. NASA CR-809, 1967.

3. Young, R. C.; Hartwig, F. J.; and Norton, C. L.: Effect of Various Atmospheres on Thermal Conductance of Refractories. Journal of the American Ceramic Society, vol. 47, no. 5, 1964, pp. 205-210.

4. Russell, H. W.: Principles of Heat Flow in Porous Insulations. Journal of the American Ceramic Society, vol. 18, no. 1, 1935, pp. 1-5.

5. Gorring, Robert L.; and Churchill, Stuart W.: Thermal Conductivity of Heterogeneous Materials. Chemical Engineering Progress, vol. 57, no. 7, July 1961, pp. 53-59.

6. Francl, J.; and Kingery, W. D.: Thermal Conductivity: IX, Experimental Investigation of the Effect of Porosity on Thermal Conductivity. Journal of the American Ceramic Society, vol. 37, no. 2, 1954, pp. 99-151.

7. Loeb, Arthur L.: Thermal Conductivity: VIII, A Theory of Thermal Conductivity of Porous Materials. Journal of the American Ceramic Society, vol. 37, no. 2, 1954, pp. 96-99.

8. Powers, A. E.: Conductivity in Aggregates. Proceedings of the Second Conference on Thermal Conductivity, Division of Applied Physics, National Research Council, Ottawa, Ontario, 1962, pp. 280-309.

9. Jakob, Max: Heat Transfer. John Wiley and Sons, Inc., New York, 1957.

10. Kreith, Frank: Principles of Heat Transfer. International Textbook Company, Scranton, Pennsylvania, 1962, pp. 318-319.

11. Verschoor, J. D.; and Greebler, Paul: Heat Transfer by Gas Conduction and Radiation in Fibrous Insulations. Transactions of the ASME, no. 74, 1952, pp. 961-968.

REFERENCES - Concluded

12. Kennard, Earle H.: Kinetic Theory of Gases. McGraw-Hill Book Company, Inc., New York, 1938, pp. 315-318.

13. Goldsmith, Alexander; Waterman, Thomas E.; and Hirschhorn, Harry J.: Thermophysical Properties of Solid Materials, Volume I - Elements (Melting temperatures above 1000°F), WADC TR 58-476, August 1960, pp. I-C-3-c.

14. WADC TR 58-476: Thermophysical Properties of Solid Materials, Volume II Alloys, Armour Research Foundation, November 1960.

15. Powell, R. W.: Proceedings of the Third Conference on Thermal Conductivity, 1963, pp. 322-341.

16. ASD-TDR-62-765: The Thermal Properties of Twenty-Six Solid Materials to 5000°F or Their Destruction Temperatures. Southern Research Institute, August 1962.

17. Pears, C. D.: Proceedings of the Third Conference on Thermal Conductivity, 1963, pp. 453-479.

18. Fieldhouse, et al: WADC TR 55-495, Part 3, 1955.

NASA-Langley, 1967 — 18 CR-966

"The aeronautical and space activities of the United States shall be conducted so as to contribute . . . to the expansion of human knowledge of phenomena in the atmosphere and space. The Administration shall provide for the widest practicable and appropriate dissemination of information concerning its activities and the results thereof."

—NATIONAL AERONAUTICS AND SPACE ACT OF 1958

NASA SCIENTIFIC AND TECHNICAL PUBLICATIONS

TECHNICAL REPORTS: Scientific and technical information considered important, complete, and a lasting contribution to existing knowledge.

TECHNICAL NOTES: Information less broad in scope but nevertheless of importance as a contribution to existing knowledge.

TECHNICAL MEMORANDUMS: Information receiving limited distribution because of preliminary data, security classification, or other reasons.

CONTRACTOR REPORTS: Scientific and technical information generated under a NASA contract or grant and considered an important contribution to existing knowledge.

TECHNICAL TRANSLATIONS: Information published in a foreign language considered to merit NASA distribution in English.

SPECIAL PUBLICATIONS: Information derived from or of value to NASA activities. Publications include conference proceedings, monographs, data compilations, handbooks, sourcebooks, and special bibliographies.

TECHNOLOGY UTILIZATION PUBLICATIONS: Information on technology used by NASA that may be of particular interest in commercial and other non-aerospace applications. Publications include Tech Briefs, Technology Utilization Reports and Notes, and Technology Surveys.

Details on the availability of these publications may be obtained from:

SCIENTIFIC AND TECHNICAL INFORMATION DIVISION

NATIONAL AERONAUTICS AND SPACE ADMINISTRATION

Washington, D.C. 20546